DISSERTATION

DEVELOPMENT AND APPLICATION OF SELF-INTERACTION CHROMATOGRAPHY AS A RATIONAL APPROACH TO MEASURING THE OSMOTIC SECOND VIRIAL COEFFICIENT (B) FOR PROTEIN FORMULATION DEVELOPMENT

Submitted by

Joseph J. Valente

Department of Chemistry

In Partial fulfillment of the requirements

For the Degree of Doctor of Philosophy

Colorado State University

Fort Collins, Colorado

Fall 2006

COLORADO STATE UNIVERSITY

July 17, 2006

WE HEREBY RECOMMEND THAT THE DISSERTATION PREPARED UNDER OUR SUPERVISION BY JOSEPH J. VALENTE ENTITLED "DEVELOPMENT AND APPLICATION OF SELF-INTERACTION CHROMATOGRAPHY AS A RATIONAL APPROACH TO MEASURING THE OSMOTIC SECOND VIRIAL COEFFICIENT (B) FOR PROTEIN FORMULATION DEVELOPMENT" BE ACCEPTED AS FULFILLING IN PART REQUIREMENTS FOR THE DEGREE OF DOCTOR OF PHILOSOPHY.

Committee on Graduate Work

Bruce A. Parkinson

Elliot R. Bernstein

Matthew P. Shores

Olve Peersen

Adivsor: Charles S. Henry

Department Head: Anthony K. Rappe

ABSTRACT OF DISSERTATION

DEVELOPMENT AND APPLICATION OF SELF-INTERACTION CHROMATOGRAPHY AS A RATIONAL APPROACH TO MEASURING THE OSMOTIC SECOND VIRIAL COEFFICIENT (B) FOR PROTEIN FORMULATION DEVELOPMENT

Formulation development is an integral step in the successful commercialization of protein-based products, both in the biotechnology and pharmaceutical industries. As the number and complexity of these protein formulations increases, so does the need for innovative approaches to characterize physical product stability. This dissertation demonstrates the development and application of self-interaction chromatography (SIC) for measuring the osmotic second virial coefficient (B) of proteins in the presence of biologically and industrially relevant mixtures of cosolvents including salts, sugars, amino acids, and polyols, and as a function of temperature and pH. Early studies focused on model proteins in very controlled systems. The application of SIC was then advanced to demonstrate rational formulation screening of three industrially relevant enzymes. SIC measured trends in B demonstrated excellent agreement with available B data from static light scattering (SLS) studies. In the absence of B measurements from other characterization approaches, SIC measured trends in B were correlated

with trends in solubility and enzymatic activity. The outcome of the work presented in this dissertation suggests that SIC is a useful means to augment current approaches to characterizing the physical stability of protein-based formulations. I believe these efforts to develop a better fundamental understanding and characterization approach of protein self-interaction in complex cosolvent systems will ultimately lead to direct improvements in macromolecular formulation chemistry and structural biology endeavors.

Joseph J. Valente

Chemistry Department

Colorado State University

Fort Collins, CO 80523

Fall 2006

ACKNOWLEDGMENTS

To my best friend and wife: Meriah Wells Neissel Valente. I love you, for all that you are, all that you have made me, and all that we will make together.

To my people (WWU): Dr. Patrick, thanks for my first chance in the lab. Good to see that 420B hasn't changed much. To "Army" Mike Lynch and Joe "MC" McClellan, best of wishes and thanks for everything, B-Ham style.

To my people (CSU): Jeff and Laura Frein, Mark Kerr, Deidre Johns (long live the Birmingham Triangle), Alan Grubbs, and The Quantum Mechanics. Thank you.

To Paninos Italian Restaurant: Thanks for helping to level my head and ease my mind, one dollar at a time.

To my lab mate: Robert W. Payne, thanks for being the other half of the project. It's all in your hands now.

To Genencor: Beth Fryksdale, Douglas Dale, and Alfred Gaertner. Thank you for the opportunity to be a part of your team. My experience with Genencor was a key stage in the development of my graduate career and will continue to positively influence my future endeavors.

To Mark C. Manning: Thank you for all your contributions to the development of the SIC project. Your support and guidance has greatly influenced the path of my graduate work.

To my committee: Dr. Parkinson, Dr. Bernstein, Dr, Dorhout, Dr. Thompson, Dr. Shores, and Dr. Peersen. Thank you all for your attention, advice, and support.

To my advisor: Dr. Charles Henry. Thank you for allowing me the freedom to explore and develop my chemistry and the guidance to maintain a proper course of work. Really though, thanks for always maintaining an open door and open mind policy towards your group.

DEDICATION

This work is dedicated to my Grandmothers

Rose Valente and Vera "Babci" Zwalinski

TABLE OF CONTENTS

LIST OF FIGURES

LIST OF TABLES

CHAPTER 1

INTRODUCTION

1.1 History and Theory of Self-Interaction Chromatography

1.1.1 The origin of SIC

Affinity chromatography, developed in the 1960s, has been loosely defined as a liquid chromatographic technique that utilizes the selective interactions occurring between a binding agent immobilized on the stationary phase (the affinity ligand) and a complementary mobile phase target (the affinity ligate) to achieve separations.[1] Similarly, bioaffinity chromatography exploits the specificity and reversibility of interactions between biological molecules as a means of purification.[2, 3] Examples of systems commonly studied with bioaffinity chromatography include, but are not limited to, the complexes formed by the interactions of enzymes and substrates, antibodies and antigens, and hormones and receptors.

SIC is a specialized adaptation of bioaffinity chromatography that measures homogenous intermolecular interactions by allowing a mobile phase analyte to interact with a stationary phase to which the same analyte has been covalently immobilized. Chiancone and coworkers are credited with the first report of a SIC

based study.[4] In 1992 these researchers were able to successfully demonstrate the separation of a mobile phase mixture of differentially modified hemoglobin using immobilized $\alpha\beta$ hemoglobin subunit dimers as the stationary phase. Inspired by this pioneering work, Patro et al. applied the principles of SIC for screening protein formulation additives as potential aggregate reducing agents.[5] This work, reported in 1996, greatly aided the emergence of SIC by stressing the technique's sensitivity to weak intermolecular interactions, ease of operation, and high throughput potential. Shortly after, a review by Przybycien highlighted SIC as a credible technique for qualitatively assessing protein-protein interactions for purposes of stabilizing and purifying pharmaceutical formulations.[6] By this time SIC had been used exclusively as a qualitative approach to biological separations and identification of solution additives that suppress aggregate formation. The next logical step was to invoke a quantitative aspect of SIC.

1.1. 2 The Osmotic Second Virial Coefficient (B)

The osmotic pressure (Π) of a thermodynamically ideal solution obeys the Van't Hoff equation (Equation 1.1),

$$\Pi = RT\frac{c}{MW} \tag{1.1}$$

where R is the universal gas constant, T is absolute temperature, and MW and c are the molecular weight and concentration (in mass units) of the solute species, respectively. In reality, dilute protein solutions are far from ideal. Protein

molecules in solution interact with one another due to their considerable size and variable surface charge. A virial expansion of the Van't Hoff equation effectively accounts for these intermolecular interactions that render protein solutions non-ideal (Equation 1.2).

$$\Pi = RTc\left(\frac{1}{MW} + Bc + \ldots\right) \tag{1.2}$$

The osmotic second virial coefficient (B) characterizes two body interactions in protein solutions by reflecting the magnitude and direction of deviation from ideality.[7] At the molecular level, positive B values indicate predominantly repulsive interactions between protein molecules, while negative values reflect predominantly attractive interactions.[8] Three body and higher order interactions make only trivial contributions to the osmotic pressure of protein solutions and have therefore been omitted from Equation 1.2.

The statistical mechanical definition of B, first derived by McMillan and Mayer[9] is defined in Equation 1.3 as

$$B = -\left(\frac{2\pi}{MW^2}\right)\int_0^\infty \left[e^{-W/kT} - 1\right] r_{12}^2 \, dr_{12} \tag{1.3}$$

where k is Boltzmann's constant, r_{12} is the intermolecular center-to-center distance between two interacting molecules, and $W(r_{12})$ is the corresponding

potential of mean force. Statistically, B represents an average over all distances and orientations of two macromolecules in solution, with each configuration weighted by a Boltzmann factor.[10]

Much of the theory used to describe the physics of protein solutions is based on traditional colloidal theories. According to Stigter and Hill, W (r_{12}) reflects the potential of average force acting between two colloidal particles in a solution approaching infinite dilution.[11] This is readily extended to protein solutions in the form of Equation 1.4.

$$W(r_{12}) = W_{HS}(r_{12}) + W_{elec}(r_{12}) + W_{disp}(r_{12}) + W_{osm}(r_{12}) + W_{solv}(r_{12}) \qquad (1.4)$$

Equation 1.4 expresses W (r_{12}) for globular proteins in simple electrolyte solutions as a sum of spherically symmetric potentials.[12] W_{HS} (r_{12}) is the protein hard sphere potential, W_{elec} (r_{12}) is the electric double layer repulsion potential, and W_{disp} (r_{12}) is the Hamaker dispersion potential. These three terms collectively describe Derjaguin-Landau-Verwey-Overbeek (DLVO) theory.[13] Unfortunately, DLVO theory is insufficient to accurately explain very short range effects, such as salt specificity and solvent effects, that are considered crucial aspects of protein crystallization.[14-16] In fact, it has been shown that protein crystallization is primarily governed by such very short range attractive forces.[15, 17] The terms

W_{osm} (r_{12}) and W_{solv} (r_{12}) have therefore been included into Equation 1.4 to respectively account for the excluded volume of electrolytes and short range solvation effects.

In summary, B correlates to physical protein stability, i.e., solubility,[10, 18-20] crystallization,[8, 21] and aggregation[22-24] by explicitly accounting for the same interactions that regulate protein phase behavior.[15, 25] Current applications and views on evaluating protein self-interaction through B, along with technological advances and direct comparison between experimental approaches, are summarized in recent reviews.[26, 27]

1.1.3 B and the Crystallization Slot

George and Wilson published the groundbreaking paper that related B to protein crystallization and demonstrated that B could be used as a rational, quantitative predictor of solution conditions conducive to protein crystal growth.[28] This seminal work utilized static light scattering (SLS) studies to identify the "crystallization slot" as a fairly narrow range of B values (-1×10^{-4} to -8×10^{-4} mol mL/ g^2) that promoted crystallization for nine previously crystallized proteins (Figure 1.1). More negative B values yielded amorphous aggregates or a mixture of aggregates and tiny crystals unfit for structure determination, while more positive B values failed to produce any solid phase at all. The idea of B, a dilute solution parameter, having the capacity to mimic the behavior of protein solutions at saturation[21] was further investigated and verified by a wave of studies

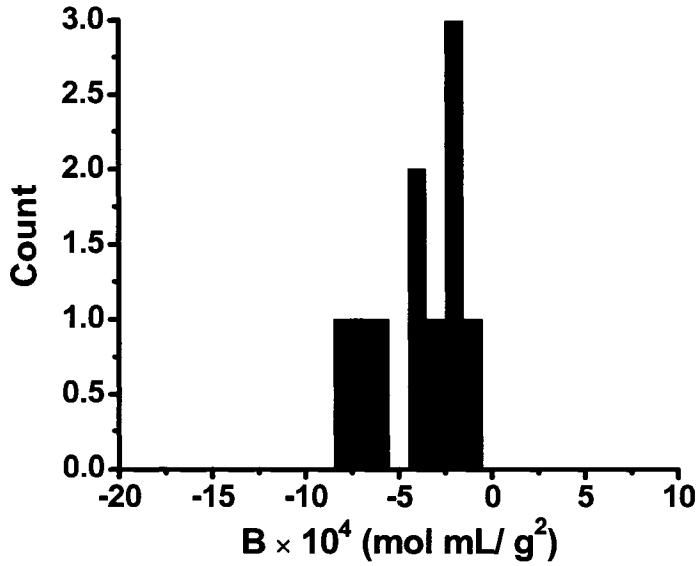

Figure 1.1. The osmotic second virial coefficient (B) crystallization slot (-1×10^{-4} to -8×10^{-4} mol mL/ g^2) for various proteins in crystallizing solvents as reported in *Predicting Protein Crystallization from a Dilute-Solution Property*, George, A.; Wilson, W. W., *Acta Crystallographica Section D-Biological Crystallography* **1994**, 50, 361-365.

following George and Wilson's findings.[15, 18, 29-31] The validity of the crystallization slot and the predictive power of B regarding protein crystallization has since become widely accepted.

1.1.4 B and Solubility

Haas et al. describe the relationship between B and solubility by stating that protein solubility, on the one hand, is determined by the intermolecular binding energy between crystalline protein molecules for very specific orientations and distances, while B, on the other hand, is a statistical average over all orientations and distances of two liquid phase proteins, with each configuration weighted by a Boltzmann factor.[10] Calculation of absolute protein solubility from B is therefore theoretically possible, but remains experimentally difficult due to the need for a pure monocrystalline form of the starting protein.[10] This topic is of great practical interest in the pharmaceutical industry, where development of high concentration formulations is critical to the efficacy of certain peptides and proteins.[32-34] While it is intuitive that enhanced protein self-interaction would lead to reduced solubility, and vice versa, there are relatively few literature reports of such a correlation.[10, 18-20, 25] In general, one finds that positive shifts in B are associated with increased solubility until the solubility reaches a limit (Table 1.1). The literature suggests that this typically occurs as B approaches zero. However, this is still a relatively unexplored area that requires more extensive experimentation prior to forming broad based conclusions.

Table 1.1. Correlation of B with solubility for various proteins from independent studies

Protein	$B \times 10^4$ (ml mol g^{-2})	Solubility (mg/ml)	Temperature (°C)	Reference
Equine Serum Albimin	-1.0	35.7	22	19
	-1.7	15.0	22	19
	-2.4	6.3	22	19
	-4.2	1.6	22	19
Ovalbumin	-0.5	46.4	30	18
	-1.6	31.0	30	18
	-3.3	15.0	30	18
	-4.2	6.9	30	18
	-4.5	3.4	30	18
Lysozyme	-7.5	4.0	25	10
	-4.3	8.0	25	10
	-2.0	24.0	25	10
	0.3	57.0	25	10
Lysozyme	-7.5	2.0	25	20
	-5.2	4.0	25	20
	-3.5	13.0	25	20
	-1.8	24.0	25	20
	-0.2	54.0	25	20

1.1.5 The synergy of B and SIC

In SIC, the protein of interest is immobilized onto a porous stationary phase and packed into a glass, stainless steel, or polymer based column. Interactions between the protein free in the mobile phase and protein immobilized onto the stationary phase are detected as shifts in the retention volume of the mobile phase protein. B values are calculated using the relation from Tessier et al., [35] modified to achieve the appropriate units (Equation 1.5)

$$B = \left(\frac{N_A}{MW^2}\right)\left(B_{HS} - \frac{k'}{\phi\rho}\right) \qquad (1.5)$$

According to Equation 1.5, B can be measured as a function of the protein excluded volume (B_{HS}), the immobilization density (ρ), the phase ratio (ϕ), and the chromatographic capacity factor (k'). Multiplying by Avogadro's' number (N_A) and dividing by the square of the protein's molecular weight (WM) produces B in units of mol mL/ g^2. The immobilization density (ρ) is the number of covalently immobilized protein molecules per unit surface area of the bare chromatographic particles. The phase ratio (ϕ) is the surface area of the protein-modified particles that is available to a mobile phase protein. Dephillips and Lenhoff characterized the protein molecular weight dependence of ϕ for the SIC stationary phase material (Figure 1.2).[36] The chromatographic capacity factor (k') is a direct measure of the strength of interaction of the mobile phase analyte with the stationary phase.[37]

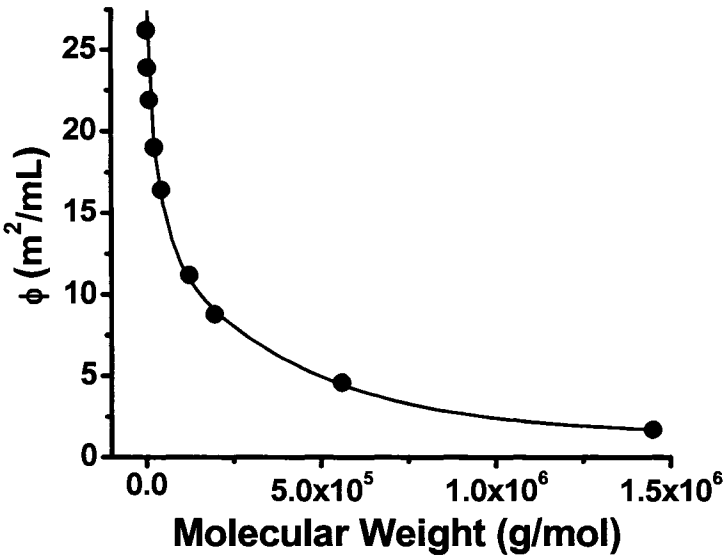

Figure 1.2. The phase ratio (ϕ) of the SIC stationary phase material as a function of protein molecular weight. The line connecting the data points has been added help guide the reader's eyes. The data points were obtained from *Pore Size Distributions of Cation-Exchange Adsorbents Determined by Inverse Size-Exclusion Chromatography*, Dephillips, P.; and Lenhoff, A. M., *J. Chrom. A.*, **2000**, 883, (1-2), 39-54.

$$k' = \frac{V_r - V_o}{V_o} \qquad (1.6)$$

Equation 1.6 characterizes SIC retentions as a function of the volumes required to elute the interacting mobile phase protein (V_r) and a non-interacting species (neutral marker) of equivalent size (V_o). A protein free column (called a dead column) effectively corrects for the size difference between proteins and acetone (the neutral marker used for SIC studies). These dead column experiments use ethanolamine or 3-hydroxypropionic acid capped particles that should have no appreciable interactions with mobile phase analytes. Additionally, all dead column mobile phases contain 5% NaCl to minimize possible nonspecific protein-surface interactions. The ratio of protein and acetone retention volumes in the dead column (V_r'/V_a') is multiplied by the retention volume of acetone in the live column (V_a) to produce a reasonable estimate for the retention volume of a hypothetically non-interacting species equivalent in size to the protein of interest in the "live" protein modified column (V_o).

For the case of globular (i.e. spherical) proteins, the excluded volume (B_{HS}) is defined as the volume of solution that is inaccessible to the center of one protein due to the presence of a second protein.[38] As seen in Equation 1.7,

$$B_{HS} = 4\upsilon_m = \frac{2}{3}\pi d^3 \qquad (1.7)$$

B_{HS} is equivalent to four molecular volumes (V_m) of a single protein. Neal and Lenhoff obtained experimental data demonstrating the relationship in Equation 1.7 (Figure 1.3).[30] Due to the relatively large size of protein molecules, B_{HS} makes a large positive[30] and often dominant[39] contribution to B values.

1.2 Modern Applications of SIC

1.2.1 SIC verses traditional methods of measuring B

The most recognized biophysical method for measuring B is static light scattering (SLS). Unfortunately, widespread application of SLS is lacking due to experimental limitations that include prohibitive quantities of protein, long sample preparation and analysis times, and substantial molecular weight limitations of cosolvents and proteins. For example, large solution additives, such as polyethylene glycols and surfactants make SLS measurements difficult because they scatter too much light. Small peptides, on the other hand, do not scatter enough light for B measurements. Alternative methods such as membrane osmometry,[39-41] analytical ultracentrifugation,[33, 42] and size exclusion chromatography[43] have also been employed for measuring B, but generally suffer from the same draw backs as SLS in terms of extensive sample preparation, consumption, and analysis times, and cannot be operated in a high-throughput screening approach. Comparatively, self-interaction chromatography (SIC) is emerging as an inexpensive, high-throughput method of reliably measuring B of proteins in complex solutions.

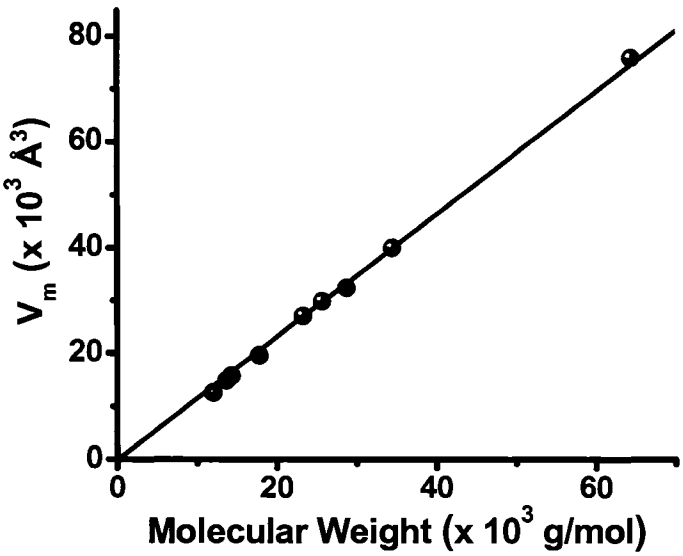

Figure 1.3. Relationship between protein molecular volume (V_m) and molecular weight for use in calculating the protein excluded volume (B_{HS}). The data points were obtained from *Excluded Volume Contribution to the Osmotic Second Virial Coefficient for Proteins*, Neal, B. L.; Lenhoff, A. M., *Aiche Journal*, **1995**, 41, (4), 1010-1014. The linear fit of data points was added (R=0.999).

1.2.2 Protein Crystallization

Tessier et al. were the first to use SIC to quantitatively measure protein-self interaction in terms of B.[35] These researchers were able to quantitatively reproduce SLS data for Lysozyme and Chymotrypsin. More impressive was the fact that the B measurements obtained by SIC required at least an order of magnitude less time and protein than what was required for the corresponding SLS experiments. Continuing on, Tessier et al. used the results of SIC experiments to grow Ribonuclease A crystals under conditions for which B values fell within the crystallization slot.[44] This was the first reported case where SIC measurements of B led to the systematic and successful growth (through ultracentrifugation) of diffraction quality protein crystals. This milestone further demonstrated the synergy of SIC and B as a rapid and rational approach to protein crystallization. In yet another study, Tessier et al. used SIC to characterize bovine serum albumin (BSA) and myoglobin self-interaction as a function of ammonium sulfate (AS).[45] SIC and SLS measurements of B for BSA demonstrated quantitative agreement. The SIC results for myoglobin were even more inspiring. Myoglobin crystals were successfully grown from solutions containing a narrow range of AS concentrations. For each solution condition that promoted the growth of diffraction quality crystals, the SIC measured B values fell within the crystallization slot. As a testament to the significance of these results it should be mentioned that a previous study, which also used AS as a crystallizing agent, was unsuccessful in attempts to grow myoglobin crystals.[46] While these two studies tested slightly different pH values and AS

concentrations, a useful comparison can still be drawn. Myoglobin crystallizes within a very narrow range of AS concentrations. The study that failed to discover the crystallization conditions randomly tested six different concentrations of AS using traditional screening technology. All trials were unsuccessful and offered no feedback as to why. The unsuccessful SIC trials, however, yielded quantitative feedback in terms of B values, which indicated a magnitude and direction of protein-self interaction. In this way Tessier et al. were able to systematically converge on the narrow range of solution conditions suitable for myoglobin crystal growth. [45]

1.2.3 Protein Formulation Development

Modern biotechnology is revolutionizing the use of proteins in pharmaceutical and industrial settings. Recombinant DNA technologies are increasing the economic feasibility of protein production, while efforts in protein engineering and directed evolution are advancing potential applications by enhancing performance and diversity.[47, 48] One area where biotechnology has played a key role is in the production and use of industrial enzymes. The impact of industrial enzymes can be seen in products and processes ranging from food and animal feed to detergents, textiles, fuel alcohol production, and chemical synthesis.[49] As with any protein-based product, enzymes pose physical stability issues (i.e., poor solubility and precipitation) that must be overcome to enable successful purification and formulation.[50] Prolonged physical stability is sometimes achieved in the solid state, but only if the protein is able to survive the stresses of

lyophilization or spray drying. More often, scientists are faced with the challenge of identifying suitable liquid phase conditions for maximum shelf life.[51] In these cases, a variety of cosolvents (also known as excipients when used in pharmaceutical preparations) serve vital roles in regulating and preserving physical protein stability. Common stabilizing cosolvents include classes of molecules such as saccharides, polyols, surfactants, and amino acids. Timasheff and colleagues pioneered the development of preferential interaction parameters and excluded volume effects, greatly improving our understanding of protein-cosolvent-water interactions.[52, 53] Nevertheless, direct measures of cosolvent-induced changes to protein behavior in solution are difficult to obtain and labor-intensive,[54] prompting continued interest in the development of more efficient and reliable characterization approaches. To the best of our knowledge, we have provided the only published accounts of cosolvent induced stabilization of proteins in terms of SIC measured trends in B.[55-57] These accounts are detailed in the following chapters of this thesis.

1.3 References

1) Hage, D. S., Affinity Chromatography. In *Handbook of HPLC*, ed.; Katz, E.; Eksteen, R.; Schoenmakers, P.; Miller, N., 'Ed.'^'Eds.' Dekker, M.: New York, 1998; 'Vol.' 78, 483-498.

2) *Protein Purification by Affinity Chromatography - Derivatizations Ofagarose and Polyacrylamide Beads,* Cuatreca.P, *Journal of Biological Chemistry* **1970,** 245, (12), 3059-&.

3) *Isolation of Antibodies to Protein Hormones by Bioaffinity Chromatography on Divinylsulfonyl Sepharose,* Sairam, M. R.; Porath, J., *Biochemical and Biophysical Research Communications* **1976,** 69, (1), 190-196.

4) *Immobilized Hemoglobin in the Purification of Hemoglobin-Based Oxygen Carriers,* Chiancone, E.; Fronticelli, C.; Gattoni, M.; Urbaitis, B. K.; Bucci, E., *Journal of Chromatography* **1992,** 604, (1), 117-123.

5) *Self-interaction chromatography: A tool for the study of protein-protein interactions in bioprocessing environments,* Patro, S. Y.; Przybycien, T. M., *Biotechnology and Bioengineering* **1996,** 52, (2), 193-203.
6) *Protein-protein interactions as a means of purification,* Przybycien, T. M., *Current Opinion in Biotechnology* **1998,** 9, (2), 164-170.
7) *Molecular origins of osmotic second virial coefficients of proteins,* Neal, B. L.; Asthagiri, D.; Lenhoff, A. M., *Biophysical Journal* **1998,** 75, (5), 2469-2477.
8) *Why is the osmotic second virial coefficient related to protein crystallization?,* Neal, B. L.; Asthagiri, D.; Velev, O. D.; Lenhoff, A. M.; Kaler, E. W., *Journal of Crystal Growth* **1999,** 196, (2-4), 377-387.
9) *The Statistical Thermodynamics of Multicomponent Systems,* McMillan, W. G.; Mayer, J. E., *Journal of Chemical Physics* **1945,** 13, (7), 276-305.
10) *Relation between the solubility of proteins in aqueous solutions and the second virial coefficient of the solution,* Haas, C.; Drenth, J.; Wilson, W. W., *Journal of Physical Chemistry B* **1999,** 103, (14), 2808-2811.
11) *Theory of the Donnan Membrane Equilibrium .2. Calculation of the Osmotic Pressure and of the Salt Distribution in a Donnan System with Highly Charged Colloid Particles,* Stigter, D.; Hill, T. L., *Journal of Physical Chemistry* **1959,** 63, (4), 551-556.
12) *Protein-protein and protein-salt interactions in aqueous protein solutions containing concentrated electrolytes,* Curtis, R. A.; Prausnitz, J. M.; Blanch, H. W., *Biotechnology and Bioengineering* **1998,** 57, (1), 11-21.
13) Verwey, E. J. W.; Overbeek, J. T. G., *Theory of the stability of lyophobic colloids*. ed.; Elsevier: Amsterdam, 2000; 'Vol.' p.
14) *Interactions in protein solutions near crystallisation: a colloid physics approach,* Piazza, R., *Journal of Crystal Growth* **1999,** 196, (2-4), 415-423.
15) *Phase behavior of small attractive colloidal particles,* Rosenbaum, D.; Zamora, P. C.; Zukoski, C. F., *Physical Review Letters* **1996,** 76, (1), 150-153.
16) *Interactions and phase transitions in protein solutions,* Piazza, R., *Current Opinion in Colloid & Interface Science* **2000,** 5, (1-2), 38-43.
17) *Calculation of phase diagrams for aqueous protein solutions,* Curtis, R. A.; Blanch, H. W.; Prausnitz, J. M., *Journal of Physical Chemistry B* **2001,** 105, (12), 2445-2452.
18) *Correlation of second virial coefficients and solubilities useful in protein crystal growth,* Guo, B.; Kao, S.; McDonald, H.; Asanov, A.; Combs, L. L.; Wilson, W. W., *Journal of Crystal Growth* **1999,** 196, (2-4), 424-433.
19) *Correlation between the osmotic second virial coefficient and solubility for equine serum albumin and ovalbumin,* Demoruelle, K.; Guo, B.; Kao, S. M.; McDonald, H. M.; Nikic, D. B.; Holman, S. C.; Wilson, W. W., *Acta Crystallographica Section D-Biological Crystallography* **2002,** 58, 1544-1548.
20) *Correlation between the osmotic second virial coefficient and the solubility of proteins,* Ruppert, S.; Sandler, S. I.; Lenhoff, A. M., *Biotechnology Progress* **2001,** 17, (1), 182-187.
21) *Second virial coefficient as predictor in protein crystal growth,* George, A.; Chiang, Y.; Guo, B.; Arabshahi, A.; Cai, Z.; Wilson, W. W., *Macromolecular Crystallography, Pt A* **1997,** 276, 100-110.

22) *Roles of conformational stability and colloidal stability in the aggregation of recombinant human granulocyte colony-stimulating factor,* Chi, E. Y.; Krishnan, S.; Kendrick, B. S.; Chang, B. S.; Carpenter, J. F.; Randolph, T. W., *Protein Science* **2003,** 12, (5), 903-913.
23) *Estimating the potential refolding yield of recombinant proteins expressed as inclusion bodies,* Ho, J. G. S.; Middelberg, A. P. J., *Biotechnology and Bioengineering* **2004,** 87, (5), 584-592.
24) *The likelihood of aggregation during protein renaturation can be assessed using the second virial coefficient,* Ho, J. G. S.; Middelberg, A. P. J.; Ramage, P.; Kocher, H. P., *Protein Science* **2003,** 12, (4), 708-716.
25) *Protein interactions and phase behavior: Sensitivity to the form of the pair potential,* Rosenbaum, D. F.; Kulkarni, A.; Ramakrishnan, S.; Zukoski, C. F., *Journal of Chemical Physics* **1999,** 111, (21), 9882-9890.
26) *Design of self-interaction chromatography as an analytical tool for predicting protein phase behavior,* Ahamed, T.; Ottens, M.; van Dedem, G. W. K.; van der Wielen, L. A. M., *Journal of Chromatography A* **2005,** 1089, (1-2), 111-124.
27) *Measurements of protein self-association as a guide to crystallization,* Tessier, P. M.; Lenhoff, A. M., *Current Opinion in Biotechnology* **2003,** 14, (5), 512-516.
28) *Predicting Protein Crystallization from a Dilute-Solution Property,* George, A.; Wilson, W. W., *Acta Crystallographica Section D-Biological Crystallography* **1994,** 50, 361-365.
29) *Protein interactions and crystallization,* Rosenbaum, D. F.; Zukoski, C. F., *Journal of Crystal Growth* **1996,** 169, (4), 752-758.
30) *Excluded volume contribution to the osmotic second virial coefficient for proteins (vol 41, pg 1010, 1995),* Neal, B. L.; Lenhoff, A. M., *Aiche Journal* **1996,** 42, (1), 258-258.
31) *Interactions in undersaturated and supersaturated lysozyme solutions: Static and dynamic light scattering results,* Muschol, M.; Rosenberger, F., *Journal of Chemical Physics* **1995,** 103, (24), 10424-10432.
32) *Commercial manufacturing scale formulation and analytical characterization of therapeutic recombinant antibodies,* Harris, R. J.; Shire, S. J.; Winter, C., *Drug Development Research* **2004,** 61, (3), 137-154.
33) *Reversible self-association increases the viscosity of a concentrated monoclonal antibody in aqueous solution,* Liu, J.; Nguyen, M. D. H.; Andya, J. D.; Shire, S. J., *Journal of Pharmaceutical Sciences* **2005,** 94, (9), 1928-1940.
34) *Challenges in the development of high protein concentration formulations,* Shire, S. J.; Shahrokh, Z.; Liu, J., *Journal of Pharmaceutical Sciences* **2004,** 93, (6), 1390-1402.
35) *Rapid measurement of protein osmotic second virial coefficients by self-interaction chromatography,* Tessier, P. M.; Lenhoff, A. M.; Sandler, S. I., *Biophysical Journal* **2002,** 82, (3), 1620-1631.
36) *Pore size distributions of cation-exchange adsorbents determined by inverse size-exclusion chromatography,* DePhillips, P.; Lenhoff, A. M., *Journal of Chromatography A* **2000,** 883, (1-2), 39-54.

37) Weston, A.; Brown, P. R., *HPLC and CE: Principles and Practice*. 1st ed.; Academic Press: San Diego, CA, 1997.
38) *Measurement of Protein Using Bicinchoninic Acid,* Smith, P. K.; Krohn, R. I.; Hermanson, G. T.; Mallia, A. K.; Gartner, F. H.; Provenzano, M. D.; Fujimoto, E. K.; Goeke, N. M.; Olson, B. J.; Klenk, D. C., *Analytical Biochemistry* **1985,** 150, (1), 76-85.
39) *Thermodynamic Properties of Aqueous Alpha-Chymotrypsin Solutions from Membrane Osmometry Measurements,* Haynes, C. A.; Tamura, K.; Korfer, H. R.; Blanch, H. W.; Prausnitz, J. M., *Journal of Physical Chemistry* **1992,** 96, (2), 905-912.
40) *Protein-protein interactions in aqueous ammonium sulfate solutions. Lysozyme and bovine serum albumin (BSA),* Moon, Y. U.; Curtis, R. A.; Anderson, C. O.; Blanch, H. W.; Prausnitz, J. M., *Journal of Solution Chemistry* **2000,** 29, (8), 699-717.
41) *Protein crystallization by design: Chymotrypsinogen without precipitants,* Pjura, P. E.; Lenhoff, A. M.; Leonard, S. A.; Gittis, A. G., *Journal of Molecular Biology* **2000,** 300, (2), 235-239.
42) *Second virial coefficients as a measure of protein-osmolyte interactions,* Weatherly, G. T.; Pielak, G. J., *Protein Science* **2001,** 10, (1), 12-16.
43) *Measurements of protein-protein interactions by size exclusion chromatography,* Bloustine, J.; Berejnov, V.; Fraden, S., *Biophysical Journal* **2003,** 85, (4), 2619-2623.
44) *Predictive crystallization of ribonuclease A via rapid screening of osmotic second virial coefficients,* Tessier, P. M.; Johnson, H. R.; Pazhianur, R.; Berger, B. W.; Prentice, J. L.; Bahnson, B. J.; Sandler, S. I.; Lenhoff, A. M., *Proteins-Structure Function and Genetics* **2003,** 50, (2), 303-311.
45) *Self-interaction chromatography: a novel screening method for rational protein crystallization,* Tessier, P. M.; Vandrey, S. D.; Berger, B. W.; Pazhianur, R.; Sandler, S. I.; Lenhoff, A. M., *Acta Crystallographica Section D-Biological Crystallography* **2002,** 58, 1531-1535.
46) *A comparison of salts for the crystallization of macromolecules,* McPherson, A., *Protein Science* **2001,** 10, (2), 418-422.
47) *Directed evolution of industrial enzymes: an update,* Cherry, J. R.; Fidantsef, A. L., *Current Opinion in Biotechnology* **2003,** 14, (4), 438-443.
48) *Enzyme technology and bioprocess engineering,* Panke, S.; Wubbolts, M. G., *Current Opinion in Biotechnology* **2002,** 13, (2), 111-116.
49) *Industrial enzyme applications,* Kirk, O.; Borchert, T. V.; Fuglsang, C. C., *Current Opinion in Biotechnology* **2002,** 13, (4), 345-351.
50) *Stability of Protein Pharmaceuticals,* Manning, M. C.; Patel, K.; Borchardt, R. T., *Pharmaceutical Research* **1989,** 6, (11), 903-918.
51) *Factors affecting short-term and long-term stabilities of proteins,* Arakawa, T.; Prestrelski, S. J.; Kenney, W. C.; Carpenter, J. F., *Advanced Drug Delivery Reviews* **2001,** 46, (1-3), 307-326.
52) *Control of protein stability and reactions by weakly interacting cosolvents: The simplicity of the complicated,* Timasheff, S. N., *Advances in Protein Chemistry, Vol 51* **1998,** 51, 355-432.

53) *The Control of Protein Stability and Association by Weak-Interactions with Water - How Do Solvents Affect These Processes,* Timasheff, S. N., *Annual Review of Biophysics and Biomolecular Structure* **1993,** 22, 67-97.
54) *Challenges in the analysis of formulated proteins in the presence of excipients,* Advant, S. J.; Komarek, D.; Adams, G.; Zhang, Y. W.; Seetharam, R., *Genetic Engineering News* **1997,** 17, (11), 20-20.
55) *Screening for the physical stability of a Pseudomonas amylase using self-interaction chromatography,* Valente, J. J.; Fryksdale, B. G.; Dale, D. A.; Gaertner, A. L.; Henry, C. S., *Analytical Biochemistry* **2006,** in press.
56) *Colloidal behavior of proteins: Effects of the second virial coefficient on solubility, crystallization and aggregation of proteins in aqueous solution,* Valente, J. J.; Payne, R. W.; Manning, M. C.; Wilson, W. W.; Henry, C. S., *Current Pharmaceutical Biotechnology* **2005,** 6, (6), 427-436.
57) *Second virial coeffcient studies of cosolvent-induced protein self-interaction,* Valente, J. J.; Verma, K. S.; Manning, M. C.; Wilson, W. W.; Henry, C. S., *Biophysical Journal* **2005,** 89, (6), 4211-4218.

CHAPTER 2

SECOND VIRIAL COEFFICIENT STUDIES OF COSOLVENT-INDUCED LYSOZYME SELF-INTERACTION

In the present chapter, SIC was employed to measure B of lysozyme (LYZ) in the presence of various cosolvents, including sucrose, trehalose, mannitol, glycine, arginine, and combinations of arginine and glutamic acid and arginine and sucrose. The primary goal of these studies was to develop a better fundamental understanding of LYZ self-interaction in complex cosolvent systems in terms of cosolvent induced trends in B. All of these cosolvents, alone or in combination, increased B, indicating a reduction in intermolecular attraction. However, the magnitude of cosolvent induced changes in B was found to be largely dependent on the ability to control long-range electrostatic repulsion (accomplished here by the used of NaCl). This study is considered broader than previous investigations because it focuses on the effects of multiple cosolvents on B of a single protein (LYZ). Existing data in the field of cosolvent induced changes in protein stability and solubility primarily comes from thermal denaturation experiments,[1, 2] hydrogen exchange studies,[3] circular dichroism spectra,[4] and surface tension[5] and partial specific volume measurements.[6] Thus, in many cases, direct comparison of our SIC results with published literature values would be difficult.

Nonetheless, SIC data presented in this chapter qualitatively agree with the results obtained by these other methods. Additionally, we have obtained limited static light scattering (SLS) results that validate the accuracy of using SIC to make B measurements of LYZ in complex cosolvent systems. Partial least squares (PLS) analysis contributed to the breadth of our studies by providing response surfaces for visualization of B trends over large amounts of solution parameter space. To the best of our knowledge, this work represented the most comprehensive virial coefficient study to date focusing on complex cosolvent-induced effects on LYZ self-interaction.

2.1Experimental

2.1.1 Stationary Phase Modification

LYZ was immobilized onto AF-Formyl-650M chromatography particles as outlined by Tessier et. al.[7] Briefly, LYZ (8 mg) was dissolved in 1.2 mL of K_2HPO_4 (1.0M, pH 7.0). AF-Formyl 650-M chromatography particles (375 μL) were washed three times with 1.2 ml of the same K_2HPO_4 buffer. The particles and LYZ solution were combined and allowed to settle. Supernatant (20 μL) was removed and diluted to 250 μL for measurement of the initial LYZ concentration by UV absorption at 280 nm using a UV-VIS spectrophotometer (Genesis 10uv, Thermo Spectronic). Sodium cyanoborohydride (15 mg) was added to the remaining LYZ-particle mixture to activate the coupling reaction. The reaction vial was then put in a room temperature rotary mixer for ~80 min, after which, a final UV measurement was taken exactly as described above. The remaining LYZ

was removed by washing the particles with 2.4 mL of K_2HPO_4 (1.0M, pH 7.0) containing 5% (w/v) NaCl. The particles were then washed with the original K_2HPO_4 buffer and placed back in the rotary mixer, along with 1.2 mL of ethanolamine (1.0 M, pH 8.0) and 10 mg sodium cyanoborohydride to cap any unreacted Formyl groups. Finally, the particles were washed with acetic acid (ACTE) (0.1 M, pH 4.5) and stored at 4°C. Ethanolamine capped AF-Formyl-650M particles (used for the dead column) were prepared according to the final step of the coupling procedure described above.

2.1.2 Self-Interaction Chromatography (SIC)

All buffers were prepared with 18 MΩ water (Nanopure, Barnstead) and the pH adjusted with either NaOH or HCl. Solution pH was followed using a digital pH meter (UB-5, Denver Instruments). All mobile phases were buffered with ACTE (0.1M, pH 4.5), except for the results in Figure 2.5 where the buffer pH was increased to 6.0. LYZ and acetone injection samples were dissolved at 15 mg/mL and 2% (v/v), respectively. The SIC column consisted of fluorinated ethylene propylene (FEP) Teflon Tubing (1/8" outer diameter, 1/16" inner diameter, Upchurch) fitted with a stainless steel frit (2 um pores, Upchurch). The column was conditioned after packing for several hours with ACTE (0.1M, pH 4.5) at 0.15 mL/min, after which, no further bed settling was observed. Generally, for all experiments where the mobile phases incrementally increased in cosolvent concentrations, two buffers were used. One buffer with no cosolvent and a second with the maximum cosolvent concentration were mixed by the HPLC

pump to achieve the entire range of desired conditions. Dead column experiments utilized identical mobile phase conditions with one exception, 5% NaCl was added to all mobile phases to suppress electrostatic interactions between mobile phase analytes and the ethanolamine capped stationary phase.

All chromatographic data were collected on a Hewlett Packard 1050 HPLC and analyzed using Chemstation software. Mobile phases were mixed and degassed online. Sample volumes of 1.0 μL were injected using a Hewlett Packard 1050 autosampler and analyzed at a flow rate of 80 μL/min. Temperatures were controlled with a digital column heater (TC-50, Eppendorf). Eluting samples were detected by UV absorption at 280nm. To ensure reproducibility, LYZ samples were run in quadruplicate, and acetone samples in triplicate. The sample chromatograms in Figure 2.1 demonstrate the sensitivity of the LYZ peak shape to changes in solution conditions, i.e., LYZ retention times increase and the peaks broaden as LYZ self-interaction becomes increasingly attractive. By contrast, the ACE peak shape is unaffected by changes in solution conditions, indicating its suitability as a neutral marker. In all cases, retention times were recorded at the maximum peak height. The methods for B calculations, as well as the relevant assumptions and uncertainties associated with SIC measurements of B values, are discussed in detail elsewhere.[7]

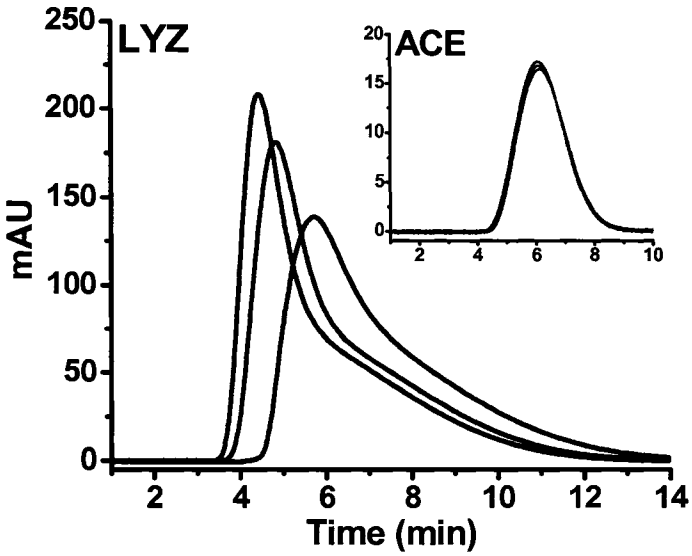

Figure 2.1. LYZ (main) and ACE (inset) elution profiles at 25°C as a function of NaCl in 0.1M ACTE, pH 4.5: 0% (w/v) NaCl (black line), 2% (w/v) NaCl (red line), 5% (w/v) NaCl (green line).

2.1.3 Static Light Scattering (SLS)

Sodium acetate buffers containing 5% (w/v) NaCl and varying cosolvent concentrations were prepared by adding 6.0 g of glacial acetic acid, 50.0 g of NaCl and the appropriate amount of excipient to ~ 900 ml of deionized water, titrating to pH 4.5 with NaOH (0.1 M) and filling with DI water to a 1.0 L mark. Lysozyme stock solutions were prepared in the desired buffer solutions at concentrations ranging from about 2-7 mg/ml, depending on the solubility of the protein. The stock solutions were filtered using 0.22 μm Millex Millipore filters. Protein concentrations were determined spectrophotometrically using ε (1%, 1cm, 280nm) = 26.3.

SLS measurements for obtaining the second virial coefficient, B, were performed using a DAWN F laser photometer from WYATT Technology. The SLS method requires that the intensity of light scattered by a protein solution be measured as a function of protein concentration. Typically, 4-5 dilutions of a particular protein stock were prepared and filtered directly into the DAWN F scattering cell. The incident light source was a vertically polarized, 5mW He-Ne laser with wavelength of 633 nm. Relative scattering intensities in excess of background (solvent, stray light) were converted to absolute scattering intensities (R_{90}) by calibrating the instrument response using toluene as the calibration standard (R_{90} = 14.06 e-6 cm^{-1} at 633 nm).

SLS data was analyzed based on the working equation (Equation 2.1) given by Kratochvil.[8]

$$\frac{Kc}{R_{90}} = \frac{1}{M} + 2Bc + \ldots \qquad (2.1)$$

where K is an optical constant given by Equation 2.2:

$$K = \frac{4\pi^2 n_0^2 (dn/dc)^2}{N_A \lambda^4} \qquad (2.2)$$

and n_0 is the refractive index of the solvent, N_A is Avogadro's number, λ is the wavelength of the incident light, dn/dc is called the refractive index increment for the protein-solvent pair and R_{90} is the excess Rayleigh factor at a scattering angle of 90° (cm^{-1}) measured as a function of protein concentration. As Equation 2.1 suggests, plotting Kc/R_{90} versus c yields the second virial coefficient, B, from the slope of the plot. Our colleagues Kusum S. Verma and William W. Wilson at Mississippi State University kindly performed all SLS experiments.

2.1.4 Partial least Squares (PLS) analysis

Much of the B data obtained during the LYZ-SIC experiments were cross-analyzed using a multivariate statistical method known as Partial Least Squares (PLS). The theoretical framework for this type of data analysis is described in detail elsewhere.[9, 10] Generally speaking, for any large matrix of values, where

there are a reasonable number of samples (together forming the so-called X-matrix), mathematical models can be constructed that explain the largest amount of variance in the dependent variable(s) of interest (the Y-matrix). The best single description of the relationship between the variation in the X-matrix and the endpoint (the Y matrix) is called the first principal component (PC1). The next important component (in terms of describing the variance in the Y-matrix) is called the second principal component (PC2). This line of rezoning can be extended to higher order PCs as needed. Quite often, only one or two PCs are required to explain most of the variance in the Y-matrix. Each of these PCs contains some contribution from each of the variables in the X-matrix. If a variable within the X-matrix contributes heavily to the construction of a given PC, then it is ranked as being significant. In fact, regression coefficients can be calculated for each variable in the X-matrix for a given model, where a model is the composite of a certain number of PCs in order to provide an adequate description of the Y-matrix. In summary, PLS takes information from the X-matrix, calculates the desired number of PCs, and constructs a suitable model. The overall coefficient of determination (r^2) indicates the quality of the model. Our colleague Mark C. Manning kindly provided all PLS analysis.

2.2 Results and Discussion: Cosolvent induced trends in B of LYZ

2.2.1. Comparing SIC to SLS: NaCl induced trends in B

Demonstrating the ability to reproduce SLS results was a critical aspect of validating the accuracy of SIC measured B values. The logical choice for such a

task was a system of LYZ in NaCl solutions, largely because this system has been very well characterized and documented in the literature.[11, 12] Generally speaking, salts affect both protein structure and solubility to various degrees.[13] For most proteins, B is steadily decreased by the concentration dependent electrostatic shielding effects of salts.[11, 14-16] This behavior corresponds to reductions in protein solubility, as discussed in previously published works.[17-20] At higher salt concentrations (>1.0 M), there is often a non-monotonic relationship,[21, 22] as excluded volume effects, solution nonideality, and direct ion binding effects begin to manifest themselves. This can cause an increase in B, but usually only at salt concentrations well above 1.0 M and only in relatively few cases.[23]

In the case of LYZ and NaCl, the salt ions interact strongly with water molecules, shielding long-range electrostatic repulsion and enhancing attractive hydrophobic effects[11]. The result is a reduction in LYZ solubility that corresponds to the decreasing trend in B seen in Figure 2.2. Our SIC results indicate that B shifts from $3.43 \pm 0.38 \times 10^{-4}$ at 0% (w/v) NaCl to $-6.50 \pm 0.04 \times 10^{-4}$ mol mL/g^2 at 5% (w/v) NaCl. Clearly, these results are in excellent quantitative agreement with those obtained from several independent SLS studies.[19, 24, 25] The line at B = 0 mol mL/g^2 (indicating a condition where there is no net attraction or repulsion between LYZ molecules) has been included as a visual aid, showing that B goes from positive to negative, reflecting a shift from repulsive to attractive intermolecular interactions. The correlation between data sets obtained by SIC

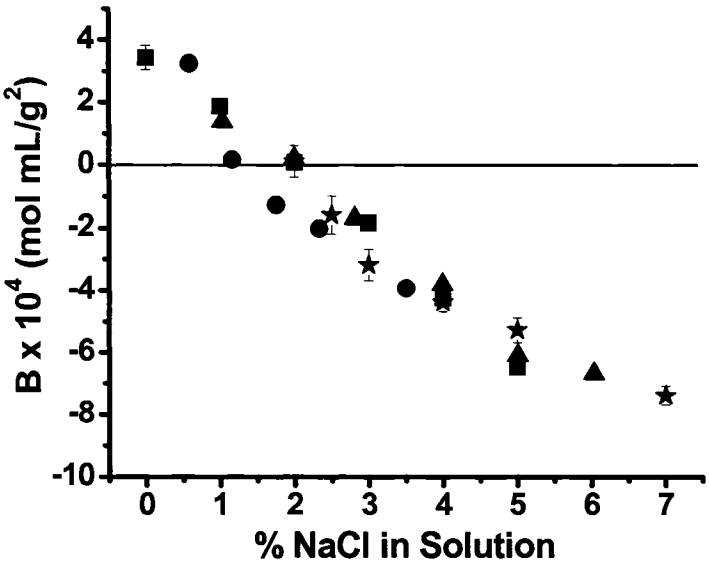

Figure 2.2. B values of LYZ at 25°C as a function of NaCl (w/v), measured by SIC (black squares, 0.1M ACTE, pH 4.5) and several independent SLS studies; (blue stars, 0.1M acetate, pH 4.2),[19] (red triangles, 0.1M ACTE, pH 4.2),[25] and (green circles, 0.04M ACTE, pH 4.6).[24]

and SLS strengthens the validity of the SIC approach. This experiment can also be employed as a control to evaluate the stability of a SIC column. Typically, lysozyme-SIC columns lasted for several weeks.

2.2.2 Saccharides and Polyols

The disaccharides sucrose and trehalose and the polyol mannitol are naturally occurring osmolytes that have long been known to stabilize protein structure.[26-28] Mechanistically, these cosolvents preferably interact with water,[29] migrating away from the protein surface, creating an excluded volume that is proportional to the protein's solvent exposed surface area.[6] Thus, in the presence of these cosolvents, proteins favor a more compact, native-like state.[3] Figure 2.3 shows the results of our SIC measurements of LYZ B trends in the presence of sucrose, trehalose, and mannitol. Interestingly, we found that the measured effects of these cosolvents were significantly dependent on the total solution ionic strength. When 2% (w/v) NaCl was added to all mobile phases, the subsequent addition of the sugar and polyol-based cosolvents had little effect on B, indicating no cosolvent-induced changes in protein self-interaction. For example, in the presence of 2% (w/v) NaCl, the B value for LYZ changed from $0.10 \pm 0.04 \times 10^{-4}$ at 0.0 M sucrose to $0.87 \pm 0.09 \times 10^{-4}$ mol mL/g^2 at 0.5 M sucrose and from 0.73 $\pm 0.29 \times 10^{-4}$ at 0.0 M mannitol to $1.03 \pm 0.19 \times 10^{-4}$ mol mL/g^2 at 0.2 M mannitol. On the other hand, addition of the cosolvents to a 5% (w/v) NaCl solution clearly reduced the magnitude of attraction between LYZ molecules. Here, the B value

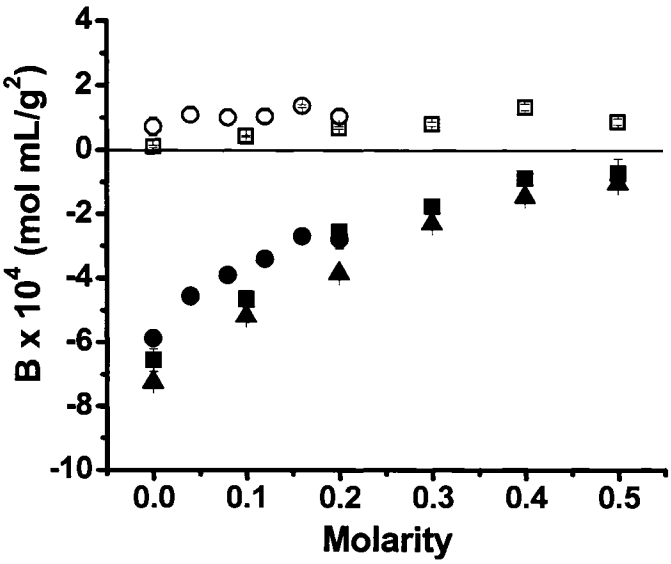

Figure 2.3. B values of LYZ at 25°C as a function of sucrose (black squares), mannitol (green circles), and trehalose (red triangles). Solution conditions: ACTE (0.1 M, pH 4.5) and 2% (w/v) NaCl (open symbols) or 5% (w/v) NaCl (closed symbols).

for LYZ changed from -6.56 ± 0.35 $\times 10^{-4}$ at 0.0 M sucrose to -0.72 ± 0.43 $\times$ 10^{-4}

mol mL/g^2 at 0.5 M sucrose, from -7.25 ± 0.11 × 10^{-4} at 0.0 M trehalose to -1.05 ± 0.06 × 10^{-4} mol mL/g^2 at 0.5 M trehalose, and from -5.89 ± 0.15 × 10^{-4} at 0.0 M mannitol to -2.81 ± 0.28 × 10^{-4} mol mL/g^2 at 0.2 M mannitol. It appears that in the presence of 2% (w/v) NaCl protein self-interaction is still being dominated by long-range electrostatics, as B values for LYZ in 2% (w/v) NaCl, pH 4.5 are slightly positive (between 0.10 ± 0.04 × 10^{-4} and 0.73 ± 0.29 × 10^{-4} mol mL/g^2), indicating weakly repulsive interactions. Increasing the NaCl concentration to 5% (w/v) lowers B to negative values (between -5.89 × 10^{-4} and -7.25 × 10^{-4} mol mL/g^2) where long-range electrostatic repulsions are fully suppressed and protein self-interaction becomes sufficiently attractive to result in self-association. To verify the accuracy of our results with respect to measuring B in the presence of saccharides and polyols, SLS experiments were performed. Table 2.1 compares B obtained by SIC and SLS for sucrose, trehalose, and mannitol. Cosolvent induced trends in B are the same for both techniques and the values between the two methods generally agree. Some variation is expected because the protein used for SLS was obtained from a different lot than the protein used for SIC. Our colleague, Dr. William Wilson, has seen as much as 25% variation between initial B values for different protein lot numbers from the same supplier.

Protein self-association is largely driven by the formation of short range, non-covalent contacts, such as the coalescence of hydrophobic surface patches between individual molecules.[30] This is one of the major ways that proteins reduce their thermodynamically unfavorable excluded volume and solvent

Table 2.1. Comparison of lysozyme osmotic second virial coefficients (B) measured by self-interaction chromatography (SIC) and static light scattering (SLS).

Cosolvent , molarity		$B \times 10^4$ (mol mL/g^2) SIC	SLS
Sucrose[†]			
	0.2	-2.56 ± 0.09	-3.5 ± 0.3
	0.3	-1.76 ± 0.05	-2.9 ± 0.6
	0.5	-0.72 ± 0.44	0.7 ± 0.8
Trehalose[†]			
	0.1	-5.19 ± 0.14	-5.80 ± 0.05
	0.2	-3.86 ± 0.12	-4.29 ± 0.06
Mannitol[†]			
	0.04	-4.57 ± 0.22	-
	0.05	-	-6.63 ± 0.35
	0.20	-2.81 ± 0.28	-2.92 ± 2.20

[†] all cosolvents were added to solution conditions of ACTE (0.1M, pH 4.5) containing 5% (w/v) NaCl at 25°C.

exposed surface area. The other major route involves intramolecular contractions of individual molecules. Notably, it has previously been reported that saccharides[3, 31] and polyols[32] influence the conformational dynamics of proteins, favoring the most compact conformation within the native-state ensemble. This reduction of protein volume is accompanied by a concomitant reduction in the hydrophobicity of the protein surface, thus reducing the tendency for self-association. The SIC results in Figure 2.3 show that once long-range electrostatics have been minimized, the addition of saccharides or polyols significantly reduces LYZ self-interaction, resulting in shifts towards more positive B.

It is important to stress that the effects of structure stabilizing cosolvents are independent of ionic strength.[4, 33] Rather, the conferred stabilization is a result of short-range excluded volume and/or hydrophobic effects, which necessarily influence conformational changes that alter a protein's solvent exposed surface area. Strong electrostatic repulsion may keep proteins sufficiently far apart such that intermolecular interactions are unaffected. Thus, at low ionic strengths and pH values far from the isoelectric point, B measurements may be similarly unaffected by the addition of these cosolvents. Conversely, at high ionic strengths where electrostatic repulsion is minimized, intermolecular distances can be reduced to the range where cosolvent-induced stabilization is reflected in the measured B trends.

2.2.3 Amino acids

Glycine and arginine are two of the most well studied amino acid cosolvents. Glycine is a naturally occurring, preferentially excluded structure stabilizer[2, 34, 35]. Conversely, the guanadinium group of arginine is believed to favorably interact with aromatic side chains,[36-38] making it a valuable aggregation suppressor, but an inefficient protein structure stabilizer. The concentration dependent effects of arginine and glycine on B are shown in Figure 2.4. The same ionic strength dependence is observed as before. For example, in the presence of 2% (w/v) NaCl, the B value for LYZ changed from $1.04 \pm 0.48 \times 10^{-4}$ at 0.0 M arginine to $0.94 \pm 0.19 \times 10^{-4}$ mol mL/g^2 at 0.1 M arginine and from $0.20 \pm 0.24 \times 10^{-4}$ at 0.0 M glycine to $0.54 \pm 0.14 \times 10^{-4}$ mol mL/g^2 at 0.1 M glycine. In the presence of 5% (w/v) NaCl, the B value for LYZ changed from $-5.97 \pm 0.05 \times 10^{-4}$ at 0.0 M arginine to $-3.11 \pm 0.31 \times 10^{-4}$ at 0.1 M arginine and from $-6.51 \pm 0.33 \times 10^{-4}$ at 0.0 M glycine to $-5.45 \pm 0.11 \times 10^{-4}$ at 0.1 M glycine. From these data it becomes clear that 0.1 M arginine has a much greater impact on B than an equivalent concentration of glycine. The increase in B as a function of arginine (from -5.97×10^{-4} at 0.0 M arginine and 5% (w/v) NaCl to -3.11×10^{-4} mol mL/g^2 at 0.1 M arginine and 5% (w/v) NaCl) signifies a reduction in LYZ self-interaction. These data are consistent with a SLS study reporting that the addition of 0.5 M arginine to the renaturation buffer significantly increases B (from $1.71 \pm 0.76 \times 10^{-3}$ mol mL/g^2 at 0.0 M arginine in a buffer containing GdnHCl (1.25 M), GSSG (6 mM), DTT (5mM), 50mM Tris, pH 8.0 to $4.76 \pm 1.02\ 10^{-3}$ mol mL/g^2 at 0.5 M arginine in the same buffer), thereby suppressing LYZ aggregation.[21]

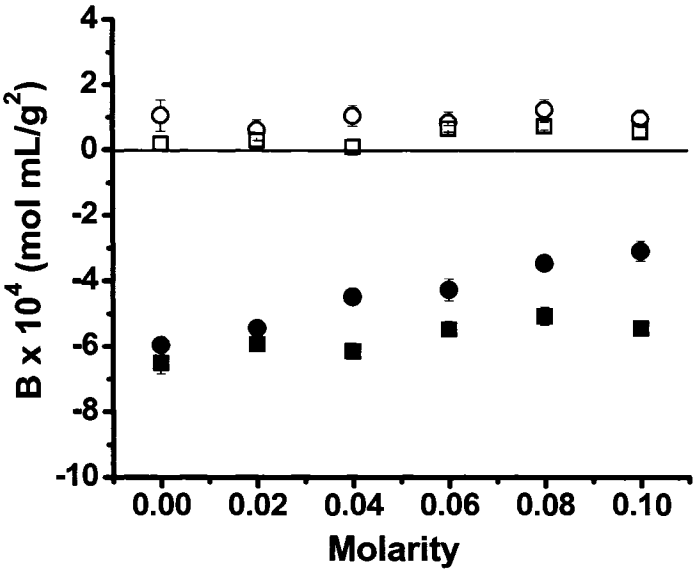

Figure 2.4. B values of LYZ at 25°C as a function of arginine (black circles) and glycine (red squares). Solution conditions: ACTE (0.1 M, pH 4.5) and 2% (w/v) NaCl (open symbols) or 5% (w/v) NaCl (closed symbols).

On the other hand, there is only a marginal increase in B as a function of glycine (from 0.20 ± 0.24 × 10^{-4} at 0.0 M glycine to 0.54 ± 0.14 × 10^{-4} mol mL/g^2 at 0.1 M glycine in the presence of 2% (w/v) NaCl and from -6.51 ± 0.33 × 10^{-4} at 0.0 M glycine to -5.45 ± 0.11 × 10^{-4} mol mL/g^2 at 0.1 M glycine in the presence of 5% (w/v) NaCl). Previous investigators found that glycine was effective at stabilizing LYZ against thermal denaturation using CD spectroscopy.[34, 35] It is quite possible that glycine could stabilize individual protein structure without affecting intermolecular interactions. The commonality between the previous cosolvents that have been shown to increase B is that they all in some way reduce attractive hydrophobic effects, either by direct interactions with surface hydrophobic patches (as with arginine [39]) or by influencing proteins to intramolecularly bury such patches (as with saccharides[3, 31] and polyols[32]). It has previously been reported that glycine does not significantly affect the native structure of LYZ, providing stabilization only against thermal denaturation (unfolding).[2] This is consistent with the observation that glycine is less effective at altering B, and thus, LYZ self-interaction (Figure 2.4).

2.2.4 Mixed cosolvents

Combined effects of two amino acids (arginine and glutamic acid) and a saccharide and amino acid (sucrose and arginine) on B were also investigated. In the presence of 5% (w/v) NaCl, increasing equimolar amounts of arginine and glutamic acid, up to a combined concentration of 0.2 M, shifted B by 5.99 ± 0.49 × 10^{-4} mol mL/g^2 (from -1.41 ± 0.41 × 10^{-3} at 0.0 M arginine + glutamic acid to

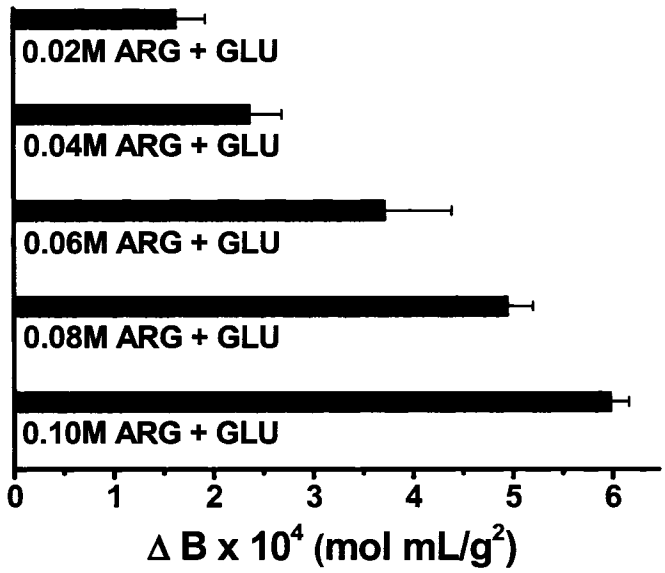

Figure 2.5. Changes in LYZ B values at 25°C as a function of equimolar amounts of arginine (ARG) and glutamic acid (GLU) added to solutions of ACTE (0.1 M, pH 6.0) containing 5 % (w/v) NaCl.

-8.13 ± 0.29 × 10^{-4} mol mL/g^2 at 0.2 M arginine + glutamic acid) (Figure 2.5). In these experiments, the initial solution conditions, representing $\Delta B = 0$, were ACTE (0.1 M, pH 6.0) containing 5 % (w/v) NaCl at 25°C.

On a per-mole basis, the combination of arginine and glutamic acid was more effective at reducing LYZ self-interaction than any single cosolvent used in this study. These data support previous findings that the simultaneous addition of arginine and glutamic acid dramatically increases protein solubility and long-term stability up to eight fold.[40] Noting that they were working with poorly soluble proteins, these same researchers speculated that the charged and aliphatic portions of arginine and glutamic acid were favorably interacting with oppositely charged and hydrophobic portions of the protein surface, respectively. Another study, using LYZ in solution conditions more comparable to ours, reported that the affinity of charged amino acids for oppositely charged groups on the protein surface is enhanced as electrostatic repulsions are minimized.[5] Drawing from these suggestions, we speculate that our data in Figure 2.5 support the theory that both arginine and glutamic acid are masking hydrophobic surface patches, thus stabilizing LYZ against self-association.

Arginine and sucrose were combined to determine the impact of two different types of cosolvents on B (Figure 2.6). The complexity of this particular two cosolvent system is compounded by the very different nature of their preferential interactions with LYZ. Sucrose stabilizes compact native conformations[3, 31] and

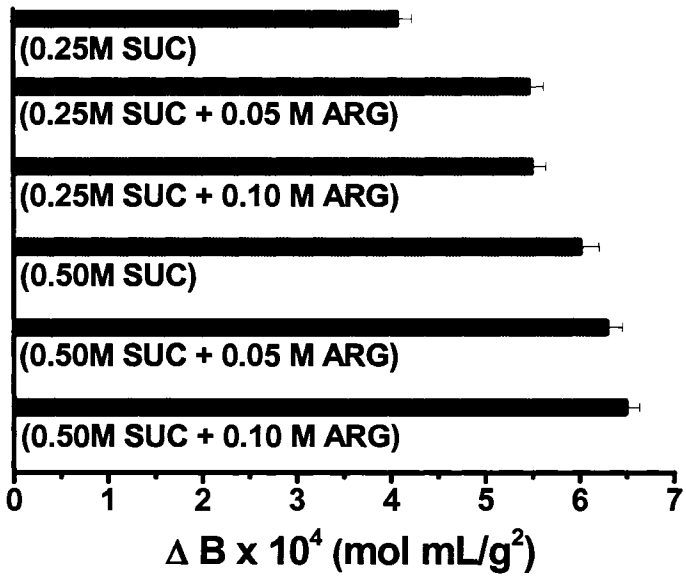

Figure 2.6. Changes in LYZ B values at 25°C as a function of arginine (ARG) and sucrose (SUC) added to solutions of ACTE (0.1 M, pH 4.5) containing 5 % (w/v) NaCl.

arginine suppresses aggregation.[36-38] The former is preferentially excluded from the protein surface and the latter displays weak binding. The link between the two is that they both decrease LYZ self-interaction by reducing attractive hydrophobic effects. These ideas are key to interpreting the data in Figure 2.6, which show a combined but not completely additive effect of arginine and sucrose on B. First consider the individual effects of sucrose on LYZ structure. It has been shown that the tendency towards more compact conformations and reduced surface hydrophobicity is proportional to sucrose concentration.[3] Consistently, SIC data indicate that higher concentrations of sucrose yield larger increases in B (Figure 2.4 and 2.6). Meanwhile, arginine is small enough to penetrate the sucrose-excluded volume and interact with LYZ. However, the degree of this interaction depends on the presence of hydrophobic side chains on the surface of LYZ, which is now proportional to the sucrose concentration. This would explain why the addition of 0.05 M arginine to a solution of 0.25 M sucrose and 5% (w/v) NaCl shifted B from $4.07 \pm 0.16 \times 10^{-4}$ to $5.46 \pm 0.16 \times 10^{-4}$ (a change of $1.39 \pm 0.23 \times 10^{-4}$ mol mL/g^2) while the addition of the same amount of arginine to a solution of 0.50 M sucrose and 5% (w/v) NaCl shifted B from $6.00 \pm 0.21 \times 10^{-4}$ to $6.28 \pm 0.17 \times 10^{-4}$ (a change of only $0.28 \pm 0.27 \times 10^{-4}$ mol mL/g^2). Furthermore, increasing the concentration of arginine from 0.05 M to 0.10 M shifted B by only $0.03 \pm 0.23 \times 10^{-4}$ in the presence of 0.25 M sucrose and only $0.20 \pm 0.23 \times 10^{-4}$ mol mL/g^2 in the presence of 0.50 M sucrose. These data suggest that there is a reduction in the number of hydrophobic patches on the protein surface, which can thus be saturated by low concentrations of arginine.

2.2.5 PLS analysis of B data from LYZ-SIC studies

Table 2.2 lists the solution parameter space investigated in the LYZ-SIC studies. A quadratic PLS model of this data was used to correlate the solution composition to B with a correlation coefficient (after full cross validation) of 0.964 (Figure 2.7). Response surfaces generated from this model are particularly useful (much more so than a tabular format) for visualizing the effects of any two formulation variables on B. For example, the response surface for combinations of NaCl and arginine is shown in Figure 2.8. Here, B becomes markedly more negative due to the electrostatic shielding afforded by the addition of up to 5% NaCl. In the presence of only 2% NaCl, the addition of up to 0.10 M arginine has little effect on B, as LYZ self-interaction is still dominated by long range electrostatics. Increasing the NaCl concentration to 5% substantially suppresses electrostatics such that the addition of 0.10 M arginine effectively shifts B to more positive values. This behavior is echoed Figure 2.9 where the strength of the trehalose induced trend in B increases with NaCl concentration. In Figure 2.10 the NaCl concentration was held at a constant 5% while the concentration of arginine and sucrose were varied. The response surface shows that the sensitivity of B to arginine was reduced as the concentration of sucrose was increased. Conversely, the dependence of sucrose induced trends in B was much less affected by changes in arginine concentration. Together the response surfaces in Figures 2.8-2.10 support the corresponding experimental SIC data and offer a more visually impressive way of interpreting trends in B of LYZ for large amounts of solution parameter space.

Table 2.2. The Effect of various cosolvents on B of lysozyme at 25°C. Solution conditions were ACTE (0.1 M, pH 4.50) (clear cells) or ACTE (0.1 M, pH 6.0) (yellow cells).

NaCl (%,w/v)	Sucrose (%,w/v)	Trehalose (%,w/v)	Mannitol (%,w/v)	Glycine (%,w/v)	Arginine (%,w/v)	Glutamic Acid (%,w/v)	B x 10^4 (mL mol g^{-2})
5	0.2	0	0	0	0	0	-2.56
5	0.3	0	0	0	0	0	-1.76
5	0.5	0	0	0	0	0	-0.72
5	0	0.1	0	0	0	0	-5.19
5	0	0.2	0	0	0	0	-3.86
5	0	0	0.04	0	0	0	-4.57
5	0	0	0.2	0	0	0	-2.81
5	0	0	0	0	0	0	-6
5	0	0	0	0	0.04	0	-4.4
5	0	0	0	0	0.1	0	-3.1
5	0	0	0	0.1	0	0	-5.3
2	0	0	0	0	0.04	0	1.1
2	0	0	0	0	0.1	0	1.1
2	0	0	0	0.04	0	0	0.2
2	0	0	0	0.1	0	0	0.7
5	0	0	0	0	0	0	-5.9
5	0	0	0	0	0	0	-6.5
5	0	0	0	0	0.02	0.02	-4.3
5	0	0	0	0	0.04	0.04	-3.7
5	0	0	0	0	0.1	0.1	-0.1
5	0.25	0	0	0	0	0	-1.9
5	0.25	0	0	0	0.05	0	-0.05
5	0.25	0	0	0	0.1	0	-0.05
5	0.5	0	0	0	0	0	0.1
5	0.5	0	0	0	0.05	0	0.3
5	0.5	0	0	0	0.1	0	0.5
2	0	0	0	0	0	0	0.2
2	0	0	0	0	0	0	1
2	0	0	0	0	0	0	0.1
2	0	0	0	0	0	0	0.7

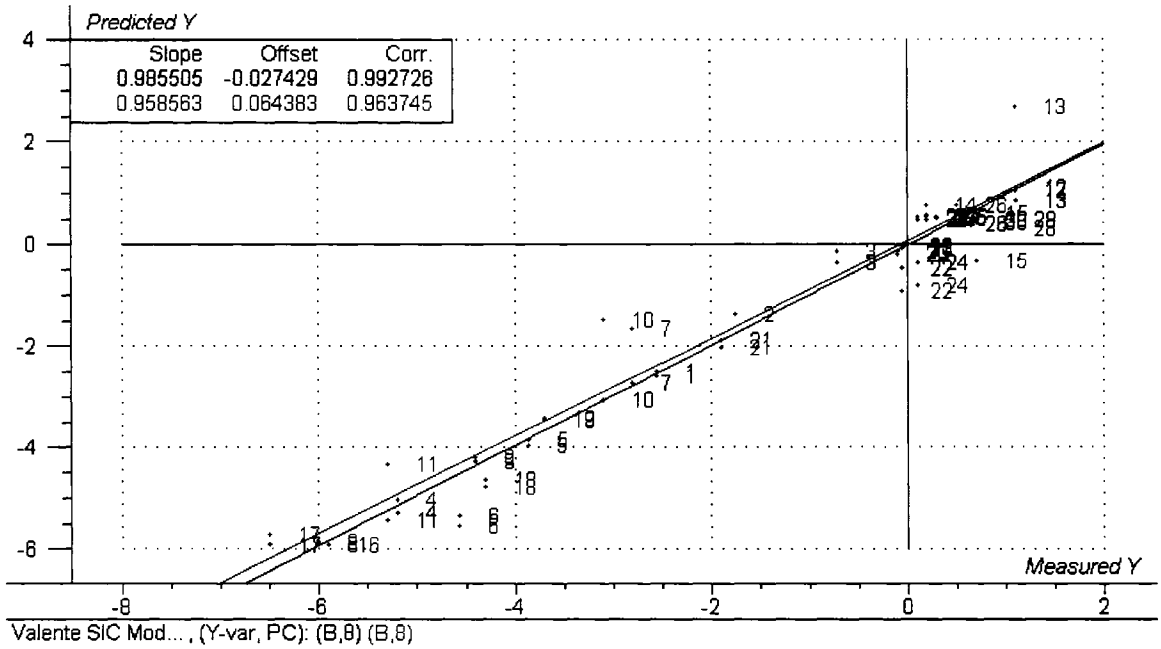

Figure 2.7. Predicted vs.SIC measured B values for a PLS model using the data in Table 2.2.

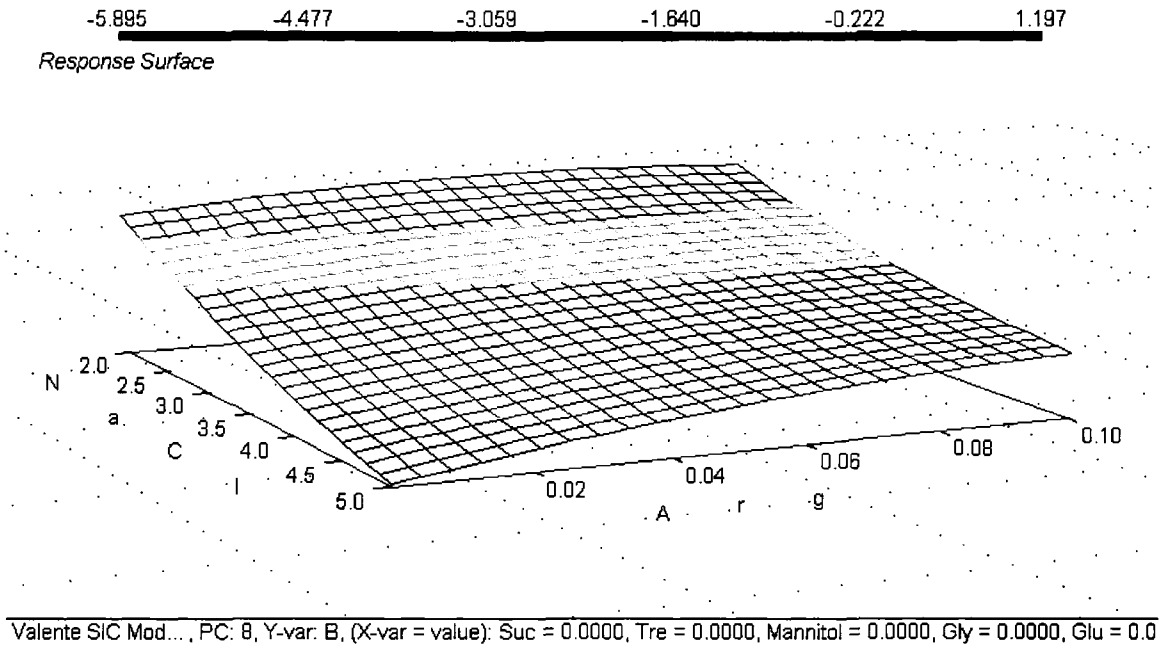

Figure 2.8. Response surface for NaCl and arginine from the PLS model of data in Table 2.2.

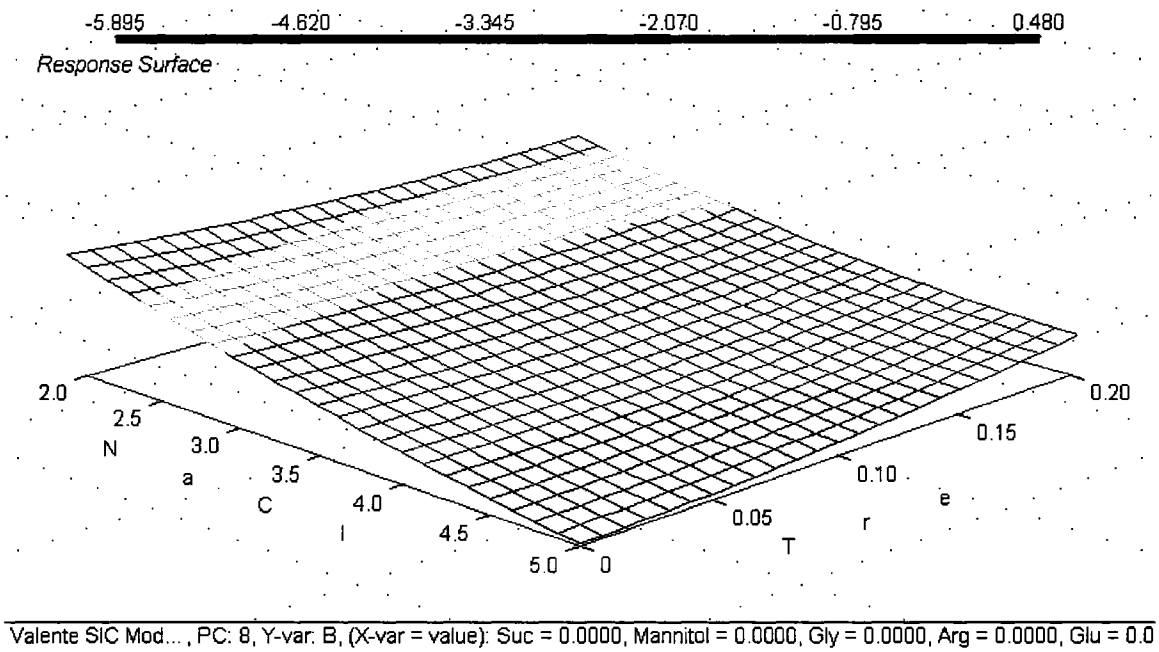

Figure 2.9. Response surface for NaCl and trehalose from the PLS model of data in Table 2.2.

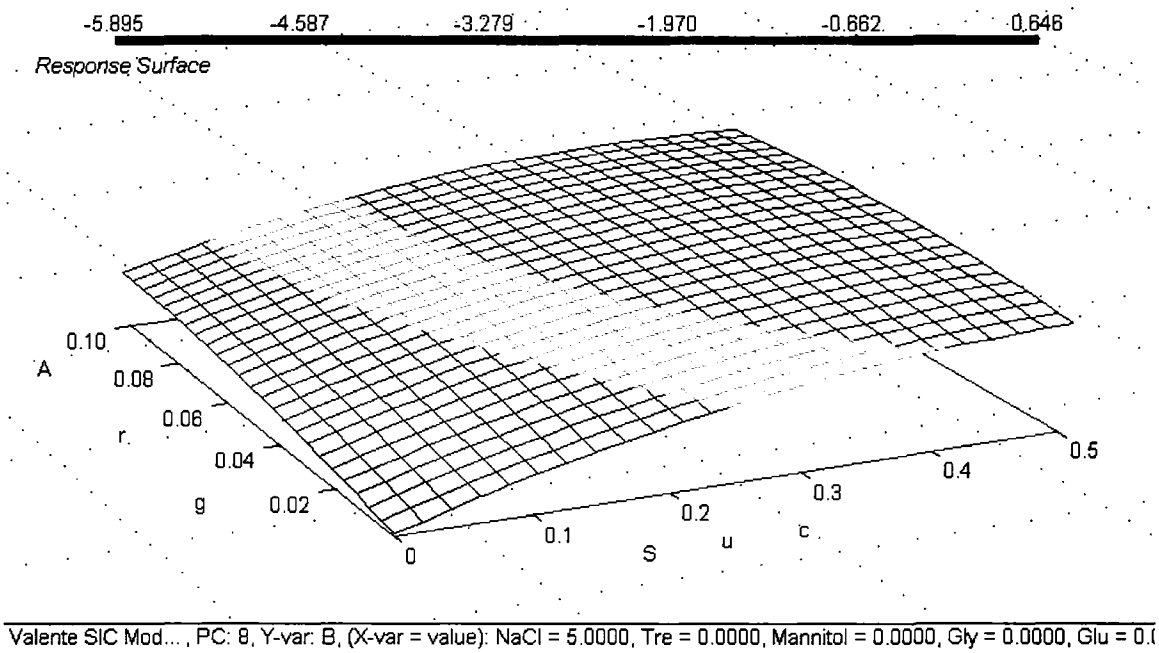

Figure 2.10. Response surface for sucrose and arginine from the PLS model of data in Table 2.2. For this surface, the NaCl concentration was set to 5%.

2.2.6 Temperature dependence of B

Introducing temperature as another solution variable served as one more incremental step towards increasing the complexity of the LYZ-SIC studies. This represented our first attempt to run SIC under variable temperature conditions. We therefore returned to our model system of LYZ in NaCl solutions as a starting point (Figure 2.2). Figure 2.11 demonstrates that increasing the temperature from 15-37°C effectively shifts B towards higher values. These data are consistent with the reported normal temperature dependent solubility of LYZ.[12, 41, 42] Notably, the sensitivity of B to differences in temperature was enhanced at elevated NaCl concentrations. For example, at 0% NaCl the average B value for all four temperatures (15, 23, 29, and 37°C) is $3.60 \pm 0.09 \times 10^{-4}$ mol mL/g^2. At 5% NaCl, on the other hand, B is $-12.91 \pm 0.26 \times 10^{-4}$ mol mL/g^2 at 15°C and $-5.86 \pm 0.12 \times 10^{-4}$ mol mL/g^2 at 37°C. This corresponds to a positive shift of $7.05 \pm 0.29 \times 10^{-4}$ mol mL/g^2 for a 22°C increase in temperature. The strength of the NaCl induced trend in B is therefore diminished by elevated temperatures. To validate our SIC results we again obtained SLS data. Figure 2.12 demonstrates excellent agreement between LYZ B values obtained by SIC and SLS. The average difference between corresponding SIC and SLS data points is $<1.0 \times 10^{-4}$ mol mL/g^2. These data, graphed with temperature on the X-axis, demonstrate that increased temperatures reduce the effect of NaCl on B. We speculate that the data trends in Figure 2.12 would continue to merge above 37°C.

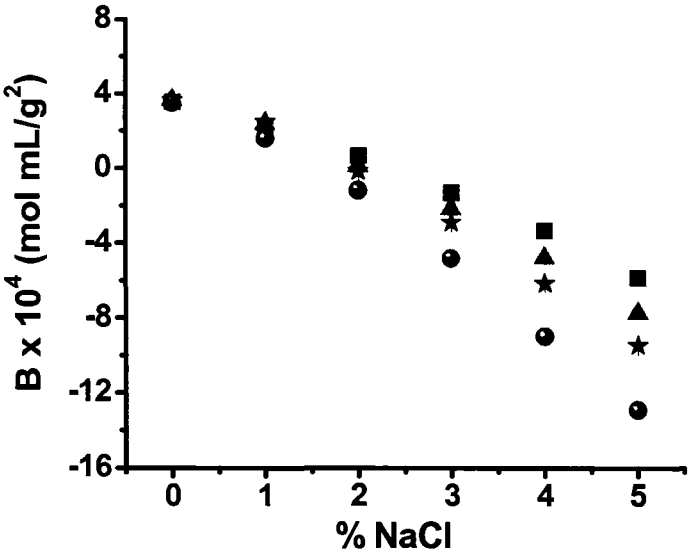

Figure 2.11. Effect of temperature on NaCl induced trends in B. Solution conditions: ACTE (0.1 M, pH 4.5) and 37°C (green squares), 29°C (orange triangles), 23°C (blue stars), 15° (black circles).

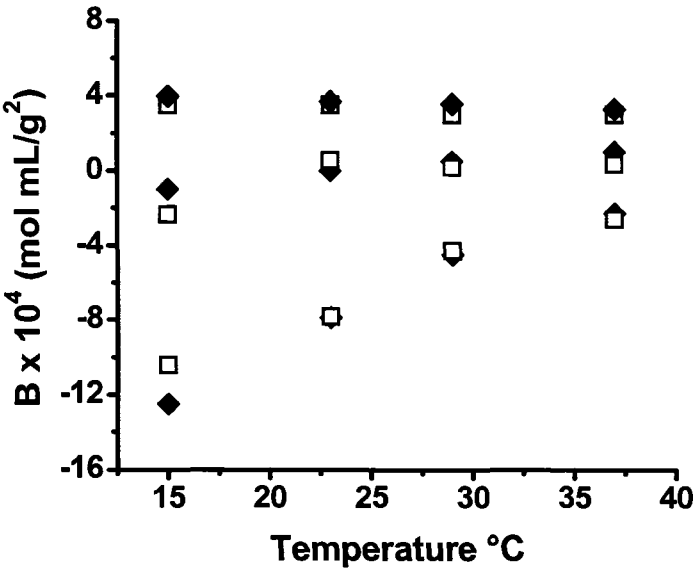

Figure 2.12. Effect of NaCl on temperature induced trends in B as measured by SIC (solid diamonds) and SLS (open squares). Solution conditions: ACTE (0.10M, pH 4.5), 0% NaCl (black symbols), 2% NaCl (red symbols), 5% NaCl (green).

The temperature studies were extended to include trehalose and sucrose solutions (Figure 2.13 and 2.14, respectively). Here again, B is shifted to higher values at elevated temperatures. The general sucrose and trehalose induced trends in B are preserved. The magnitudes of the trends, however, are reduced at elevated temperatures. This behavior is expected based on the results in Figure 2.11 and 2.12. Increasing the temperature raises B, overcoming the salting out effect of NaCl. Subsequent addition of sucrose or trehalose further improves B, but only to a certain point. The large shift in trehalose induced B trends between 25 and 37°C verses the much smaller shift between 37° and 50°C confirms the results in Figure 2.12 and supports the idea that B continues to merge and becomes less sensitive to temperature induced stabilization above 37°C. The eventual leveling off of B trends is an indication of the finite degree to which individual solution parameters (i.e. cosolvents, temperature) contribute to the overall stabilization of LYZ.

2.3 Conclusions

In this chapter, SIC was used to measure B for LYZ self-interaction as a function of several cosolvents, including sucrose, trehalose, mannitol, glycine, arginine, and combinations of arginine and glutamic acid and arginine and sucrose. All of these cosolvents (including cases of combined cosolvents) lead to increased B, reflecting a reduction of LZY self-interaction. An interesting outcome of this study was that B was most affected by these cosolvents once electrostatic repulsions between lysozyme molecules had been fully suppressed (accomplished here by

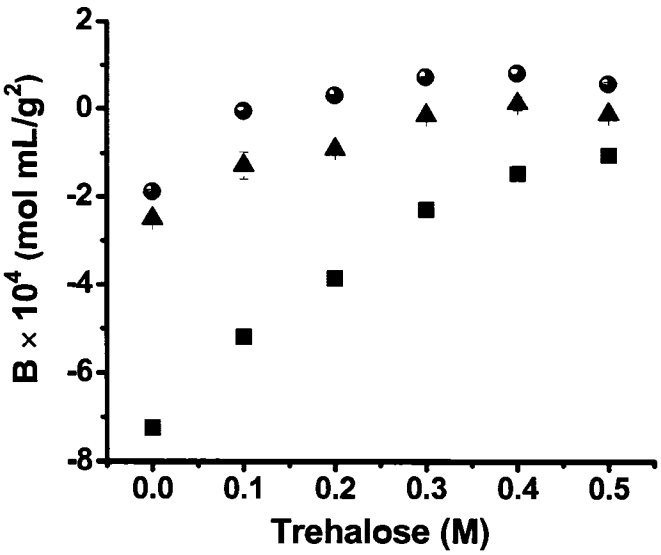

Figure 2.13. Effect of temperature on trehalose induced trends in B. Solution conditions: ACTE (0.1M, pH 4.5) containing 5% NaCl at 50°C (red circles), 37°C (green triangles), 25°C (blue squares).

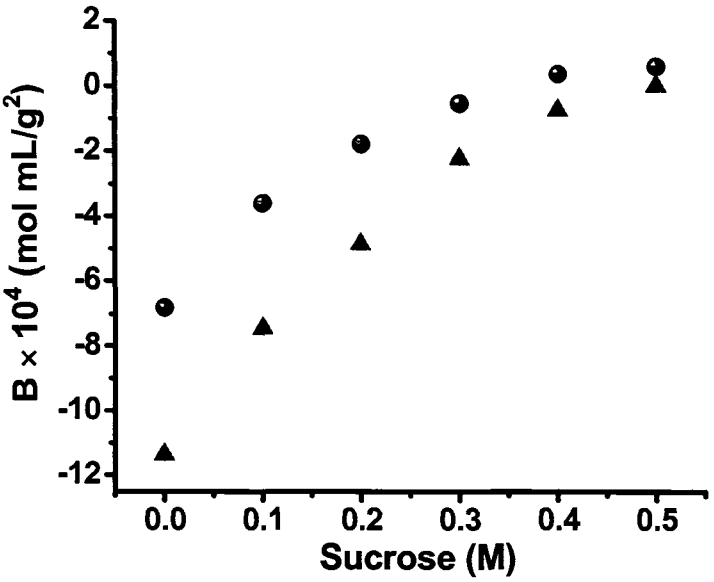

Figure 2.14. Effect of temperature on sucrose induced trends in B. Solution conditions: ACTE (0.1M, pH 4.5) containing 5% NaCl at 27°C (red circles), 19°C (green triangles), 23°C (blue squares).

the addition of 5 % (w/v) NaCl). This was not completely unexpected since cosolvent induced stabilization is mechanistically explained in terms of hydration and excluded volume effects, which are much shorter range than electrostatic forces. Temperature induced trends in B similarly depended on NaCl concentration. SIC measured trends in B were verified by SLS data and accurately modeled with PLS response surfaces. To the best of our knowledge, this work represents the most comprehensive study on the ability of cosolvents to affect the self-interaction and therefore B of LYZ. Virtually all previous protein B studies have focused on salting out effects for crystallization purposes. Overall, this work demonstrates that SIC offers an efficient, high-throughput approach to measuring B of a model protein (LYZ) in complex solutions. More studies of this nature are needed to fully explore all potential advantages and limitations of SIC as well as to develop a fundamental understanding of protein self-interaction in complex solutions.

2.4 Acknowledgments

The author would like to extend gratitude to the following people for their contributions to the above studies of LYZ: Kusum S. Verma and Dr. William W. Wilson (SLS data) and Dr. Mark C. Manning (PLS data).

2.5 References

1) *Increased Thermal-Stability of Proteins in the Presence of Naturally-Occurring Osmolytes,* Santoro, M. M.; Liu, Y. F.; Khan, S. M. A.; Hou, L. X.; Bolen, D. W., *Biochemistry* **1992,** 31, (23), 5278-5283.

2) *The Stabilization of Proteins by Osmolytes,* Arakawa, T.; Timasheff, S. N., *Biophysical Journal* **1985,** 47, (3), 411-414.
3) *Effects of sucrose on conformational equilibria and fluctuations within the native-state ensemble of proteins,* Kim, Y. S.; Jones, L. S.; Dong, A. C.; Kendrick, B. S.; Chang, B. S.; Manning, M. C.; Randolph, T. W.; Carpenter, J. F., *Protein Science* **2003,** 12, (6), 1252-1261.
4) *Sugar-induced molten-globule model,* Davis-Searles, P. R.; Morar, A. S.; Saunders, A. J.; Erie, D. A.; Pielak, G. J., *Biochemistry* **1998,** 37, (48), 17048-17053.
5) *Contribution of the Surface Free-Energy Perturbation to Protein Solvent Interactions,* Kita, Y.; Arakawa, T.; Lin, T. Y.; Timasheff, S. N., *Biochemistry* **1994,** 33, (50), 15178-15189.
6) *Mechanism of Stabilization of Proteins by Glycerol and Sucrose,* Arakawa, T.; Timasheff, S. N., *Seikagaku* **1982,** 54, (11), 1255-1259.
7) *Rapid measurement of protein osmotic second virial coefficients by self-interaction chromatography,* Tessier, P. M.; Lenhoff, A. M.; Sandler, S. I., *Biophysical Journal* **2002,** 82, (3), 1620-1631.
8) Kratochvil, P., In *Light Scattering from Polymer Solutions.*; Huglin, M. ed.; Academic Press: London, **1972**; p 333.
9) *PLS regression methods,* Höskuldsson, A., *Journal of Chemometrics* **1988,** 3, (2), 211-228.
10) Wold, S.; Martens, H.; Wold, H., *The Multivariate Calibration Problem in Chemistry Solved by PLS.* ed.; Springer: Heidelberg, 1983; 'Vol.' Lecture Notes in Mathematics, p 286-293.
11) *Protein-protein and protein-salt interactions in aqueous protein solutions containing concentrated electrolytes,* Curtis, R. A.; Prausnitz, J. M.; Blanch, H. W., *Biotechnology and Bioengineering* **1998,** 57, (1), 11-21.
12) *Tetragonal chicken egg white lysozyme solubility in sodium chloride solutions,* Forsythe, E. L.; Judge, R. A.; Pusey, M. L., *Journal of Chemical and Engineering Data* **1999,** 44, (3), 637-640.
13) *Protein-protein interactions in concentrated electrolyte solutions - Hofmeister-series effects,* Curtis, R. A.; Ulrich, J.; Montaser, A.; Prausnitz, J. M.; Blanch, H. W., *Biotechnology and Bioengineering* **2002,** 79, (4), 367-380.
14) *Correlation between the osmotic second virial coefficient and solubility for equine serum albumin and ovalbumin,* Demoruelle, K.; Guo, B.; Kao, S. M.; McDonald, H. M.; Nikic, D. B.; Holman, S. C.; Wilson, W. W., *Acta Crystallographica Section D-Biological Crystallography* **2002,** 58, 1544-1548.
15) *Protein-protein interactions in aqueous ammonium sulfate solutions. Lysozyme and bovine serum albumin (BSA),* Moon, Y. U.; Curtis, R. A.; Anderson, C. O.; Blanch, H. W.; Prausnitz, J. M., *Journal of Solution Chemistry* **2000,** 29, (8), 699-717.
16) *Effect of alcohols on aqueous lysozyme-lysozyme interactions from static light-scattering measurements,* Liu, W.; Bratko, D.; Prausnitz, J. M.; Blanch, H. W., *Biophys Chem* **2004,** 107, (3), 289-298.

17) *Correlation between the osmotic second virial coefficient and the solubility of proteins,* Ruppert, S.; Sandler, S. I.; Lenhoff, A. M., *Biotechnology Progress* **2001,** 17, (1), 182-187.
18) *Relation between the solubility of proteins in aqueous solutions and the second virial coefficient of the solution,* Haas, C.; Drenth, J.; Wilson, W. W., *Journal of Physical Chemistry B* **1999,** 103, (14), 2808-2811.
19) *Correlation of second virial coefficients and solubilities useful in protein crystal growth,* Guo, B.; Kao, S.; McDonald, H.; Asanov, A.; Combs, L. L.; Wilson, W. W., *Journal of Crystal Growth* **1999,** 196, (2-4), 424-433.
20) *Self-interaction chromatography: a novel screening method for rational protein crystallization,* Tessier, P. M.; Vandrey, S. D.; Berger, B. W.; Pazhianur, R.; Sandler, S. I.; Lenhoff, A. M., *Acta Crystallographica Section D-Biological Crystallography* **2002,** 58, 1531-1535.
21) *The likelihood of aggregation during protein renaturation can be assessed using the second virial coefficient,* Ho, J. G. S.; Middelberg, A. P. J.; Ramage, P.; Kocher, H. P., *Protein Science* **2003,** 12, (4), 708-716.
22) *Nonmonotonic variation with salt concentration of the second virial coefficient in protein solutions,* Allahyarov, E.; Lowen, H.; Hansen, J. P.; Louis, A. A., *Physical Review E* **2003,** 67, (5).
23) *Design of self-interaction chromatography as an analytical tool for predicting protein phase behavior,* Ahamed, T.; Ottens, M.; van Dedem, G. W. K.; van der Wielen, L. A. M., *Journal of Chromatography A* **2005,** 1089, (1-2), 111-124.
24) *Protein interactions and crystallization,* Rosenbaum, D. F.; Zukoski, C. F., *Journal of Crystal Growth* **1996,** 169, (4), 752-758.
25) *Screening of protein-ligand interactions by affinity chromatography,* Garcia, C. D.; Holman, S. C.; Henry, C. S.; Wilson, W. W., *Biotechnology Progress* **2003,** 19, (2), 575-579.
26) *The thermodynamic mechanism of protein stabilization by trehalose,* Xie, G. F.; Timasheff, S. N., *Biophysical Chemistry* **1997,** 64, (1-3), 25-43.
27) *The Stabilization of Proteins by Sucrose,* Lee, J. C.; Timasheff, S. N., *Journal of Biological Chemistry* **1981,** 256, (14), 7193-7201.
28) *Thermodynamics of Polyol-Induced Thermal Stabilization of Chymotrypsinogen,* Gekko, K.; Morikawa, T., *Journal of Biochemistry* **1981,** 90, (1), 51-60.
29) *Interaction of Tubulin and Other Proteins with Structure-Stabilizing Solvents,* Timasheff, S. N.; Lee, J. C.; Pittz, E. P.; Tweedy, N., *Journal of Colloid and Interface Science* **1976,** 55, (3), 658-663.
30) *Hydrophobic forces between protein molecules in aqueous solutions of concentrated electrolyte,* Curtis, R. A.; Steinbrecher, C.; Heinemann, A.; Blanch, H. W.; Prausnitz, J. M., *Biophysical Chemistry* **2002,** 98, (3), 249-265.
31) *A transient expansion of the native state precedes aggregation of recombinant human interferon-gamma,* Kendrick, B. S.; Carpenter, J. F.; Cleland, J. L.; Randolph, T. W., *Proceedings of the National Academy of Sciences of the United States of America* **1998,** 95, (24), 14142-14146.

32) *Thermal stability of proteins in aqueous polyol solutions: Role of the surface tension of water in the stabilizing effect of polyols,* Kaushik, J. K.; Bhat, R., *Journal of Physical Chemistry B* **1998,** 102, (36), 7058-7066.
33) *Osmolyte-induced changes in protein conformation equilibria,* Saunders, A. J.; Davis-Searles, P. R.; Allen, D. L.; Pielak, G. J.; Erie, D. A., *Biopolymers* **2000,** 53, (4), 293-307.
34) *Preferential Interactions of Proteins with Solvent Components in Aqueous Amino-Acid Solutions,* Arakawa, T.; Timasheff, S. N., *Archives of Biochemistry and Biophysics* **1983,** 224, (1), 169-177.
35) *Differential Scanning Calorimetric Study of the Interactions of Some Stabilizing Amino-Acids and Oligopeptides with Hen Egg-White Lysozyme,* Sabulal, B.; Kishore, N., *Journal of the Chemical Society-Faraday Transactions* **1995,** 91, (14), 2101-2106.
36) *Role of arginine in protein refolding, solubilization, and purification,* Tsumoto, K.; Umetsu, M.; Kumagai, I.; Ejima, D.; Philo, J. S.; Arakawa, T., *Biotechnology Progress* **2004,** 20, (5), 1301-1308.
37) *Role of arginine in the stabilization of proteins against aggregation,* Baynes, B. M.; Wang, D. I. C.; Trout, B. L., *Biochemistry* **2005,** 44, (12), 4919-4925.
38) *L-Arginine increases the solubility of unfolded species of hen egg white lysozyme,* Reddy, R. C.; Lilie, H.; Rudolph, R.; Lange, C., *Protein Science* **2005,** 14, (4), 929-935.
39) Clark, E. D.; Schwarz, E.; Rudolph, R., Inhibition of aggregation side reactions during in vitro protein folding. In *Amyloid, Prions, and Other Protein Aggregates*, ed.; **1999**; 'Vol.' 309, p 217-236.
40) *A simple method for improving protein solubility and long-term stability,* Golovanov, A. P.; Hautbergue, G. M.; Wilson, S. A.; Lian, L. Y., *Journal of the American Chemical Society* **2004,** 126, (29), 8933-8939.
41) *Protein solubility modeling,* Agena, S. M.; Pusey, M. L.; Bogle, I. D. L., *Biotechnology and Bioengineering* **1999,** 64, (2), 144-150.
42) *Variation of Lysozyme Solubility as a Function of Temperature in the Presence of Organic and Inorganic Salts,* Guilloteau, J. P.; Rieskautt, M. M.; Ducruix, A. F., *Journal of Crystal Growth* **1992,** 122, (1-4), 223-230.

CHAPTER 3

CONCANAVALIN A AND EQUINE SERUM ALBUMIN STUDIES

In this chapter I turn my attention away from Lysozyme (LYZ) and begin to explore the potential of SIC for analyzing more complex, and less characterized proteins. Doing so required a more fundamental approach and analysis of the SIC methodology. Concanavalin A (Con A) and equine serum albumin (ESA) were chosen as study subjects. Existing B data for both proteins was available from only a few static light scattering studies.[1,2] The SIC literature contained a single study of ESA that lacked B data and reported only the chromatographic capacity factor (k', Equation 1.6).[3] The next closest source was B data from a bovine serum albumin (BSA)-SIC study.[4] These few resources provided valuable reference and guidelines for our investigations.

Preliminary work with Con A and ESA began with size exclusion chromatography (SEC) for purity analysis. Next, protein-particle coupling studies were performed. B was obtained for both proteins as a function of ammonium sulfate and temperature. These data were compared with literature reports whenever applicable. During the SIC studies, special attention was paid to the retention behavior of Con A, ESA, and acetone on both the live and dead columns.

3.1Experimental

3.1.1 Size Exclusion Chromatography (SEC)

All SEC data was collected on a Thermo Spectra Physics Analytical HPLC and analyzed using Chrome Quest software. The column consisted of Omnifit precision bore borosilicate glass (250 x 25 mm) packed with Toyopearl HW-55F SEC resin and fitted with porous 0.25 μm polyethylene frits and polytetrafluoroethylene (PTFE) end fittings. Mobile phases were degassed online and buffered with either Tris (0.1 M, pH 6.0) or K_2HPO_4 (0.1 M, pH 7.0). Sample volumes of 25.0 μL were injected using a Thermo Spectra System AS3000 autosampler and analyzed at a flow rate of 1.0 μL/min at room temperature (22 ± 2°C). Eluting samples were detected at 280 nm.

3.1.2 Determination of extinction coefficient (ε)

Con A (1.0 mg/mL) and ESA (4.0 mg/mL) were dissolved in K_2HPO_4 (1.0 M, pH 7.5). The absorption of serial dilutions between 1.0 and 0.1 mg/mL were measured at 280 nm in a UV-VIS spectrophotometer (Genesys 10uv, Thermo Spectronic). Each dilution sample was run only once. Each protein was run separately. Data points for each protein were fitted to a linear equation with the Y-intercept forced through zero (R= 0.999). The extinction coefficient (ε) was determined by the slope of the line.

3.1.3 Stationary Phase Modification: Con A

Con A (20 mg) was dissolved in 1.2 mL K_2HPO_4 (1.0 M, pH 7.0). AF-Formyl 650-M chromatography particles (600 μL) were washed three times with 1.2 mL of the same K_2HPO_4 buffer. The particles and Con A solution were combined and allowed to settle. Supernatant (25 μL) was removed and diluted to 250 μL for measurement of the initial Con A concentration by UV absorption at 280 nm using a UV-VIS spectrophotometer (Genesis 10uv, Thermo Spectronic). Sodium cyanoborohydride (16 mg) was added to the remaining Con A-particle slurry. The reaction vial was put in a room temperature rotary mixer for 75 min, after which, a final UV measurement was taken exactly as described above. The remaining Con A was removed by washing the particles with 3.6 mL of K_2HPO_4 (1.0 M, pH 7.0) containing 5% (w/v) NaCl. The particles were then washed with the original K_2HPO_4 buffer and placed back in the rotary mixer, along with 1.2 mL of ethanolamine (1.0 M, pH 8.0) and 12 mg sodium cyanoborohydride to cap any unreacted Formyl groups. Finally, the particles were washed with Tris (0.1 M, pH 6.0) and stored at 4° C. Ethanolamine capped AF-Formyl-650M particles (used for the protein-free dead column) were prepared according to the final step of the coupling procedure described above.

3.1.4 Stationary Phase Modification: ESA

ESA (40 mg) was dissolved in 1.2 mL K_2HPO_4 (1.0 M, pH 7.0). AF-Formyl 650-M chromatography particles (600 μL) were washed three times with 1.2 ml of the same K_2HPO_4 buffer. The particles and ESA solution were combined and

allowed to settle. Supernatant (10 μL) was removed and diluted to 250 μL for measurement of the initial ESA concentration by UV absorption at 280 nm using a UV-VIS spectrophotometer (Genesis 10uv, Thermo Spectronic). Sodium cyanoborohydride (20 mg) was added to the remaining ESA-particle slurry. The reaction vial was put in a room temperature rotary mixer for 95 min, after which, a final UV measurement was taken exactly as described above. The remaining ESA was removed by washing the particles with 3.6 mL of K_2HPO_4 (1.0 M, pH 7.0) containing 5% (w/v) NaCl. The particles were then washed with the original K_2HPO_4 buffer and placed back in the rotary mixer, along with 1.2 mL of ethanolamine (1.0 M, pH 8.0) and 15 mg sodium cyanoborohydride to cap any unreacted Formyl groups. Finally, the particles were washed with acetic acid (ACTE) (0.1 M, pH 5.6) and stored at 4°C. Ethanolamine capped AF-Formyl-650M particles (used for the protein-free dead column) were prepared according to the final step of the coupling procedure described above.

3.1.5 Self-Interaction Chromatography (SIC)

All buffers were prepared with 18 MΩ water (Nanopure, Barnstead) and the pH adjusted with either NaOH or HCl. pH was followed using a digital pH meter (UB-5, Denver Instruments). All mobile phases for Con A-SIC were buffered with Tris (0.1 M, pH 6.0). Con A and acetone samples were dissolved at 20 mg/mL and 2% (v/v), respectively. The SIC column consisted of Teflon fluorinated ethylene propylene (FEP) Tubing (1/8" outer diameter, 1/16" inner diameter, Upchurch) fitted with a stainless steel frit (2 μm pores, Upchurch). The column was

conditioned after packing for several hours with Tris (0.1 M, pH 6.0) at 0.30 mL/min, after which no further bed settling was observed. Generally, for all experiments where the mobile phases incrementally increased in cosolvent concentrations, two buffers were used. One buffer with no cosolvent and another with the maximum cosolvent concentration were mixed by the HPLC pump to achieve the entire range of desired conditions. Dead column experiments utilized identical mobile phase conditions with one exception, 5% NaCl was added to all mobile phases to suppress electrostatic interactions between mobile phase analytes and the ethanolamine capped stationary phase.

All chromatographic data were collected on a Hewlett Packard 1050 HPLC and analyzed using Chemstation software. Mobile phases were mixed and degassed online. Sample volumes of 8.0 μL were injected using a Hewlett Packard 1050 autosampler and analyzed at a flow rate of 300 μL/min. Temperatures were controlled with a digital column heater (TC-50, Eppendorf). Eluting samples were detected by UV absorption at 280nm. To ensure reproducibility, Con A samples were run in quadruplicate, and acetone samples in triplicate.

For the ESA-SIC experiments, all mobile phases were buffered with ACTE (0.1 M, pH 5.6). ESA and acetone samples were dissolved at 30 mg/mL and 3% (v/v), respectively. The ESA-SIC column was conditioned after packing for several hours with ACTE (0.1 M, pH 5.6) at 0.20 mL/min, after which no further bed settling was observed. Sample volumes of 1.0 μL were injected using a Hewlett

Packard 1050 autosampler and analyzed at a flow rate of 150 μL/min. All other parameters of the ESA-SIC experiments were equivalent to those used for the Con A-SIC experiments.

3.2 Results and discussion

3.2.1 Purity analysis by SEC

Con A and ESA had to be checked for purity prior to use for SIC experiments. Previous light scattering studies of ESA reported the appearance of dimers and trimers at conditions of Na_2HPO_4 (0.1 M, pH 6.7) and Na_2SO_4 (0.1 M, pH 6.7).[2] Con A, on the other hand, engages in a reversible dimer-tetramer equilibrium. Reports of the exact equilibrium conditions vary, but there is a general consensus. The Con A dimer dominates at slightly acidic pH with the tetramer becoming increasingly favored at alkaline pH.[5-7] Figure 3.1 contains SEC results for the Con A and ESA samples used throughout this chapter, under solution conditions that would closely resemble those used in the protein-particle coupling studies and SIC experiments. Apoferritin (APO, 460 kDa), Human serum albumin (HSA, 66 kDa), and Cymotrypsinogen (CYM, 26 kDa) were used as molecular weight markers. Con A was the first and last protein injected to ensure that column conditions remained constant. At both conditions (Tris (0.1 M, ph 6.0), Figure 3.1A, and K_2HPO_4 (0.1 M, pH 7.0), Figure 3.1B) Con A elutes after HSA (66 kDa) and ESA (64 kDa) but before CYM (26 kDa) indicating the presence of the Con A dimer (51 kDa). Figures 3.1C and 3.1D are the respective close ups

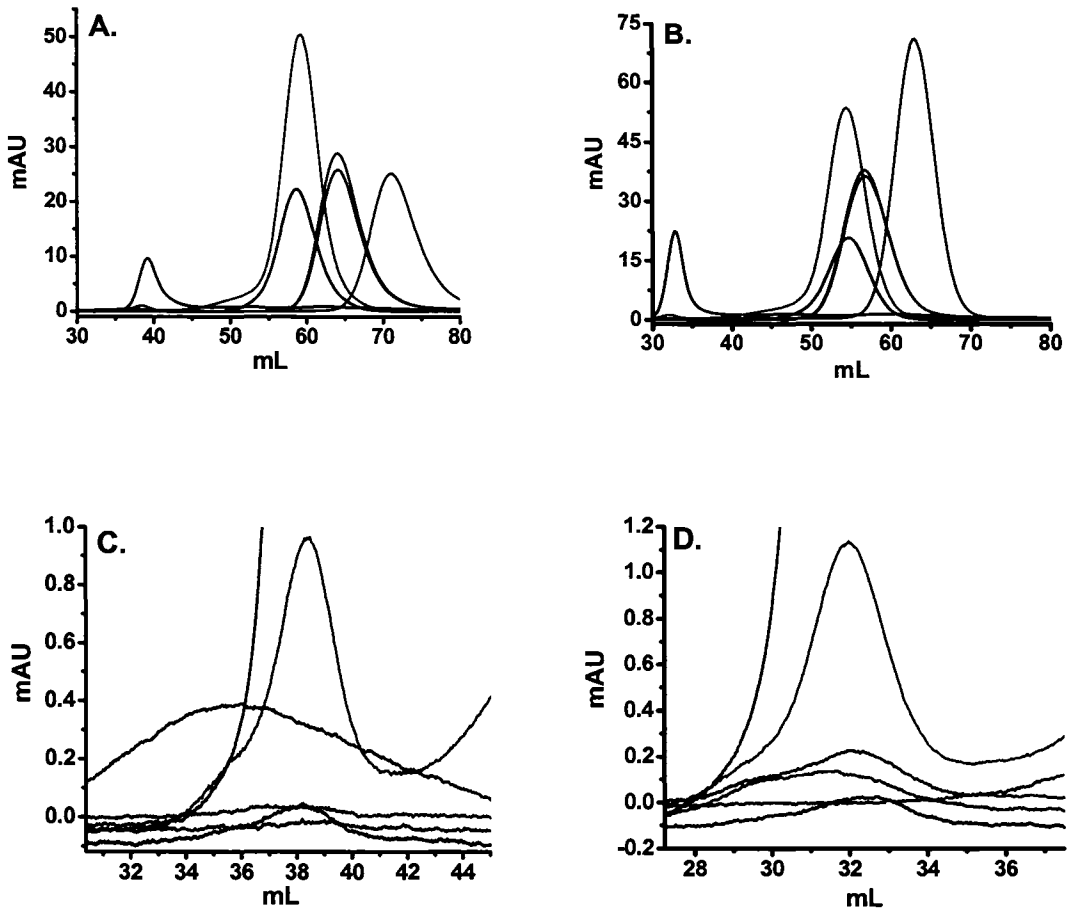

Figure 3.1. Size Exclusion Chromatography (SEC) of Apoferritin (black line, 460 kDa), Human Serum Albumin (light blue line, 66 kDa), Equine Serum Albumin (dark blue line, 64 kDa), Concanavalin A (red and green lines, 51 kDa), and Cymotrypsinogen (pink line, 26 kDa). Buffer conditions: TRIS (0.1 M, pH6.0) (A. and C.) or K_2HPO_4 (0.1 M, pH 7.0) (B. and D.) at room temperature (22 ± 2°C). Graph C. is a close-up of A. and graph D. is a close-up of B.

of Figures 3.1A and 3.1B. HSA and ESA dimers (132 kDa and 128 kDa, respectively) are present at both pH 6.0 and 7.0. Only at pH 7.0 does a peak begin to appear where the Con A tetramer (102 kDa) would be expected to elute. These data are consistent with the previously mentioned equilibrium conditions. It is not clear why the primary APO peak, the Con A tetramer, and the HSA and ESA dimers all elute at nearly the same time. A very likely explanation is that we were approaching the selectivity limit of the resin, despite the manufacturers report that the resin is effective in the range of 1-700 kDa. Nonetheless, this SEC data indicated relatively low amounts of Con A tetramer and ESA dimer impurities.

3.2.2 Protein-particle coupling studies

The coupling density (CD) of protein covalently immobilized to the stationary phase particles was calculated from UV measurements. As a first step, the proteins' extinction coefficient (ε) must be experimentally determined. Figure 3.2 demonstrates that ε of Con A and ESA was measured as 0.935 and 0.434 mL/ mg cm at 280nm, respectively. These values were used to quantify the difference in absorbance between the pre- and post- coupling concentration of each protein in solution. The result is a CD in units of mg of protein/ mL of Formyl particles, which is then converted to molecules of protein/ m^2 of Formyl particle surface area. The later units represent (ρ) and are directly used in the calculation of B.

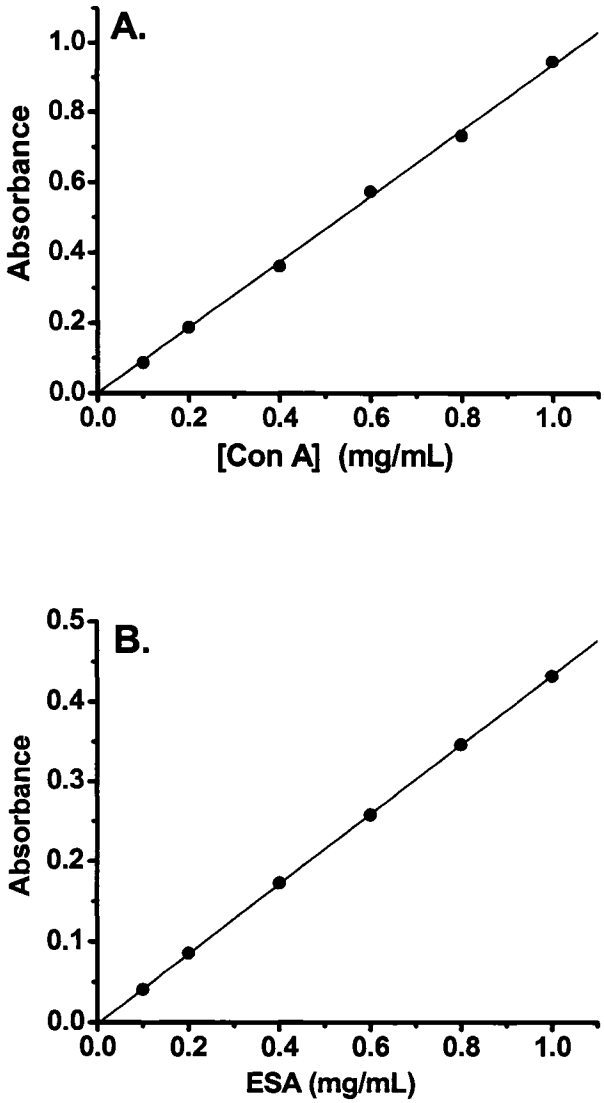

Figure 3.2: Con A (A) and ESA (B) calibration curves for the determination of the molar extinction coefficient (ε) at 280 nm. Con A and ESA dilutions (black dots) were produced from stock samples (1.0 and 4.0 mg/mL, respectively). Linear fits (red lines, R=0.999) were forced through zero. ε = 0.935 mL/ mg cm (Con A) and 0.434 mL/ mg cm (ESA).

Previous LYZ-SIC experiments have suggested that a minimum CD is required for accurate self-interaction measurements.[8] Slower flow rates and longer columns may help counter the effects of low immobilization densities, but also 650M particles have the lowest density of reactive ligands (20 μmol/mL). The only published accounts of SIC experiments using these particles neglected to report a CD and calculated only k' values, without the use of a dead column.[3, 9] Formyl particles, on the other hand, contain a three-fold increase in the density of chemically reactive ligands (60 μmol/mL). These particles were successfully used throughout the LYZ-SIC studies in chapter 2. Table 3.1 lists the physical parameters used in calculating CDs and summarizes the results of protein-Formyl particle coupling studies for Con A, ESA, and LYZ. The CD Con A and ESA modified particles used for SIC studies was were 2.81×10^{16} and 1.35×10^{16} protein molecules/m^2 Formyl particle surface area, respectively. These values are equivalent to 57% and 27% of the average LYZ CD (4.92×10^{16} protein molecules/m^2 Formyl particle surface area). In terms of mg of protein/mL of Formyl particles, the manufacturer (Toyopearl) quotes a CD of 14 mg/ mL for BSA. This value is consistent with our reported CD of 15.2 ± 2.2 mg ESA/ mL Formyl particles (Table 3.1). The only quote for Con A was 13 mg Con A/ mL of Tresyl particles. Since Formyl particles contain three times as many reactive ligands as Tresyl particles, our reported CD of 25.6 ± 5.7 mg of Con A/ mL of Formyl particles was considered acceptable. The error associated with our CD

Table 3.1: Hydrodynamic radius (R_H), coupling densities (ρ), and excluded volume (B_{HS}) of proteins for which SIC data has been obtained.

Protein	MW (kDa)	R_H (nm)	Coupling density (ρ) (mg/mL)	(molecs/m^2)	B_{HS} (cm^3) (radius)	B_{HS} (cm^3) (MW)
LYZ	14.6	1.55	16.6 ± 0.6	4.92×10^{16}	6.24×10^{-20}	6.76×10^{-20}
Con A	51	2.55	25.6 ± 5.7	2.81×10^{16}	2.78×10^{-19}	2.36×10^{-18}
ESA	64	3.8	15.2 ± 2.2	1.35×10^{16}	9.19×10^{-19}	3.12×10^{-19}

values (when reported in units of mg/mL) arises from multiple trials (n= 4-6) where protein concentration and particle volume were varied during the coupling studies.

3.2.3 Dead Column Experiments

Dead columns are prepared by capping Formyl particles exclusively with ethanolamine (1.0 M, pH 8.0). The primary purpose of a dead column is to provide V_o', which is the ratio of the protein retention volume and the acetone retention volume (V_p'/V_a'). This parameter is then multiplied by the retention volume of acetone in the live protein-modified column (V_a) to yield a reasonable estimate for the retention volume of a non-retained species (neutral marker) of equivalent size to the protein (V_o). While V_o' is the desired product of dead column experiments, valuable information can also be extracted from individual analysis of V_p' and V_a' as a function of solution conditions.

Dead column experiments are normally run with mobile phases containing 5% NaCl to suppress the potential for electrostatic interaction between the mobile phase analytes and the stationary phase. To verify the utility of this practice we ran dead column experiments with and without 5% NaCl. The retention behavior of acetone and Con A as a function of ammonium sulfate (AS) and temperature on a dead column without 5% NaCl is shown in Figure 3.3. The retention of acetone (V_a') is increased both by the addition of ammonium sulfate and elevated temperatures. Considering that there should be no appreciable interactions

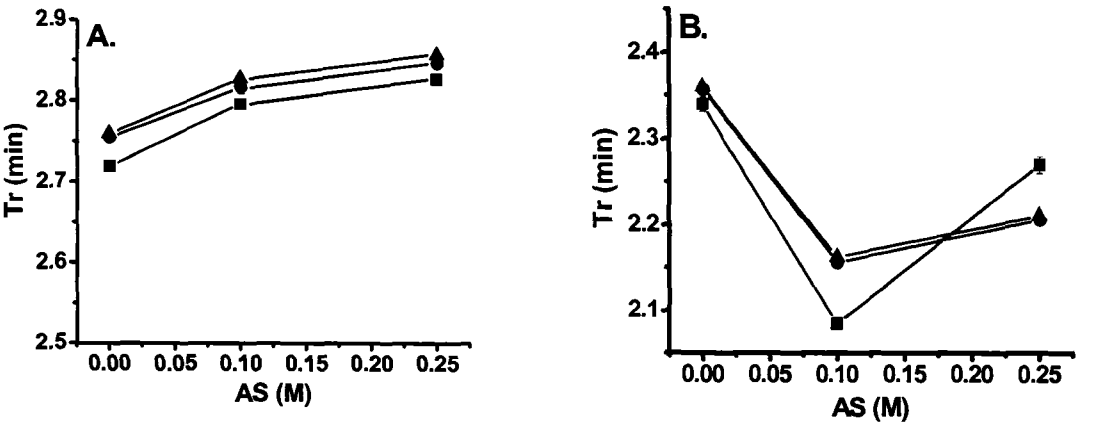

Figure 3.3. Retention of acetone (A) and Con A (B) as a function of ammonium sulfate (AS) on an ethanolamine capped dead column. Buffer Conditions: Tris (0.1 M, pH 6.0) containing 0% NaCl at 37°C (red triangles), 25°C (green circles), 17°C (black squares). Lines connecting data points have been added to help guide the eye.

between acetone and stationary phase, the V_a' trend most likely is an indication of stationary phase particle swelling. The Con A (V_p') trend, on the other hand, likely reflects electrostatic protein-particle surface interactions. Addition of up to 0.1 M AS shifts V_p' to shorter times (from 2.36 ± 0.01 to 2.15 ± 0.01 min). At the same conditions V_a' increased, indicating that the V_p' trend cannot be due to a decrease in stationary phase volume. Further increasing the AS concentration to 0.25 M shifts V_p' back to longer times (from 2.15 ± 0.01 to 2.20 ± 0.01 min). The behavior of V_p' in this range of ionic strengths (0.0-0.25 M AS) is consistent with classic salting in, salting out theory.[10] In terms of temperature, V_a' is increased from 10-37°C at all AS concentration. V_p' also increases as a function of temperature but only at the 0.0 M and 0.1 M AS data points, and the majority of the temperature shift is observed between 17 and 25°C. In the presence of 0.1 M AS, V_p' is shifted from 2.08 ± 0.01 to 2.15 ± 0.01 min by raising the temperature from 17 to 25°C. Further raising the temperature to 37°C produced no significant shift in V_p' (2.16 ± 0.01 min). This temperature induced trend is reversed in the presence of 0.25 M AS, where V_p' is higher at 17° than at 25 and 37°C. When 5% NaCl is added to the mobile phases, the V_o' trend is preserved but the V_p' trend is significantly altered (Figure 3.4). Both V_o' and V_p' are shifted to higher values as a function of AS. At 25°C the addition of 0.25 M AS shifts V_a' by 0.04 ± 0.01 min (from 2.91 ± 0.01 to 2.95 ± 0.01 min) and V_p' by 0.07 ± 0.01 min (from 2.31 ± 0.01 to 2.38 ± 0.01 min). Only V_a' demonstrated a temperature dependence. V_a' was shifted by 0.05 ± 0.01 min at all AS concentrations by raising the temperature from 17-37°C.

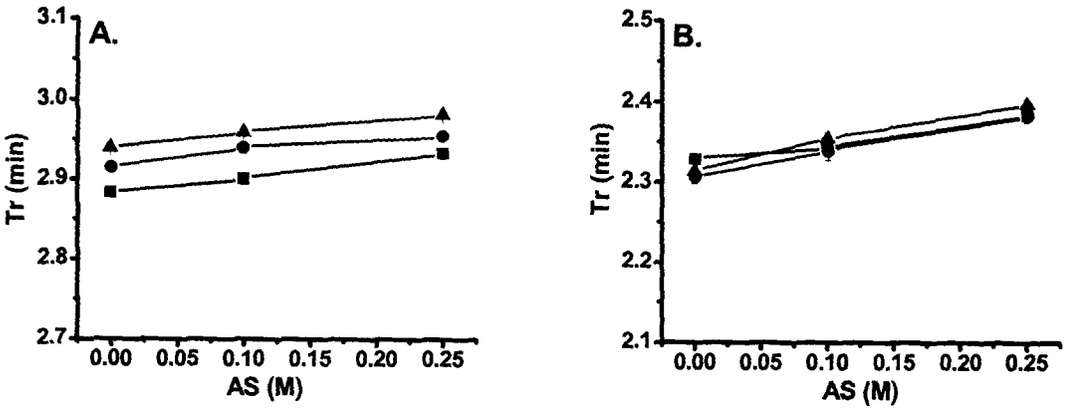

Figure 3.4. Retention of acetone (A) and Con A (B) as a function of ammonium sulfate (AS) on an ethanolamine capped dead column. Buffer Conditions: Tris (0.1 M, pH 6.0) containing 5% NaCl at 37°C (red triangles), 25°C (green circles), 17°C (black squares). Lines connecting data points have been added to help guide the eye.

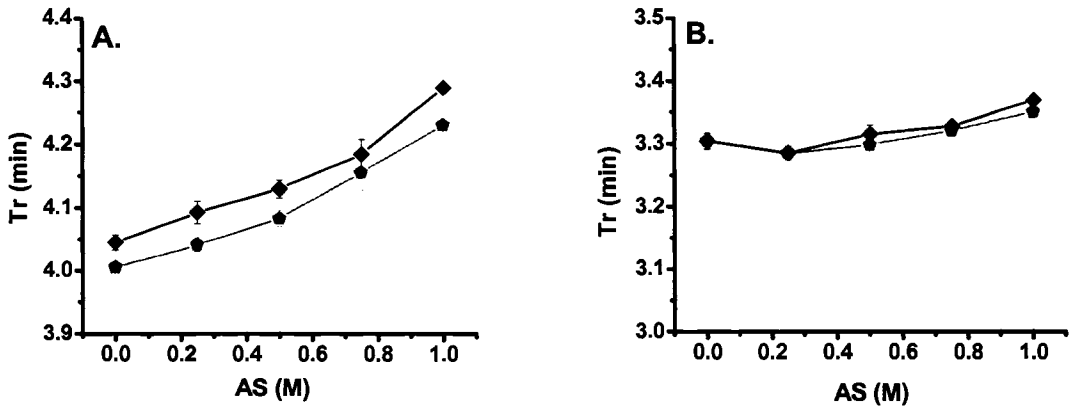

Figure 3.5. Retention of acetone (A) and ESA (B) as a function of ammonium sulfate (AS) on an ethanolamine capped dead column. Buffer Conditions: ACTE (0.1 M, pH 5.6) containing 0% NaCl, 29°C (blue diamonds), 22°C (orange pentagons). Lines connecting data points have been added to help guide the eye.

Similar experiments were run with ESA. Figure 3.5 demonstrates the behavior of V_a' and V_p' (for ESA) on an ethanolamine-Formyl column in the absence of 5% NaCl. V_a' is clearly more affected by the addition of up to 1.0 M AS and a shift in temperature from 22-29°C than V_p'. At 22°C, V_a' is raised by 0.22 ± 0.01 min (from 4.01 ± 0.0.1 to 4.23 ± 0.01 min) by the addition of 1.0 M AS. Under the same conditions V_p' is only raised by 0.04 ± 0.01 min (from 3.31 ± 0.01 to 3.35 ± 0.01 min). The average shift in V_a' for an increase in temperature from 22-29°C was 0.04 ± 0.02 min. No measurable shift in Vp' was produced in the same thermal range. When 5% NaCl was added to the mobile phases, both the V_o' and V_p' trends are largely preserved (Figure 3.6). These data probed a larger thermal range (17-37°C) than the data in Figure 3.5. The data again indicate that V_a' is significantly more sensitive to changes in temperature and AS concentration than V_p'. In the absence of 5% NaCl, V_p' for ESA was shifted by 0.07 ± 0.01 min (from 3.30 ± 0.01 to 3.37 ± 0.01) by the addition of 1.0 M AS at 29°C. In the presence of 5% NaCl, V_p' was shifted by 0.12 ± 0.01 min (from 3.28 ± 0.01 to 3.40 ± 0.01 min) at the same temperature and AS concentration (Figure 3.6).

Together, the data in Figures 3.3-3.6 verify that 5% NaCl should be used in all dead column mobile phases. In the absence of 5% NaCl, some interactions between the mobile phase proteins and the stationary phase are observed. These effects appear to be protein specific and more pronounced at lower ionic strengths. This is expected since it is the total ionic strength, rather than the specific salt that is required for electrostatic suppression. However, NaCl appears

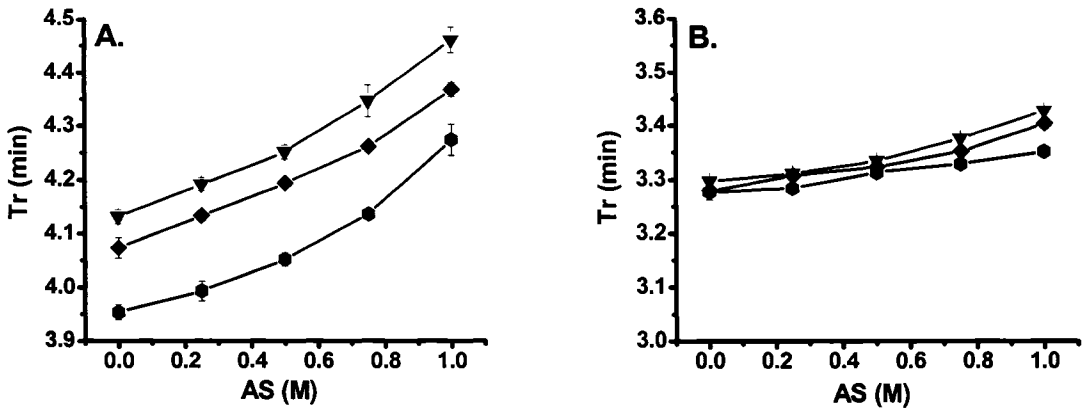

Figure 3.6. Retention times of acetone (A) and ESA (B) as a function of ammonium sulfate (AS) on an ethanolamine capped dead column. Buffer Conditions: ACTE (0.1M, pH 5.6) containing 5% NaCl, 37°C (inverted red triangles), 29°C (blue diamonds), 17°C (black hexagons). Lines connecting data points have been added to help guide the eye.

to be a more ideal salt for the purposes of dead column experiments than AS. Our results indicate that the stationary phase material swells as a function of AS (up to 1.0 M) and temperature (between 17 and 37°C). Both of these effects are more prominent in the acetone trends (V_a'). These results are explained by the fact that acetone accesses considerably more pore space than a protein will therefore be more sensitive to slight changes in the intra particle pore space.

Another interesting outcome of these studies is seen when comparing V_o' (V_p'/V_a') for Con A and ESA (Figure 3.7). It is unclear to us why V_o' increases for Con A and decreases for ESA in the range of 0.00-0.25 M AS. We assume that V_a' is affected only by the particle swelling which should be the same in both systems. At 17°C V_o' for ESA is consistently larger than V_o' for Con A, indicating that ESA is accessing more pore space. At 37°C V_o' values intersect at ~0.09 M AS, with ESA having the larger V_o' at lower AS concentrations and Con A having the larger Vo' as higher AS concentrations. Con A has a smaller MW and R_H (see Table 3.1) and should therefore consistently have a higher V_o' than ESA b virtue of the ability to access more of the stationary phase pore space. There are several possible explanations for our data. Presumably, the highly ellipsoidal nature of the Con A dimer (84 x 40 x 39 Å)[11] may disproportionately restricting the amount of available pore space due to orientations where the long axis is perpendicular to the stationary phase pores. It is also possible that our results reflect changes in the protein structure and hydration layers as combined functions of temperature and AS concentration. The data trends must then be

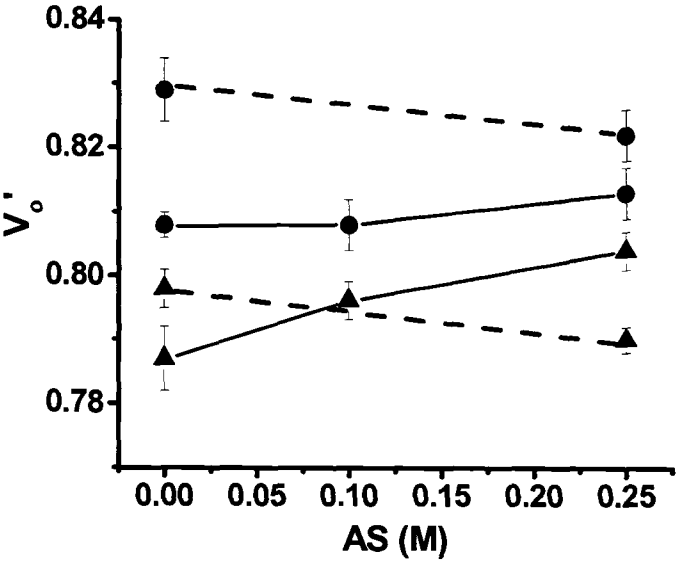

Figure 3.7. Vo' for Con A (red data) and ESA (black data). Solution conditions: Tris (0.1 M, pH 6.0) (red data) or ACTE (0.1 M, pH 5.6) (black data) containing 5% NaCl (all data) at 17°C (circles) or 37°C (triangles). Dashed and solid lines have been added to help guide the eye.

explained in terms of interactions between the AS and the protein surface, an area of extensive complexity that is described in detail elsewhere.[12-15] Furthermore, it should be noted that V_o' for LYZ in the presence of 5% NaCl was ~0.76. Both Con A and ESA are larger than LYZ. They should thus access less pore space and produce lower V_o' values. All of the V_o' values in Figure 3.7 are larger than 0.76. These results are significant because they suggest that the dead column does not necessarily perform according to the theoretical framework discussed in Chapter 1. This impacts the accuracy (in terms of absolute value) of our SIC measured B values for proteins other than LYZ. However, overall trends in V_o' and B are preserved. We therefore focus all subsequent discussions of SIC B data in terms of shifts in B, rather than absolute B values.

Clearly, the issue of available pore space is an important one in both live and dead columns. Accessible pore space in a live column (ϕ) is determined from the protein's molecular weight (MW).[16] The protein excluded volume (B_{HS}), which directly effects ϕ, is most commonly calculated from the protein's hydrodynamic radius (R_H) but can also be obtained from the MW. For relatively globular proteins such as LYZ, there is little difference between B_{HS} values based on MW vs. R_H (Table 3.1). Unfortunately, discrepancies scale with protein asymmetry. For example, Con A B_{HS} values differ by nearly an order of magnitude. For ESA, B_{HS} calculated from R_H is three times larger than B_{HS} calculated from MW. For consistency, all B data in this chapter, as well as in the LYZ-SIC chapter were calculated with B_{HS} as a function of R_H.

3.2.4 Con A-SIC

The results of Con A SIC experiments are plotted in Figure 3.8. Con A displays retrograde temperature dependent physical stability, as indicated by shifts towards lower B values at increased temperatures. In the absence of AS, B is reduced by 1.94 ± 0.16 (from -0.44 ± 0.06 to -2.38 ± 0.15 × 10^{-4} mol mL/ g^2) by increasing the temperature from 17-37°C. Addition of 0.1 M AS shifts B to higher values (from –0.44 ± 0.74 ± 0.07 × 10^{-4} mol mL/ g^2 at 17°C and from –2.38 ± 0.15 to –0.38 ± 0.12) indicating a shift towards favorable Con A-solvent interactions, consistent with salting-in theory.[17] The overall temperature induced lowering of B is preserved at these conditions. Further increasing the AS concentration to 0.25 M does not significantly alter B in any way. Christopher et al.[18] observed a similar retrograde temperature dependent solubility for Con A in phosphate buffer at pH 7.4 in the same thermal range. Conversely, Agena et al. report a solubility trend that changed from retrograde to normal temperature dependence.[19] The opposite trend was reported by Mikol and Geige.[20] Both experimental sets were performed at pH 6.0, but each was at a different ammonium sulfate concentration. Our Con A-SIC experiments were also performed at pH 6.0. Ultimately, it was determined that more SIC experiments over a broader range of solution conditions were needed to better interpret and compare our B data to literature reports.

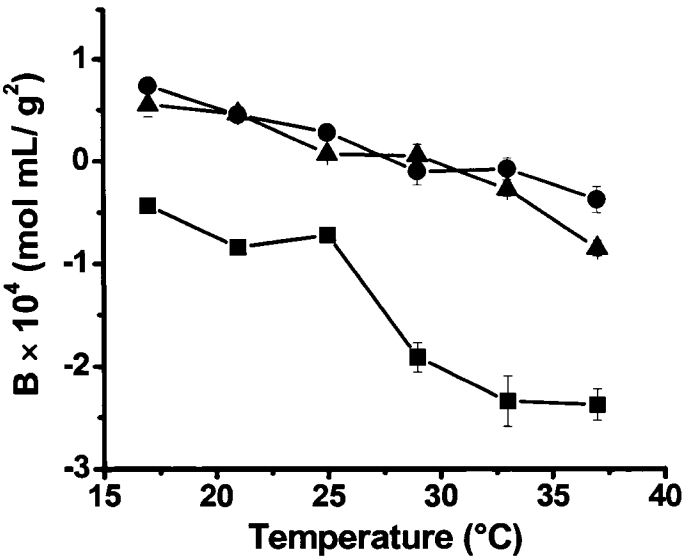

Figure 3.8. Effect of ammonium sulfate (AS) concentration on temperature induced trends in B of Con A. Solution conditions: Tris (0.1 M, pH 6.0) containing 0.0 M AS (black squares), 0.1 M AS (red circles), 0.25 M AS (green triangles). Lines connecting data points have been added to help guide the eye.

3.2.5 ESA-SIC

ESA-SIC data is plotted as a function of temperature in Figure 3.9. The temperature dependence of B was investigated at five different AS concentrations up to 1.0 M. For clarity, only the 0.0, 0.5, and 1.0 M AS trends have been graphed. The data indicate no temperature dependent shift in B in the range of 17-37°C. B was shifted to slightly higher values as a function of AS. At 17°C, B was shifted by $0.33 \pm 0.13 \times 10^{-4}$ mol mL/ g^2 (from 1.60 ± 0.12 to $1.93 \pm 0.04 \times 10^{-4}$ mol mL/ g^2) by the addition of 1.0 M AS. The same concentration of AS shifted B by $0.53 \pm 0.17 \times 10^{-4}$ mol mL/ g^2 (from 1.44 ± 0.11 to $1.97 \pm 0.13 \times 10^{-4}$ mol mL/ g^2) at 37°C. By contrast, literature reports indicate that ESA as retrograde temperature dependent solubility.[18, 21, 22] Furthermore, Demorelle et al. reported a reduction in B of ESA (from 2.0 ± 0.3 to $0.1 \pm 0.8 \times 10^{-4}$ mol mL/ g^2) from the addition of 1.0 M AS at the same buffer conditions used in our SIC studies.[2]

We suspect that the discrepancy between our SIC data and literature reports of B for ESA was due to an insufficient CD of the ESA-Formyl particles. The CD of the particles used to collect the SIC data in Figure 3.9 was 13.8 mg of ESA/ mL of Formyl particles. While this values was right in line with the manufacturers reported value of 14.0 mg of ESA/ mL of Formyl particles, there were no reports of these particles being used for measuring ESA self-interaction. The closest literature reference to our studies was a report by Tessier et al. of BSA-SIC using Amino particles with a CD of 19.1 ± 2.3 mg/ mL.[4] At the time of the ESA-

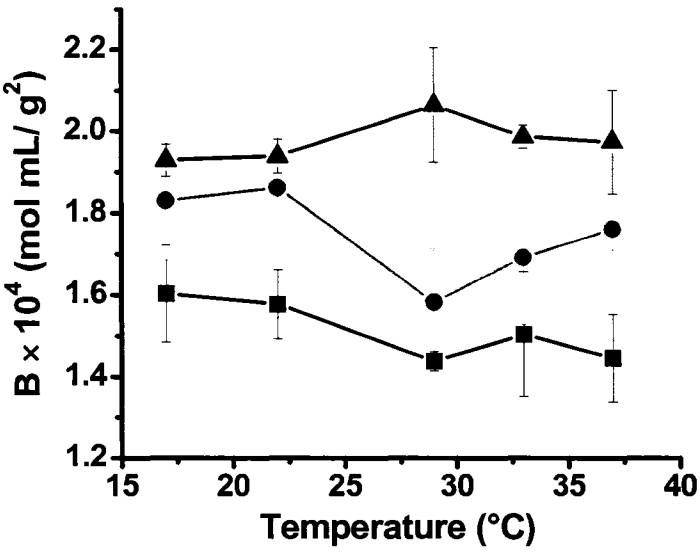

Figure 3.9. Effect of ammonium sulfate (AS) and temperature on B of ESA. Solution conditions: ACTE (0.1 M, pH 5.6) containing 0.0 M AS (dark green squares), 0.5 M AS (orange circles), 1.0 M AS (blue triangles). Lines connecting data points have been added to help guide the eye.

SIC studies we were unfamiliar with the use Amino particles. It is likely that future ESA-SIC studies, as well as SIC of other proteins, would benefit from the use of Amino particles.

The most convincing data indicating the need to increase the CD of the ESA-Formyl particles is seen in Figure 3.10. V_o for the live ESA-Formyl column and V_o' for the dead ethanolamine-Formyl column are graphed as a function of AS concentration. These data were collect under identical solution conditions. The only differences were in the columns. Aside from the obvious difference due to the presence of immobilized ESA in the live column, there was also a considerable difference between column lengths (23 cm for the dead column and 34 cm for the live column). Both V_o and V_o' are reduced by the addition of up to 1.0 M AS. The V_o trend is vertically shifted lower than the V_o' trend. Both parameters are independent of column length. The difference between the V_o and V_o' value is therefore attributed to the presence of immobilized ESA in the live column. This would reduce the available pore space relative to a dead column. The ESA accessible pore space is expected to be reduced more than the acetone accessible pore space because immobilized ESA already occupying pore space will prevent the passage of a mobile phase ESA molecule before preventing the passage of a much smaller acetone molecule. The result will be a reduction in V_o (V_p/V_a) just as seen in Figure 3.10. It was therefore concluded that the ESA-Formyl live column was acting as an ethanolamine-Formyl dead

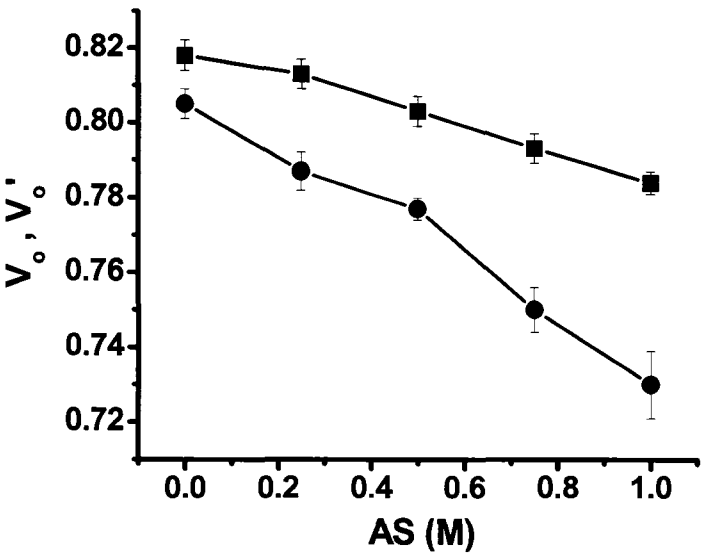

Figure 3.10. Ratios of available pore space in an ESA-Formyl column (Vo= Vp/ Va) (black squares) and an ethanolamine-Formyl column (Vo'= Vp'/ Va') (red circles) as a function of ammonium sulfate (AS). Solution conditions: ACTE (0.1 M, pH 5.6) containing 5% NaCl at 22°C.

column. There simply may not have been enough immobilized ESA to measure changes in ESA self-interaction. As previously suggested, this situation could potentially be remedied with the use of amino particles.

3.3 Conclusions

This work represented largely uncharted territory for SIC and therefore took a course more along the lines of method development, rather than novel applications as with LYZ in Chapter 2. In this chapter, the effects of AS and temperature on Con A and ESA self-interaction were investigated by SIC. B of Con A was increased by the addition of up to 0.25M AS and decreased by raising the temperature from 17-37°C. B of ESA, on the other hand, was unaffected by temperature in the range of 17-37°C and was increased by the addition of up to 1.0 M AS. These results were later attributed to temperature and AS induced effects on the stationary phase rather than changes in ESA self-interaction. Careful examination of ethanolamine-dead column data indicated that the stationary phase material expanded as a function of both AS and temperature. The practice of using 5% NaCl, or equivalent ionic strength in all dead column mobile phases was verified as a necessary approach to suppress potential interactions between the mobile phase proteins and the stationary phase. Analysis of the ratios of available pore space for acetone and LYZ, Con A, and ESA systems indicated that some interactions may still occur between mobile phase proteins and the stationary phase even at ionic strength in excess of 1.0 M. The method by which the protein excluded volume is calculated was also

shown to incorporate some degree of uncertainty into SIC measurements of B. In the absence of extensive B data for all proteins studied by SIC it remains unclear to what extent SIC measurements of B are skewed in relation to absolute B values. Nonetheless, overall trends in B induced by changes in solvent parameters are preserved. Subsequent discussion of SIC measurement of B therefore focuses in shifts in relative B values rather than absolute values. In the next chapter we continue our divergence away from model proteins in simple solution conditions. We demonstrate that the results of the methodology studies in the current chapter were instrumental in broadening the application of SIC to more complex systems and verify the utility of measuring trends in relative B as predictors of physical protein stability.

3.4 References

1) *Predicting Protein Crystallization from a Dilute-Solution Property,* George, A.; Wilson, W. W., *Acta Crystallographica Section D-Biological Crystallography* **1994,** 50, 361-365.
2) *Correlation between the osmotic second virial coefficient and solubility for equine serum albumin and ovalbumin,* Demoruelle, K.; Guo, B.; Kao, S. M.; McDonald, H. M.; Nikic, D. B.; Holman, S. C.; Wilson, W. W., *Acta Crystallographica Section D-Biological Crystallography* **2002,** 58, 1544-1548.
3) *Screening of protein-ligand interactions by affinity chromatography,* Garcia, C. D.; Holman, S. C.; Henry, C. S.; Wilson, W. W., *Biotechnology Progress* **2003,** 19, (2), 575-579.
4) *Self-interaction chromatography: a novel screening method for rational protein crystallization,* Tessier, P. M.; Vandrey, S. D.; Berger, B. W.; Pazhianur, R.; Sandler, S. I.; Lenhoff, A. M., *Acta Crystallographica Section D-Biological Crystallography* **2002,** 58, 1531-1535.
5) *Sedimentation Studies of Reversible Dimer-Tetramer Transition Kinetics of Concanavalin-A,* Huet, M.; Claverie, J. M., *Biochemistry* **1978,** 17, (2), 236-241.
6) *Thermodynamics of Concanavalin-a Dimer-Tetramer Self-Association - Sedimentation Equilibrium Studies,* Senear, D. F.; Teller, D. C., *Biochemistry* **1981,** 20, (11), 3076-3083.

7) *Structure of concanavalin A at pH 8: bound solvent and crystal contacts,* Lopez-Jaramillo, F. J.; Gonzalez-Ramirez, L. A.; Albert, A.; Santoyo-Gonzalez, F.; Vargas-Berenguel, A.; Otalora, F., *Acta Crystallographica Section D-Biological Crystallography* **2004,** 60, 1048-1056.
8) *Rapid measurement of protein osmotic second virial coefficients by self-interaction chromatography,* Tessier, P. M.; Lenhoff, A. M.; Sandler, S. I., *Biophysical Journal* **2002,** 82, (3), 1620-1631.
9) *Measuring protein interactions by microchip self-interaction chromatography,* Garcia, C. D.; Hadley, D. J.; Wilson, W. W.; Henry, C. S., *Biotechnology Progress* **2003,** 19, (3), 1006-1010.
10) *Protein-protein interactions in concentrated electrolyte solutions - Hofmeister-series effects,* Curtis, R. A.; Ulrich, J.; Montaser, A.; Prausnitz, J. M.; Blanch, H. W., *Biotechnology and Bioengineering* **2002,** 79, (4), 367-380.
11) *Covalent and 3-Dimensional Structure of Concanavalin-A .4. Atomic Coordinates, Hydrogen-Bonding, and Quaternary Structure,* Reeke, G. N.; Becker, J. W.; Edelman, G. M., *Journal of Biological Chemistry* **1975,** 250, (4), 1525-1547.
12) *Protein-protein and protein-salt interactions in aqueous protein solutions containing concentrated electrolytes,* Curtis, R. A.; Prausnitz, J. M.; Blanch, H. W., *Biotechnology and Bioengineering* **1998,** 57, (1), 11-21.
13) *Calculation of phase diagrams for aqueous protein solutions,* Curtis, R. A.; Blanch, H. W.; Prausnitz, J. M., *Journal of Physical Chemistry B* **2001,** 105, (12), 2445-2452.
14) *The Control of Protein Stability and Association by Weak-Interactions with Water - How Do Solvents Affect These Processes,* Timasheff, S. N., *Annual Review of Biophysics and Biomolecular Structure* **1993,** 22, 67-97.
15) Timasheff, S. N., Control of protein stability and reactions by weakly interacting cosolvents: The simplicity of the complicated. In *Advances in Protein Chemistry, Vol 51*, ed.; 'Ed.'^'Eds.' 1998; 'Vol.' 51, p^pp 355-432.
16) *Pore size distributions of cation-exchange adsorbents determined by inverse size-exclusion chromatography,* DePhillips, P.; Lenhoff, A. M., *Journal of Chromatography A* **2000,** 883, (1-2), 39-54.
17) *Abnormal Solubility Behavior of Beta-Lactoglobulin - Salting-in by Glycine and Nacl,* Arakawa, T.; Timasheff, S. N., *Biochemistry* **1987,** 26, (16), 5147-5153.
18) *Temperature-dependent solubility of selected proteins,* Christopher, G. K.; Phipps, A. G.; Gray, R. J., *Journal of Crystal Growth* **1998,** 191, (4), 820-826.
19) *Protein solubility modeling,* Agena, S. M.; Pusey, M. L.; Bogle, I. D. L., *Biotechnology and Bioengineering* **1999,** 64, (2), 144-150.
20) *Phase-Diagram of a Crystalline Protein - Determination of the Solubility of Concanavalin a by a Microquantitation Assay,* Mikol, V.; Giege, R., *Journal of Crystal Growth* **1989,** 97, (2), 324-332.
21) *Thermal Methods for Crystallizing Biological Macromolecules,* Dematteі, R. C.; Feigelson, R. S., *Journal of Crystal Growth* **1993,** 128, (1-4), 1225-1231.
22) *Interactions in undersaturated and supersaturated lysozyme solutions: Static and dynamic light scattering results,* Muschol, M.; Rosenberger, F., *Journal of Chemical Physics* **1995,** 103, (24), 10424-10432.

CHAPTER 4

SCREENING FOR PHYSICAL STABILITY OF A NEUTRAL CELLULASE USING SELF-INTERACTION CHROMATOGRAPHY

The final stage of research on the SIC project involved a joint collaboration and internship with Genencor International. The primary objective of this collaboration was to investigate the ability of SIC to predict the physical stability of commercially relevant enzymes during formulation development studies. Up until this point only pure crystallized proteins had been analyzed by SIC. Moving away from these model proteins posed unique challenges that required adaptations of our experimental approach. For example, no longer could we dissolve pure protein crystals in solution conditions of our choice. Instead, we were dealing with ultra filtrate (UF) containing protein amidst a milieu of other compounds. Despite the inherent obstacles, we realized that this was a necessary step in the evolution of SIC methodology. Therefore, our work plan with Genencor was designed to begin with a relatively simple and pure enzyme. We would then progress towards more complex enzymes and solution conditions, adapting our approach so as to handle conditions commonly encountered in the industrial

production of such protein formulations. Ultimately, we aimed to determine the limits of applicability of SIC as a formulation screening development tool for industrial systems.

In this chapter, we summarize the research conducted during the summer internship portion of the collaboration with Genencor. During this initial stage, the physical stability of a neutral cellulase (NC) provided by Genencor was studied via SIC as a function of multiple conditions including pH, temperature, buffer species, and common cosolvents. Much of the initial work focused on enzyme-stationary phase coupling chemistry studies and instrument parameter adjustments. Discussion of the results therefore focuses on trends in B, rather than absolute B values. Notably, no absolute B values for NC, or any of the other Genencor enzymes we studied, were available. Therefore, to support the validity of our experimental approach, we compare trends in B with data trends from experimental approaches that are more commonplace in the biotechnology industry, such as bench scale phase stability (precipitation) studies and activity assay measurements.

4.1 Experimental

4.1.1 Determination of extinction coefficient (ε)

Purified NC (250 mL) formulated at 12.5 mg/mL in K_2HPO_4 (0.5 M, pH 7.5) was obtained from Genencor (this sample will be referred to as the NC "stock" sample throughout this chapter). The absorption of serial dilutions between 0.6 and 0.1

mg/mL were measured at 280 nm in a Genesys 10uv spectrophotometer (Thermo Spectronic, Rochester, NY). Each NC dilution was run only once. Data points were fitted to a linear equation with the Y-intercept forced through zero (R= 0.999).

4.1.2 Immobilization of NC to SIC stationary phase

The following procedure describes NC-Formyl particle coupling procedures for five individual trials. Aliquots (5.0 mL) of NC stock solution were pH adjusted with either 5% ACTE or K_2HPO_4 to obtain pH values in the range of 7.2 - 7.9 and K_2HPO_4 concentrations in the range of 0.5 – 1.0 M. Five sets of Formyl particles (400 μL each) were washed four times with 1.2 mL portions of K_2HPO_4 solution (0.5-2.0 M, pH 7.2-7.9). Exact conditions for both the wash solutions and the NC solutions are listed in Table 4.1. Supernatant from each washed particle sample was removed and replaced by one of the NC solutions described above (1.2 mL each). The slurry was hand mixed (20 sec) and centrifuged briefly (10 k rpm, 30 sec). Supernatant (15 μL) was removed and diluted to 250 μL with K_2HPO_4 solution (1.0 M, pH 8.0). The concentration (pre-coupling) of NC was measured at 280 nm using the K_2HPO_4 solution (1.0M, pH 8.0) as a blank. $NaCNBH_3$ (12 mg) was added to each NC-Formyl particle mixture. Each reaction vial was placed in a room temperature (21 ± 2°C) rotary mixer for 90 min. After brief centrifugation (10k rpm, 30 sec) supernatant was removed, diluted, and analyzed by UV absorption as described above. This measurement indicated the post-coupling concentration of NC remaining in solution. The difference between the

pre- and post-coupling absorbance values was used to quantity the amount of NC covalently immobilized to the Formyl particles. The NC-Formyl particles were washed with 1.2mL K_2HPO_4 (1.0 M, pH 8.0) four times. The supernatant was removed and replaced with 1.2 mL ethanolamine (1.0 M, pH 8.0) and $NaCNBH_3$ (10 mg). The reaction vial was returned to the rotary mixer for another 90 minutes. Afterwards, the NC-Formyl particles were again washed with 1.2 mL of K_2HPO_4 (0.1 M, pH 8.0) and stored at 4°C. Protein free columns (used in the dead column experiments) were capped exclusively with ethanolamine using the procedure described above.

4.1.3 SIC procedures

All buffers were prepared with 18 MΩ water (Nanopure, Barnstead) and pH adjusted with either NaOH or HCl. The pH was followed using a digital pH meter (UB-5, Denver Instruments). All mobile phases were buffered at pH 8.0 with either K_2HPO_4 (0.05-0.20 M) or Na_2HPO_4 (0.10 M), except for the results in Figure 4.4 where the pH was varied from 5.0-8.0. NC and acetone injection samples were dissolved at 12.5 mg/mL and 2% (v/v), respectively. The SIC column consisted of Teflon FEP Tubing (1/8" outer diameter, 1/16" inner diameter, Upchurch) fitted with a stainless steel frit (2 μm pores, Upchurch). The column was conditioned after packing for several hours with K_2HPO_4 (0.1 M, pH 4.5) at 0.15 mL/min, after which, no further bed settling was observed. Generally, for all experiments where cosolvent concentrations were incrementally increased,

one buffer with no cosolvent and another with the maximum cosolvent concentration used were mixed online by the HPLC pump to achieve the entire range of desired conditions. Mobile phases for dead column experiments mimicked those of the NC-SIC experiments with the one exception of a constant 5% NaCl concentration for the purpose of suppressing electrostatic interactions between mobile phase analytes and the ethanolamine capped stationary phase. Chromatographic data were collected on Hewlett Packard 1050 and 1090 HPLCs and analyzed using Chemstation software. Mobile phases were degassed online. NC and acetone sample (1.0 μL) were injected using a Hewlett Packard 1050 autosampler and analyzed at a flow rate of 80 μL/min (except where otherwise noted). Temperatures were controlled with an external digital column heater (HP 1050) (TC-50, Eppendorf) or built in temperature controlled column compartment (HP 1090). Eluting samples were detected by UV absorption at 280nm. LYZ samples were run in quadruplicate, and acetone samples in triplicate

4.1.4 Dialysis of NC ultra filtrate

Precipitated NC ultra filtrate (500mL, pH 6.00) was obtained from Genencor. The material was stirred to obtain a slurry. Four slurry samples (5 mL each) were transferred into 10 kDa MWCO dialysis tubing (Pierce). Each sample was dialyzed for 24 hours against 500 mL of a Na_2HPO_4 buffered solution (0.1M, pH 8.0) containing one of the following sodium citrate ($Na_3C_6H_5O_7$) concentrations:

0.0M, 0.1M, 0.2M, or 0.3M. Aliquots (3.5 mL) of the dialyzed slurry samples were transferred to scintillation vials. These samples were photographed after settling for 24 hours at room temperature (21 ± 2°C).

4.1.5 Activity Measurements

All NC activity assays were performed at Genencor. All assayed samples were prepared with NC ultra filtrate. Solution conditions for these experiments matched those of the SIC experiments. Cosolvents and buffers were added directly to ultra filtrate samples (10 mL each). Sample pH was adjusted with either 10% NaOH or 5% HCL. Enzyme activity was measured by an endpoint assay. The substrate used was para-nitrophenylcellobioside (pNPC), from Megazyme International Ireland Ltd. (Wicklow, Ireland). pNPC was prepared at 100 mg/ml in dimethyl sulfoxide (DMSO). The assay buffer consisted of Na_2PO_4 (0.1 M, pH 8.0). Substrate solution was prepared by diluting 5 μL of the above pNPC solution per mL assay buffer. A dilution factor of 500 parts assay buffer to 1 part sample was used for all assayed samples. The reaction was started by the addition of 20 μL of suitably diluted sample into 180 μL of substrate solution. The reaction was allowed to proceed for 8 minutes at 30°C. Upon hydrolysis of pNPC by NC, *o*-nitrophenol was released, generating a yellow colored solution. The color intensity was quantified by measured absorbance at 405 nm. A standard curve was made by the same method, using NC enzyme samples of known activity. A regression equation determined from the standard curve, was used to calculate the activity of the unknown NC samples. Activity values were calculated by

multiplying the absorption of the assayed sample by 500 and the necessary dilution correction factor to account for the difference in the final volume of each sample that resulted from buffer, NaCl, and pH adjustment. The assay was run in an automated format on a Konelab Aqua 20 auto analyzer (Thermo Electron Corporation, Waltham, MA).

4.2 Results and Discussion

4.2.1 Optimization of NC-Formyl coupling chemistry

At the current stage of the SIC project, the coupling density (CD) of protein covalently immobilized to the stationary phase particles was still being calculated from UV measurements. As a first step in this process, the proteins' extinction coefficient (ε) must be experimentally determined. Figure 4.1 demonstrate that ε of NC was measured as 1.59 mL/mg cm at 280nm. This value was used to quantify the difference in absorbance between the pre- and post- coupling concentration of NC in solution. The result is a CD in units of mg of NC/ mL of Formyl particles.

The NC-Formyl particle CD was optimized by screening conditions within a set of solution parameters that proved successful for previously studied proteins (see Chapter 2 and 3). The results of this study are summarized in Table 4.1. Of the five conditions tested, trial 5 yielded the highest CD (12.7 mg NC/ mL Formyl particles). Trial 2 and 4 both yielded a CD of 12.0 mg NC/mL Formyl particles.

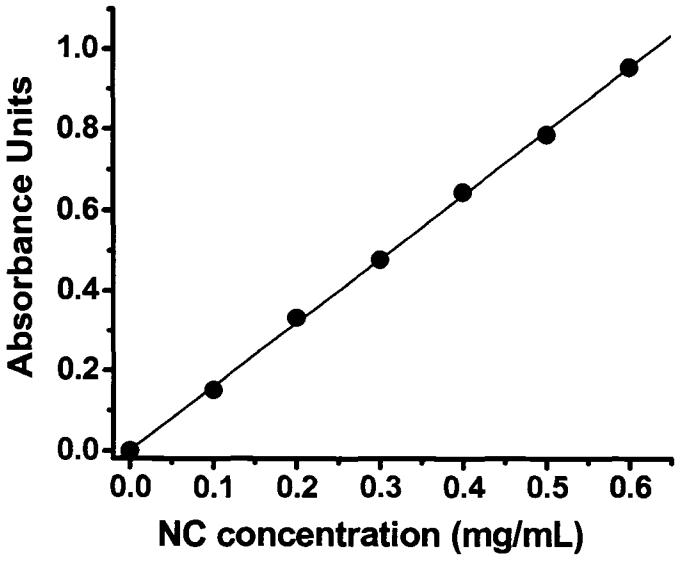

Figure 4.1. NC calibration curve for the determination of the molar extinction coefficient (ε) at 280 nm. NC dilutions (black dots) were produced from a stock sample (12.5 mg/mL). The linear fit (red line) was forced through zero (R= 0.999). ε = 1.59 mL/ mg cm.

Table 4.1: Summary of NC-Formyl particle coupling studies. The term molecs/m^2 refers to the number NC molecules/m^2 of Formyl particle surface area.

Trial #	Wash Solution		Stock NC Sample		CD (NC/Formyl)	
	K_2HPO_4 (M)	pH	K_2HPO_4 (M)	pH	mg/mL	molecs/m^2
1	0.5	7.2	0.5	7.2	2.60	5.10×10^{15}
2	1.0	7.9	1.0	7.9	12.0	2.37×10^{16}
3	2.0	7.0	0.5	7.2	7.58	1.48×10^{16}
4	1.0	7.4	1.0	7.9	12.0	2.37×10^{16}
5	1.0	7.9	1.0	7.9	12.7	2.51×10^{16}

Since only one measurements per trial was obtained it is unclear whether there is any statistical difference between these three CDs. Overall, the results in Table 4.1 suggest that NC-Formyl particle CD is optimized when the particles have been washed with 1.0 M K_2HPO_4, pH 7.4-7.9 and the stock NC sample conditions have been adjusted to 1.0 M K_2HPO_4, pH 7.9. For consistency, all subsequent batches of NC-Formyl particles were prepared according to the conditions used in trial 5. Notably, the CDs in Table 4.1 are reported in units of mg of NC/mL Formyl particles and in units of NC molecules/m^2 Formyl particle surface area. The latter units represent ρ, which is directly used in the calculation of B (see Equation 1.5).

4.2.2 Introducing the concept of SIC to Genencor

An important goal of the collaboration work plan with Genencor was to demonstrate and understand how the NC-SIC data would correlate with bench scale stability studies and activity assay measurements. Figure 4.2 served as a visual aide for bridging the gap between our unique experimental approach (SIC) and those more commonly employed in industrial biotechnology settings. Four buffer conditions varying only in sodium citrate ($Na_3C_6H_5O_7$) concentration were investigated by SIC and bench scale precipitation studies for their effects on NC physical stability. Figure 4.2 clearly demonstrates how $Na_3C_6H_5O_7$ induced reductions in NC physical stability were observed with SIC as increases in both the width and retention time at maximum absorption of the NC peak. This enhanced NC self-interaction is then conveyed to the SIC novice through the

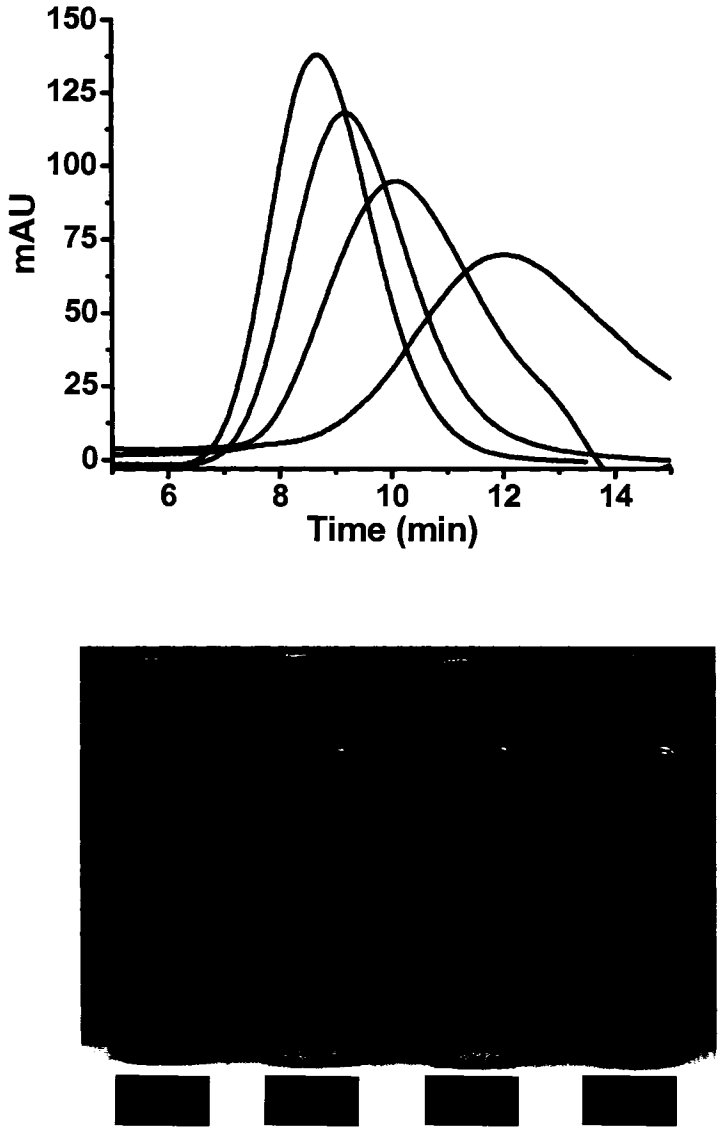

Figure 4.2. Correlation between NC elution profile (chromatograms) and bench scale precipitation behavior (photograph) as a function of sodium citrate ($Na_3C_6H_5O_7$). Solution conditions were Na_2HPO_4 (0.1 M, pH 8.0) containing 0.0 M $Na_3C_6H_5O_7$ (black line), 0.1 M $Na_3C_6H_5O_7$ (red line), 0.2 M $Na_3C_6H_5O_7$ (green line), or 0.3 M $Na_3C_6H_5O_7$ (blue line), at ambient temperature (21 ± 2°C). The colors in the chromatogram correspond with the colors beneath each vial in the photograph.

photographs of bench scale NC stability studies (Figure 4.2). Here, the fraction of precipitated NC scales with $Na_3C_6H_5O_7$ concentration. The Citrate anion ($C_6H_5O_7^{3-}$) demonstrates stronger preferential interactions with water than sulfate (SO_4^{2-}), which is ranked first in the Hofmeister series as the strongest salting-out anion.[1, 2] The hydration of $C_6H_5O_7^{3-}$ reduces the amount of free water, therefore increasing the effective concentration of the protein (NC in this case). The outcome is often supersaturation and subsequent precipitation of the protein, consistent with our observations for NC in Figure 4.2. Due to the extreme salting out nature $C_6H_5O_7^{3-}$, further studies using this particular buffer species were not pursued. Notably, all subsequent discussions of NC-SIC data are conducted in terms of cosolvent induced trends in B, which are directly calculated from NC elution profiles such as the ones observed in Figure 4.2.

4.2.3 Effect of NC-SIC column parameters on NaCl induced trends in B

Figure 4.3 demonstrates the effect of NaCl on B and the effect of NC-SIC column parameters such as length, CD, and temperature, on the strength of the NaCl induced trend in B. In all cases, the addition of 5% NaCl to the mobile phase shifts B towards higher values, thus indicating enhanced physical stability. Notably, NaCl is classified as a mild salting out agent.[3] It should therefore enhance protein-self interaction, and shift B towards lower values. While somewhat counterintuitive, our results are not one of a kind. Similar NaCl induced trends in B [4, 5] and solubility [6, 7] have been previously reported. The

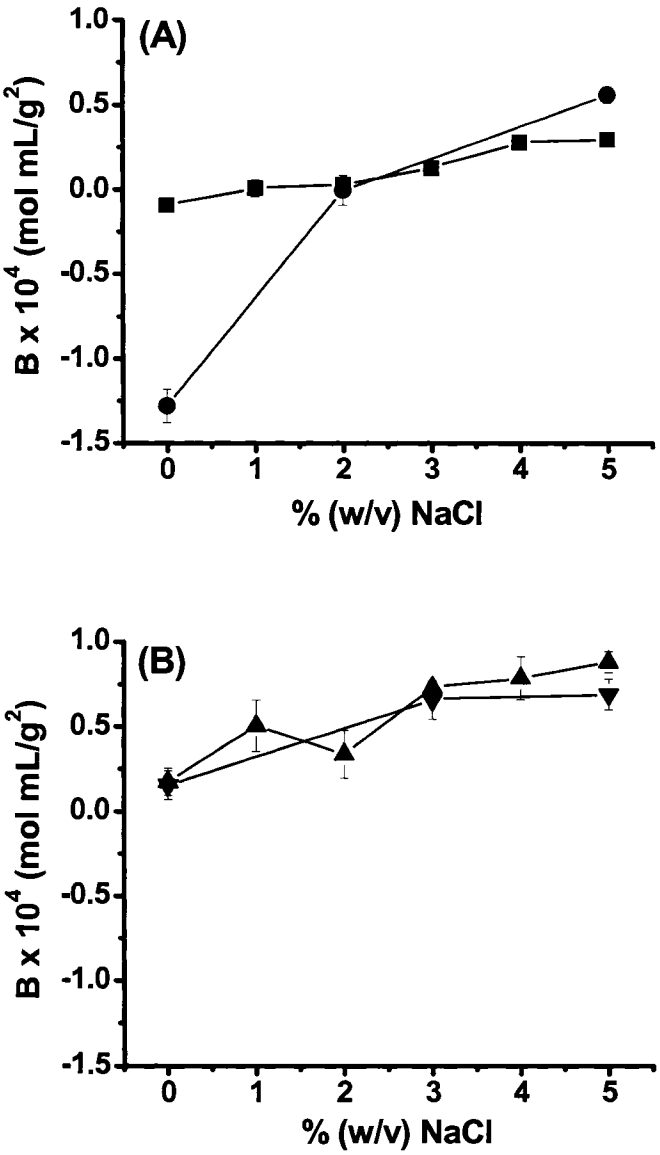

Figure 4.3. B of NC as a function of NaCl and the effects of NC-column parameters on the NaCl induced trend in B. Buffer conditions were (0.1 M, K_2HPO_4) (A and B). A) Constant temperature (19°C, all symbols), Column lengths and CDS were 25cm and 1.65 x 10^{16} NC molecules/m^2 Formyl particle surface area (black squares) or 16cm and 3.51 x 10^{16} NC molecules/m^2 Formyl particle surface area (red circles). B) Constant column length and CD of 22cm and 2.75 x 10^{16} NC molecules/m^2 Formyl particle surface area (all symbols). Temperatures was 15°C (green triangles) or (10°C, upside down blue triangles). Axes in (A) and (B) are scaled the same to facilitate comparison. Lines connecting data points have been added to help guide the reader's eye.

extent to which B is raised by the addition of NaCl is, however, largely dependent on the column length and CD. In Figure 4.3A, two different columns were used that varied in length and CD. The column temperature, on the other hand, was a constant 19°C. The data indicate that the longer column (25 cm) with a lower CD (1.65×10^{16} NC molecules/m^2 Formyl particle surface area) was more sensitive to the NaCl induced trend in B than the shorter column (16 cm) with the higher CD (3.51×10^{16} NC molecules/m^2 Formyl particle surface area). In Figure 4.3B, a single column was used at two different temperatures (10 and 15°C). The data here indicate that a medium column length (22 cm) and CD (2.75×10^{16} NC molecules/m^2 Formyl particle surface area) yielded a mid range sensitivity to the NaCl induced trend in B.

In terms of column length and CD, the data in Figure 4.3A and 4.3B suggest that longer columns lead to enhanced sensitivity of cosolvent (here NaCl) induced changes in B. The effect of CD is more difficult to assess. We were unable to vary column length while holding the column CD constant due to a limited amount of particles. Notably, the conditions for trial 5 in Table 4.1 were used to produce all three batches of particles discussed in Figure 4.3A and 4.3B. The average CD for these batches is $2.64 \pm 0.94 \times 10^{16}$ NC molecules/m^2 Formyl particle surface area. We thus concluded that the observed differences in CD represented normal batch-to-batch variability and controlling particle batch size, and therefore column length, would be the more feasible approach to optimization. In terms of column temperature, we observed a retrograde

temperature dependent physical stability of NC in the range of 15-19°C, but not in the rage of 10-15°C. Under all conditions, B values were raised by the addition of up to 5% NaCl. These data are consistent with results from independent stability studies (performed at Genencor) that reported reduced precipitation and increased activity levels of NC as a function of NaCl added to the ultra filtrate. Therefore, it appears that the NaCl induced trend in NC physical stability is preserved both in the presence and absence of the ultra filtrate components.

4.2.4 pH and temperature induced trends in B

Independent studies at Genencor reported that the activity of NC in its ultra filtrate displayed retrograde temperature dependence from 4 to 37°C and was largely independent of changes in pH between pH 5.0 and 8.0. SIC studies of these reported properties are demonstrated in Figure 4.4. The data indicated that B of NC was shifted to lower values by raising the NC-SIC column temperature from 17-21°C. The B data also lacked any significant pH dependent trend. The one exception was a reduction in B when the pH was increased from 7.0 to 8.0 at 17°C. The two B trends obtained at 19°C indicate the day-to-day reproducibility of the SIC experimental approach. The pH 6.0 and pH 8.0 data points are statistically similar. The difference in the data points obtained at pH 5.0 does indicate some variability, but it is not significant enough to change the conclusions drawn from this study.

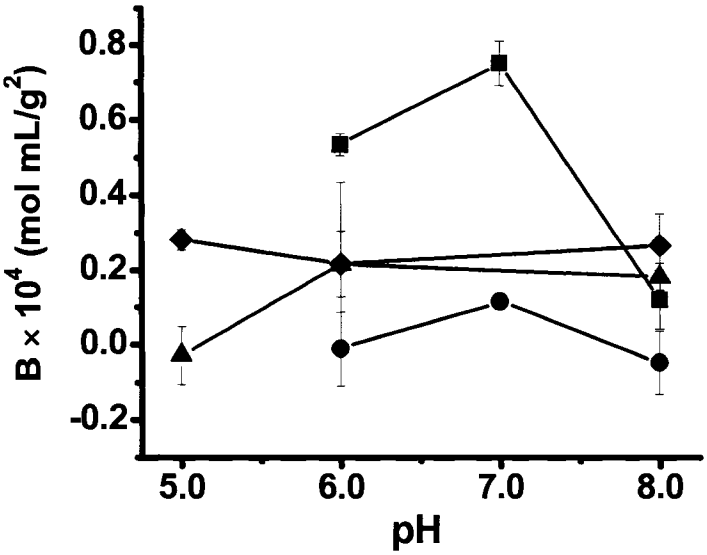

Figure 4.4. pH and temperature induced trends in B of NC. Solution conditions were K_2HPO_4 (0.1M) at 17°C (black squares), 19°C (green triangles and blue diamonds, 21°C (red circles). Lines connecting data points have been added to help guide the reader's eye. The column length and CD were16cm and 3.51 x 1^{16} NC molecules/m^2 Formyl particle surface area, respectively.

4.2.5 Saccharide induced trends in B

Saccharides are commonly used cosolvents for industrial and pharmaceutical protein formulations.[8, 9] The degree of structure stabilization afforded by this class of molecules is concentration and molecular weight dependent. Both of these trends are apparent in the NC-SIC data presented in Figure 4.5. Here, NC physical stability is enhanced by the addition of cosolvent (up to 1.0M), as indicated by positive shifts in B. The data also indicate that sucrose (a disaccharide) is a more effective stabilizer than glucose (a monosaccharide). Furthermore, Figure 4.5 again confirms the retrograde temperature dependence of NC stability in the rage of 15°C -19°C.

Saccharide based cosolvents stabilize biological molecules by altering short-range, attractive hydrophobic effects.[10] At low ionic strengths intermolecular distances generally exceed the range of hydrophobic effects due to much longer-range electrostatic repulsion. Increasing the solution ionic strength suppresses electrostatic interaction, enabling reductions in intermolecular distances to within the range where hydrophobic interaction will dictate protein self-interaction. Only under such conditions will cosolvent induced stabilization be reflected in B trends Therefore, the buffer used for this particular set of experiments (and subsequent cosolvent experiments) contained 5% NaCl (0.86 M). The exact salt is not as important as the total ionic strength of the solution. However, strong salting out agents, such as $C_6H_5O_7^{3-}$ or SO_4^{2-} should be avoided since they may readily precipitate the protein. In the case of NC and NaCl, the addition of 5% NaCl

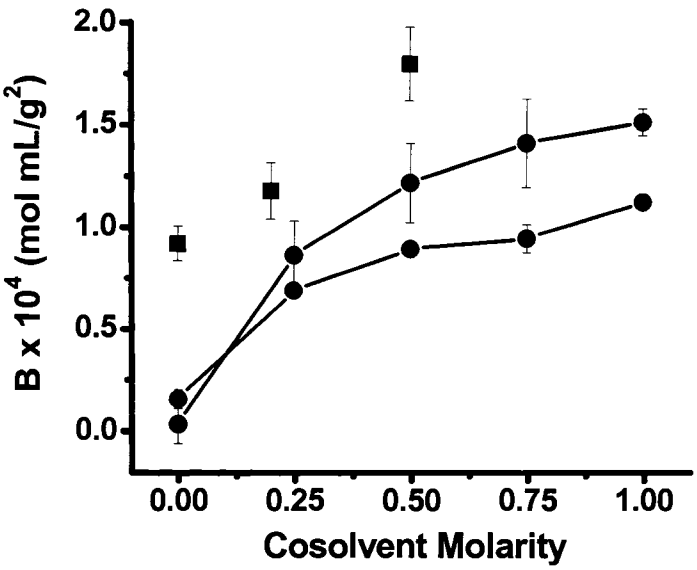

Figure 4.5. Glucose (red circles) and Sucrose (black circles and squares) induced trends in B. Solution conditions were K_2HPO_4 (0.1 M, pH 8.0) containing 5% NaCl at 15°C (black squares) or 19°C (black and red circles). Lines connecting data points have been added to help guide the reader's eye. Column length and CD were 24cm and 5.00 x 10^{16} NC molecules/m^2 of Formyl particle surface area.

4.2.6 Arginine induced trends in B

Arginine is a unique structure stabilizing amino acid by virtue of its guanadinium side chain.[11] As with the saccharides, 5% NaCl was added to all buffer conditions to provide the necessary electrostatic shielding such that cosolvent induced changes in enzyme hydrophobicity will affect intermolecular interactions. The data in Figure 4.6 show that stabilization conferred by arginine (in terms of increasing B) is greatest at 0.2M and then falls and levels off between 0.4 and 0.5M. Arginine interacts with both charged and hydrophobic protein surface patches (as discussed in Chapter 2). As the degree of these motifs change, so do the protein-arginine interactions. Thus, it is possible that B is raised by the addition of up to 0.2 M arginine because NC-arginine interactions are replacing attractive NC self-interaction. Above this concentration, the surface of NC may become saturated with arginine and the remaining free arginine in solution may then be acting as a salting out agent, decreasing B. However, it is still somewhat unclear as to why B levels off between 0.4 and 0.5 M arginine.

The arginine data sets in Figure 4.6 again address the issue of NC-SIC column length and CD. For this set of experiments, the two columns lengths were within 1 cm of each other (27 cm vs. 28 cm) while immobilization densities differed by a factor of 2.3 (1.48 vs. 3.51 x 10^{16} NC molecules/m^2 Formyl particle surface area). The overall strength of the arginine induced trend in B was larger with the lower CD column. Similar behavior was observed in Figure 4.3. The primary difference between the two studies, in terms of experimental parameters, is that a flow rate

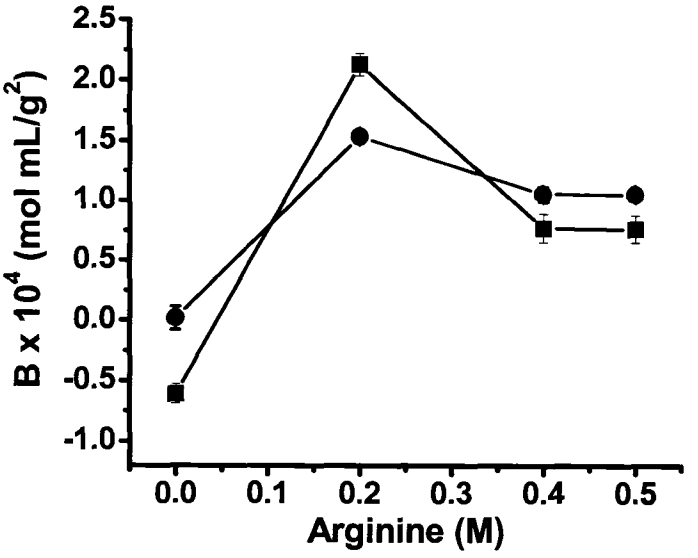

Figure 4.6. Arginine induced trends in B as a function of column length and CD. Solution conditions were K_2HPO_4 (50 mM, pH 8.0) containing 5% NaCl at 19°C. Column lengths and CDs were 27cm and 1.48 x 10^{16} NC molecule /m^2 Formyl particle surface area (black squares) or 28 cm and 3.51 x 10^{16} NC molecules/m^2 Formyl particle surface area (red circles). Lines connecting data points have been added to help guide the reader's eye.

of 80μL/min was used for the NaCl studies while a flow rate of 60 μL/min was used for the arginine studies. The data in both figures agree that increased residence time of mobile phase NC on the column enhances the sensitivity of the technique and that higher immobilization densities do not necessarily correlated with enhanced sensitivity of B trends. Notably, the flow rate for all other NC-SIC experiments was kept at 80 μL/min due to substantial NC peak broadening and extended analysis times at 60 μL/min.

4.2.7 Polyol induced trends in B

Polyols are another class of stabilizing cosolvents commonly added to protein-based formulations.[12] They too display stabilizing strengths that are molecular weight and concentration dependent. The sorbitol and propylene glycol induced trends in B of NC are shown in Figure 4.7 and 4.8, respectively. In Figure 4.7, 5% NaCl was present in all mobile phase conditions to suppress electrostatics as discussed in the previous sections. The data show that increasing the K_2HPO_4 concentration from 0.1 to 0.2 M has a salting-out effect, lowering B and thus the physical stability of NC. A non-monotonic trend in B is obtained from the addition of sorbitol at the 0.2 M K_2HPO_4 buffer conditions. At the 0.1 M K_2HPO_4 buffer condition B is raised by the addition of up to 15% sorbitol. The majority of the trend in B is observed between 5% and 10% sorbitol.

In Figure 4.8, up to 15% propylene glycol was added to solution conditions of constant K_2HPO_4 concentration (50 mM) and either 0% or 5% NaCl. For both

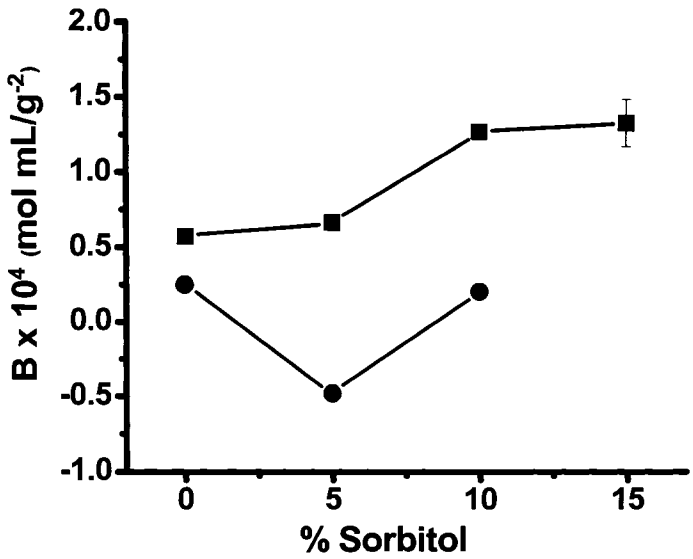

Figure 4.7. Sorbitol induced trends in B at different K_2HPO_4 concentrations. Buffer conditions were K_2HPO_4 (0.1 M, pH 8.0) (black squares) or K_2HPO_4 (0.2 M, pH 8.0) containing 5% NaCl (red circles) at 19°C. Column length and CD were 27cm and 1.93 x 10^{16} NC molecules/m^2 of Formyl particle surface area, respectively. Lines connecting data points have been added to help guide the reader's eye.

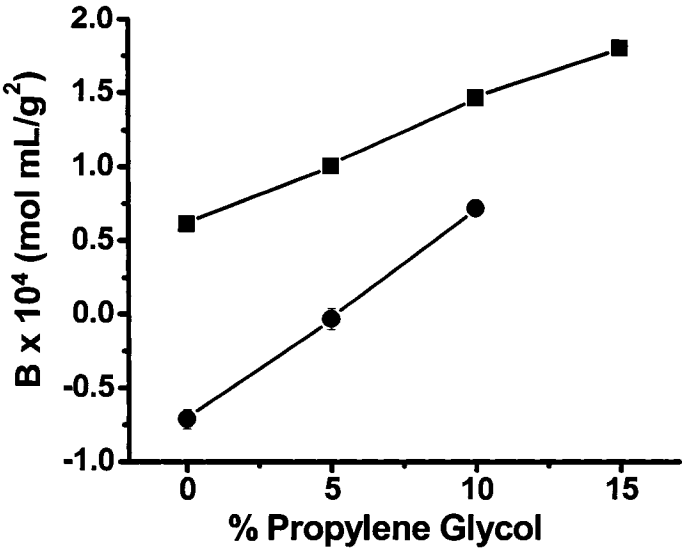

Figure 4.8. Propylene glycol induced trends in B in the presence and absence of 5% NaCl. Buffer conditions were K_2HPO_4 (50 mM, pH 8.0) containing 0% NaCl (red circles) or 5% NaCl (black squares) at 19°C. Column length and CD were 27cm and 1.93 x 10^{16} NC molecules/m^2 of Formyl particle surface area, respectively. Lines connecting data points have been added to help guide the reader's eye.

data sets the propylene glycol induced trend in B scales more evenly than with sorbitol. The presence of 5% NaCl shifts to B to higher values supporting previous results (Figure 4.3). An interesting outcome of the polyol studies was the observation that propylene glycol effectively increases B independent of the solution ionic strength, at least between 0%-5% NaCl. These results are contrary to those obtained for the saccharides and arginine (discussed both in this Chapter and in Chapter 4). Propylene glycol, unique from any of the other cosolvents we have investigated, is a water-soluble organic solvent. It is one of the most common organic solvents found in small-molecule injectable and oral formulations.[13] Unfortunately, propylene glycol is not one of the common polyols added to protein formulations. Notably, Arakawa et al. recently reported that propylene glycol effectively protected Ciliary Neurotrophic Factor from agitation induced aggregation but not from thermally induced aggregation.[14] In the absence of more literature references, or further studies on our behalf, it is difficult to form conclusive arguments regarding the propylene glycol induced shifts in B shown in Figure 4.8. Nonetheless, we speculate that propylene glycol alters bulk water properties (i.e. structure, ordering, polarity, dielectric constant) to an extent that affects intermolecular interactions even in the presence of long-range electrostatics.

Formulation development scientists are often more concerned with the percent of the formulation space occupied by a cosolvent rather than the cosolvent molarity. However, to compare the relative effectiveness of cosolvents it is more useful to

convert percent into molarity. For example, 15% propylene glycol and 15% sorbitol convert to 1.97 M and 0.82 M, respectively. In the presence of 5% NaCl these cosolvent concentrations raised B by 1.19 ± 0.02 x 10^{-4} mol mL/g^2 (from 0.61 ± 0.02 x 10^{-4} to 1.80 ± 0.01 x 10^{-4} mol mL/g^2) for propylene glycol and 0.75 ± 0.16 x 10^{-4} mol mL/g^2 (from 0.57 ± 0.04 x 10^{-4} to 1.32 ± 0.16 x 10^{-4} mol mL/g^2) for sorbitol. These numbers can again be converted to show that B is increased by 0.60 x 10^{-4} mol mL/g^2 per mole of propylene glycol and 0.91 x 10^{-4} mol mL/g^2 per mol of sorbitol. The SIC data therefore reflect the expected trend that sorbitol ($C_6H_{14}0_6$, 182.17 g/mol) is a stronger stabilizing cosolvent (in terms of trends in B) than propylene glycol ($C_3H_8O_2$, 76.10 g/mol).

4.2.8 Summary of formulation parameter space investigated by SIC

Figure 4.9 combines most of the formulation parameter space investigated during the NC-SIC studies into one graph. Not included are the pH (Figure 4.4) and temperature studies (Figure 4.4 and 4.5). The 10% and 15% propylene glycol data points have also been excluded because they convert to 1.3 M and 2.0 M respectively. Due to variation in column length and CD used through out these studies, comparison between absolute B values is not appropriate. Instead, the focus is on the overall cosolvent induced trends in B. Together, the graph and table in Figure 4.9 represent a simple method presenting NC trends in B for a large amount of formulation parameter space. More extensive studies of this nature would enable three-dimensional mapping of physical protein stability (in terms of trends in B) in a rapid and rational manner.

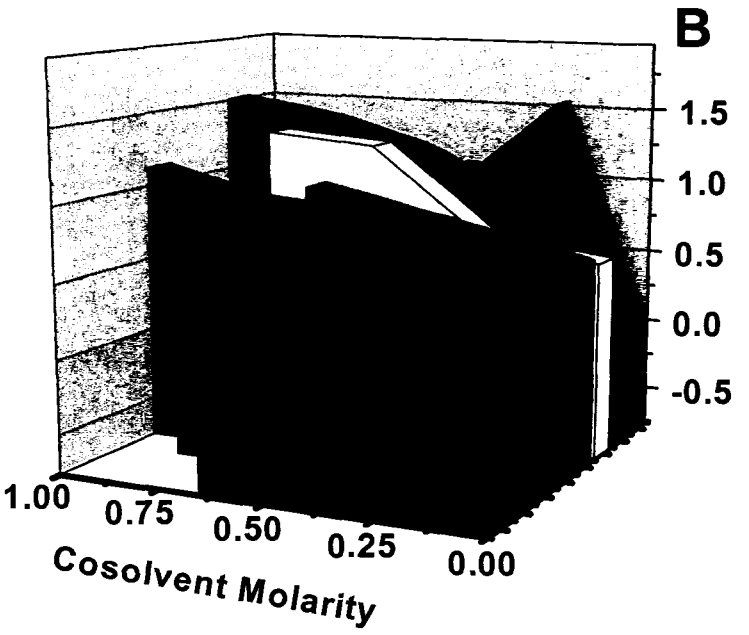

Cosolvent, maximum (M), (increments)	K_2HPO_4 (M)	NaCl
Propylene Glycol , 0.7		
NaCl , 5% (+1%)	0.1	
Propylene Glycol , 0.7	0.05	5%
Sorbitol , 0.8 (+0.2)	**0.1**	**5%**
Sucrose , 1.0 (+ 0.25)	0.1	5%
Arginine , 0.5 , (+0.1)	0.1	5%

Figure 4.9. Summary of formulation parameter space investigated during NC-SIC studies (see text for exceptions). All data was collected at 19°C. Colors in the graph correspond to those in the table.

4.2.9 NC activity assay data

NaCl, glucose, propylene glycol, and sucrose induced trends in NC activity were investigated. Buffers and cosolvents were added to assayed samples so as to mimic those conditions investigated during the NC-SIC experiments. All activity assay experiments, except the sucrose studies, included either multiple runs of a single set of samples or comparison between data sets from multiple sample sets. Consequently, The sucrose results are omitted from the following discussion that focuses on day-to-day and sample-to-sample reproducibility of activity assay measurements. It is important the stress that all NC activity assay samples were prepared from the NC ultra filtrate while all NC-SIC studies were performed with purified NC. The ultra filtrate is a complex milieu of cosolvents that could potentially affect NC-self interaction. At this point in the NC studies, it was still unclear how the ultra filtrate materials affected the physical stability NC.

Figure 4.10 demonstrates that the addition of up to 5% NaCl to NC ultra filtrate induced two completely different trends in NC activity (one increasing and one decreasing). The four data sets were generated from two sample sets. Each data trend was measured on a different day. The two data sets within each NaCl induced trend are statistically similar, having overlapping error bars and percent coefficients of variation (%CVs) ranging from 0.3 to 3.9%. Conversely, day-to-day %CVs for the three replicate analyses of sample set 1 range from 2.2 to 5.5%, and result in two entirely different NaCl induced trends in activity. Glucose induced trends in NC activity were also generated from two sample sets and run

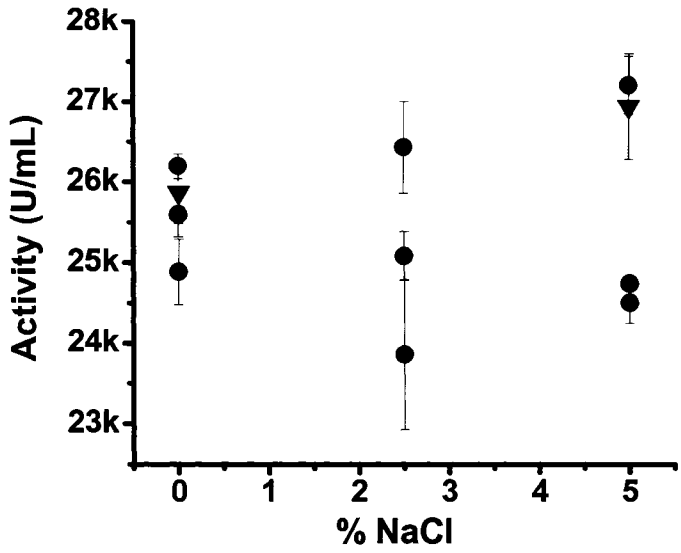

Figure 4.10. NaCl induced trends in NC activity. Buffer conditions were K_2HPO_4 (0.1 M, pH 8.0) containing 5% NaCl at 21 ± 2°C. Circular data points were obtained from sample set 1 and inverted triangular points from set 2. Chronological order of measurement from first to last was black circles, red circles, green circles, and inverted blue triangles).

on separate days (Figure 4.11). Again, considerable day-to-day and sample-to-sample variability is observed. The %CVs between the three data trends range from 0.6 to 5.2%. Overall, there is no clearly identifiable glucose induced trend in NC activity. The propylene glycol induced trends in NC activity are shown in Figure 4.12. Both trends were generated from a single sample set. Here, the data indicate that NC activity is reduced by the addition of up to 10% propylene glycol and then increased by further increasing the propylene glycol concentration from 10 to 20%. For the samples containing 0%-15% propylene glycol the %CVs for replicate measurements of individual data points ranged from 0.7 to 4.1%. Day-to-day %CVs ranged from 0.9 to 3.3%. The two data points for the 20% propylene glycol samples yield activity values of 25.9 k ± 1.1 k and 54.6 K ± 1.4 k U/mL (a spread of 28.7 k ± 1.8 k U/mL). This converts to a 29.7% CV. While this last point likely represents an extreme case, day-to-day variability as high as 8-10% CV is not uncommon for the current enzymatic assay approach.

4.2.10 SIC vs. Activity Assay

An important goal of the NC studies was to determine whether trends in B (measured by SIC) would correlate with trends in NC activity. Intuitively, enzymatic activity trends should correlate with B trends. Shifts toward larger B values indicate concomitant shifts towards enhanced enzyme-solvent interaction. This in turn leads to enhanced enzyme solubility, and therefore activity. Again we stress that all SIC studies were performed with purified NC while activity studies were performed with NC in the presence of unpurified ultra filtrate. Graphically

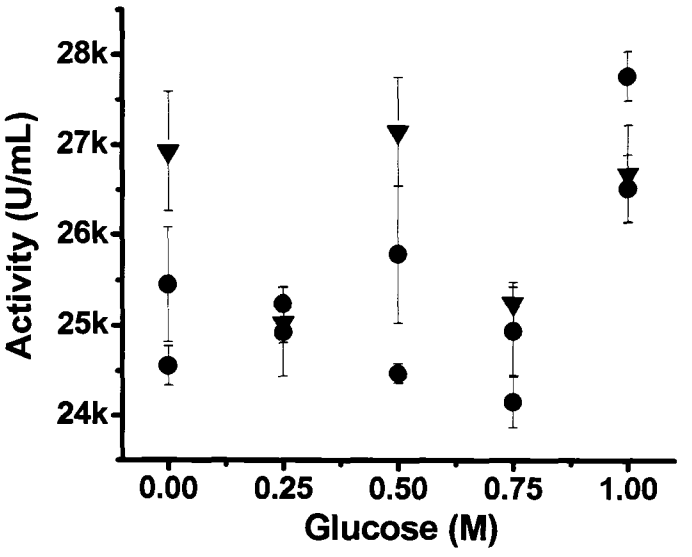

Figure 4.11. Glucose induced trends in NC activity. Buffer conditions were K_2HPO_4 (0.1 M, pH 8.0) containing 5% NaCl at 21 ± 2°C. Circular data points were obtained from sample set 1 and inverted triangular points from set 2. Chronological order of measurement from first to last was black circles, red circles, and inverted blue triangles.

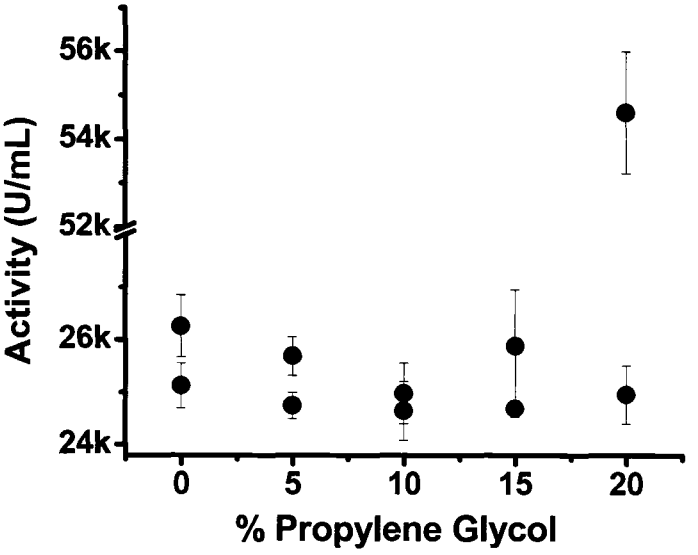

Figure 4.12. Propylene glycol induced trends in NC activity. Buffer conditions were K_2HPO_4 (50 mM, pH 8.0) containing 5% NaCl at 21 ± 2°C. Both data trends were obtained from a single sample set. Chronological order of measurement from first to last was black circles and then red circles.

combining SIC B data and activity assay data facilitates meaningful comparison between the two experimental approaches. The data in Figures 4.13-4.15 are represented by graphing the activity assay scale on the left Y-axis and the SIC scale on the right, with a common X-axis. The end points of the data sets are easily matched by adjusting the scales of the Y-axes. The agreement between interior data points, and the relative amount of error associated with each approach are respectively discussed as measures of correlation between B and activity and measures of sensitivity between SIC and the activity assay. The correlation between sucrose induced trends in B and activity was the best of any cosolvent system tested (Figure 4.13). The data show that all but the 0.75 M sucrose points are statistically similar. Instinctively, the 0.75 M sucrose assay data point is an outlier. However, this set of assayed samples was only run once, so that point cannot statistically be thrown out. In comparing B and activity values, it is not appropriate to compare %CVs due to the large difference in magnitude of the measured parameters. For example, the assay data point for the 0.50 M sucrose condition was measured as 26.0 ± 0.5 k U/mL (a %CV of 1.9). The corresponding SIC data point was measured as 1.2 ± 0.2 x 10^{-4} mol mL/g^2 (a %CV of 16.7). According to the %CVs the SIC data has a much larger variance for replicate measurements. Conversely, visual examination of the data in Figure 4.13 indicates a much larger error bar associated with the assay data point than with the SIC data point. Determining what percent of the entire data trend (the difference between the highest and lowest measured values) is incorporated by the average error (the average of all error bars within the data

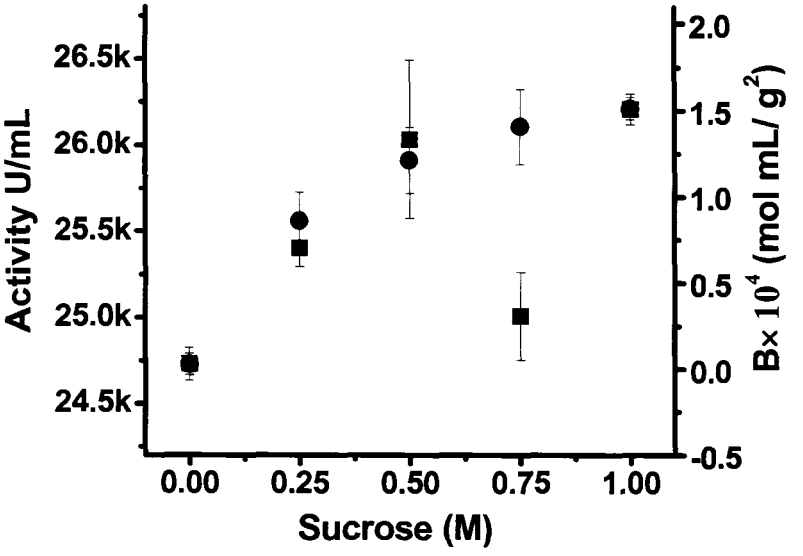

Figure 4.13. Comparison of sucrose induced trends in B (red circles) and activity (black squares) of NC. Buffer conditions were K_2HPO_4 (0.1 M, pH 8.0) containing 5% NaCl at 19°C (red circles) or 21 ± 2°C (black squares).

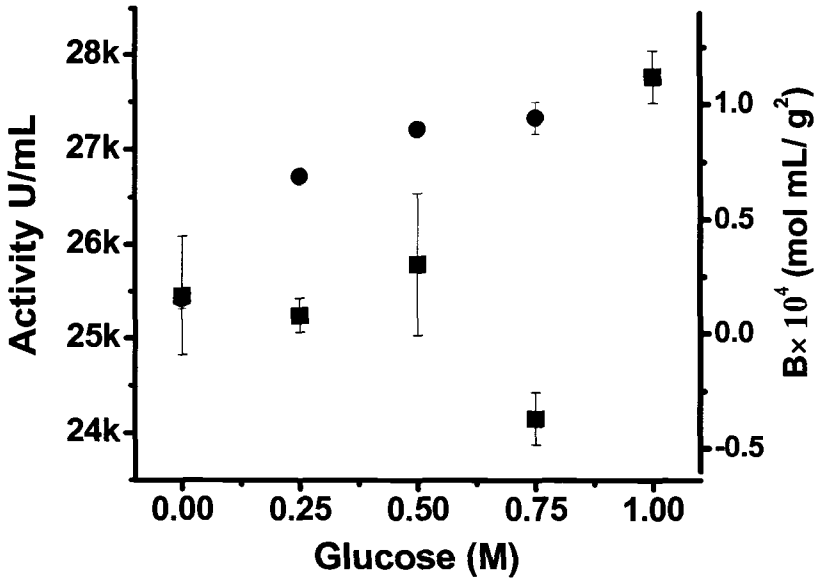

Figure 4.14. Comparison of glucose induced trends in B (red circles) and activity (black squares) of NC. Buffer conditions were K_2HPO_4 (0.1 M, pH 8.0) containing 5% NaCl at 19°C (red circles) or 21 ± 2°C (black squares).

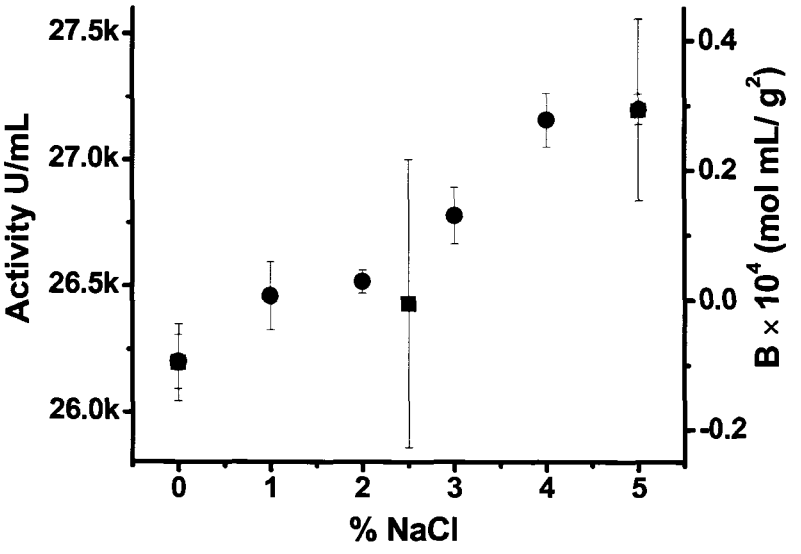

Figure 4.15. Comparison of NaCl induced trends in B (red circles) and activity (black squares) of NC. Buffer conditions were K_2HPO_4 (0.1 M, pH 8.0) containing 5% NaCl, at 19°C (red circles) or 21 ± 2°C (black squares).

trend) makes for a much more useful comparison. For example, the assay data show that adding 1.0 M sucrose increases the activity of NC from 24.7 ± 0.1 k U/mL to 26.2 ± 0.1 k (a change of 1.5 ± 0.1 k U/mL). The average error for the five assayed data points is 0.2 k U/mL. Here, the average error incorporates 13.3% of the entire data trend. The same analysis of the SIC data show an increase in B from 0.0 ± 0.1 to 1.5 ± 0.1 x 10^{-4} moL mL/g^2 with an average error of 0.1 x 10^{-4} moL mL/g^2 (only 6.7% of the entire data trend). Continuing this type of analysis, we see that the glucose induced trends in B and activity are poorly correlated, showing no overlapping of interior data points (Figure 4.14). The average assay error incorporates 11.8% of the total data trend, where as the SIC data incorporates only 3.8%. The correlation of the SIC data with the other two assay data sets for glucose solutions was equally poor. Lastly, Figure 4.15 compares B and activity data trends as a function of NaCl. Here again, the assay data contains relatively larger error bars than the SIC data. B is increased by 0.39 ± 0.05 x 10^{-4} mol mL/g^2 with 12.3 % of this data trend incorporated within the average experimental error. The assay data indicates that NC activity increases by 1.00 k U/mL with a 36.1 % of the data trend being within the average experimental error. For all three cases (Figures 4.13-4.15) SIC appears to be the more sensitive approach in terms of being able to track small changes in NC physical stability via trends in B.

4.3 Conclusions

Trends in B of NC as a function of several commercially relevant solution conditions were studied by SIC. The data indicated that NaCl, sucrose, glucose, sorbitol, and propylene glycol all effectively increased the physical stability of NC, as determined by shifts towards more positive B values. Reduced temperatures also enhanced B, indicating retrograde temperature dependent stability of NC. No pH dependent stability of NC was observed between pH 5.0 and pH 8.0. Parallel assay experiments were used to compare the activity of NC in the complex background of the ultra filtrate to the self-interaction of NC in a much more controlled solution environment. Together, these studies indicated that the SIC approach was capable of measuring minor changes in NC physical stability (in terms of trends in B) that were well within the normal error of the current assay approach. While no established correlation between B and activity exists, empirical results indicated varying degrees of qualitative agreement. The effect of the ultra filtrate on the error associated with the activity measurements or on the self-interaction of NC remains unclear. Attempts to perform SIC of NC in the presence of the ultra filtrate were unsuccessful due to unacceptably high absorbance of the solution at the same wavelength where NC is detected. This works represents the first use of SIC as a formulation development screening tool for a commercially produced enzyme. Continued investigations into other commercial enzymes and increasingly complex solution conditions are necessary to ultimately determine the broadness of applicability of SIC to formulation screening studies in industrial settings.

4.4 Acknowledgments

The author would like to extend gratitude to Beth Fryksdale, Michael Bodo, Douglas Dale, and Dr. Alfred Gaertner for their contributions to the above studies of NC.

4.5 References

1) *Protein-protein interactions in concentrated electrolyte solutions - Hofmeister-series effects,* Curtis, R. A.; Ulrich, J.; Montaser, A.; Prausnitz, J. M.; Blanch, H. W., *Biotechnology and Bioengineering* **2002,** 79, (4), 367-380.
2) *Salting-out of Aqueous Proteins - Phase-Equilibria and Intermolecular Potentials,* Coen, C. J.; Blanch, H. W.; Prausnitz, J. M., *Aiche Journal* **1995,** 41, (4), 996-1004.
3) *Salt Effects on Hydrophobic Interactions in Precipitation and Chromatography of Proteins - Interpretation of Lyotropic Series,* Melander, W.; Horvath, C., *Archives of Biochemistry and Biophysics* **1977,** 183, (1), 200-215.
4) *Interactions and aggregation of apoferritin molecules in solution: Effects of added electrolytes,* Petsev, D. N.; Thomas, B. R.; Yau, S. T.; Vekilov, P. G., *Biophysical Journal* **2000,** 78, (4), 2060-2069.
5) *Protein interactions in solution characterized by light and neutron scattering: Comparison of lysozyme and chymotrypsinogen,* Velev, O. D.; Kaler, E. W.; Lenhoff, A. M., *Biophysical Journal* **1998,** 75, (6), 2682-2697.
6) *Abnormal Solubility Behavior of Beta-Lactoglobulin - Salting-in by Glycine and Nacl,* Arakawa, T.; Timasheff, S. N., *Biochemistry* **1987,** 26, (16), 5147-5153.
7) *Effect of salts on the solubility of thermolysin: A remarkable increase in the solubility as well as the activity by the addition of salts without aggregation or dispersion of thermolysin,* Inouye, K.; Kuzuya, K.; Tonomura, B., *Journal of Biochemistry* **1998,** 123, (5), 847-852.
8) *Protein-Solvent Interactions in Pharmaceutical Formulations,* Arakawa, T.; Kita, Y.; Carpenter, J. F., *Pharmaceutical Research* **1991,** 8, (3), 285-291.
9) *Stability of Protein Pharmaceuticals,* Manning, M. C.; Patel, K.; Borchardt, R. T., *Pharmaceutical Research* **1989,** 6, (11), 903-918.
10) *The Control of Protein Stability and Association by Weak-Interactions with Water - How Do Solvents Affect These Processes,* Timasheff, S. N., *Annual Review of Biophysics and Biomolecular Structure* **1993,** 22, 67-97.
11) *Role of arginine in protein refolding, solubilization, and purification,* Tsumoto, K.; Umetsu, M.; Kumagai, I.; Ejima, D.; Philo, J. S.; Arakawa, T., *Biotechnology Progress* **2004,** 20, (5), 1301-1308.
12) *Thermal stability of proteins in aqueous polyol solutions: Role of the surface tension of water in the stabilizing effect of polyols,* Kaushik, J. K.; Bhat, R., *Journal of Physical Chemistry B* **1998,** 102, (36), 7058-7066.

13) *Solubilizing excipients in oral and injectable formulations,* Strickley, R. G., *Pharmaceutical Research* **2004,** 21, (2), 201-230.
14) *The effects of protein stabilizers on aggregation induced by multiple-stresses,* Arakawa, T.; Dix, D. B.; Chang, B. S., *Yakugaku Zasshi-Journal of the Pharmaceutical Society of Japan* **2003,** 123, (11), 957-961.

CHAPTER 5

SCREENING FOR PHYSICAL STABILITY OF A *PSEUDOMONAS* AMYLASE USING SELF-INTERACTION CHROMATOGRAPHY

In this chapter, B of a commercial amylase (*P*A) was evaluated by SIC as an innovative approach to characterize physical protein stability. B was measured as a function of pH and several common formulation additives (cosolvents) including NaCl, sucrose, and sorbitol. Cosolvent and pH induced physical stabilization of amylase is discussed in terms of positive shifts in B. Liquid chromatographic (LC) measurements of total soluble amylase and enzymatic activity demonstrated excellent qualitative correlation with trends in B, except near the pI of amylase where physical stability was minimal. This work builds upon our previous report of using SIC measurements of B to quantify lysozyme self-interaction as a function of common formulation additive mixtures. We now demonstrate that this chemistry can be extended from a model system of lysozyme solutions to industrially relevant conditions of the type encountered in the production and formulation of a non-model, commercial enzyme. Notably, this worked marked our first attempt to extend the accepted correlation between trends in B and solubility to include trends in enzymatic activity.

5.1 Experimental

5.1.1 Purification of *P*A

The following bench scale purification process was followed according to protocols previously developed at Genencor. Stock *P*A ultra filtrate (500 mL) was obtained from Genencor. The pH of a 60 mL sample was lowered to 4.50 with 10% (v/v) acetic acid, causing significant precipitation. The sample was stirred to an even consistency and portioned into 15 mL centrifuge tubes. After centrifugation (5k rpm, 3 min), the supernatant was removed and replaced with an equal amount of deionized water. This washing process was repeated 3 times. The remaining precipitate (4 mL) was diluted back to its original volume (15 mL). Purified *P*A for immediate use was stored at 4°C. A -10°C freezer was used for long term storage of purified and stock *P*A samples.

5.1.2 SEC

All SEC data were collected on a Hewlett Packard 1090 HPLC and analyzed using Chemstation software. Stock *P*A concentrate (ultra filtrate), supernatants from washing steps of the purification process, and purified *P*A redisolved in K_2HPO_4 (100 mM, pH 7.5) were analyzed on a Biosep-SEC-3000-S, 600 x 7.8 mm column. The mobile phase for all SEC experiments contained K_2HPO_4 (50 mM, pH 6.80). In all cases, 5 μL of sample was injected onto the column at a flow rate of 0.5 mL/min. Eluting samples were detected at 254 nm. The column was used at ambient temperature (21 ± 2°C).

5.1.3 IEF

Isoelectric focusing (IEF) of purified *P*A was performed using a Novex Pre-Cast gel (pH 3-7) and an Xcell II mini cell unit obtained from Invitrogen (Carlsbad, CA). Novex running buffers, sample buffer and Serva IEF 3-10 markers were also obtained from Invitrogen. Each lane was loaded with a 10 µL mixture of sample buffer (5 µL), deionized water (3 µL), and either *P*A concentrate (2 µL) or IEF markers (2 µL). The gel was run under constant current conditions (5 mA) at 100 V for 1 h, 200 V for 2 h, and 300 V for 45 min. After focusing, the gel was fixed in a solution of 12% (w/v) trichloroacetic acid and 0.35% (w/v) sulfosalicylic acid for 30 minutes. Staining was performed with Coomassie Brilliant Blue R-250 obtained from Bio-Rad (Hercules, CA).

5.1.4 DLS

Dynamic light scattering (DLS) of purified amylase was performed on a DynaPro-801 molecular sizing instrument (Protein Solution, Inc.). Purified *P*A (50 µL) was diluted to 1.0 mL and manually pumped through a 0.2 µM polyethersulfone (PES) filter five times. This sample was loaded into a Hellma quarts precision cell (3 mm path length) that was placed in a temperature-controlled microsampler set to 21°C. The viscosity and refractive index of water were used for all measurements. The solid state laser was tuned to 780 nm and adjusted to 25% power (5 mW) for 10-second acquisition times. Laser counts were typically 1-2 × 10^6. The hydrodynamic radius (R_H) and molecular weight (MW) distributions were processed with the DYNAMICS (version 3.30) software package.

5.1.5 Immobilization of *P*A to stationary phase

AF-Amino-650 M chromatography particles (1.0 mL) were washed with 5.0 mL of 4-Morpholineethansulfonic acid (MES) (50 mM, pH 6.00) containing 3% (w/v) NaCl, and then combined with 0.7 mL of purified *P*A solution (21 mg/ mL). 1-Ethyl-3-[3-dimethylaminopropyl] carbodiimide hydrochloride (EDC) (2.0 mg) and N-hydroxysulfosuccinimide (NHS) (0.5 mg) were added to the reaction mixture to promote *P*A-particle coupling through amide bond formation. This chemistry was allowed to proceed in a room temperature (21 ± 2°C) rotary mixer, overnight. The remaining free *P*A was removed by washing with the original MES buffer. The *P*A-modified particles were placed back in the rotary mixer, overnight, with 3-hydroxypropionic acid (3HP) (0.7 mL, 0.2 M), EDC (2.0 mg) and NHS (0.5 mg) for the purpose of capping any unreacted amine groups. These particles were washed with the original MES buffer and stored at 4°C until use. Additionally, 3HP capped AF-Amino particles (used for the enzyme-free "dead" column) were prepared according to the final step of the coupling chemistry described above.

5.1.6 SIC Procedures

All mobile phase solutions were prepared with 18 MΩ water (Nanopure, Barnstead) and buffered with 50 mM MES. Buffer pH was adjusted with either NaOH or HCl and measured using a digital pH meter (UB-5, Denver Instruments). The pH meter was calibrated before each measurement. Measured pH values were reproducible to within ± 0.01 units as determined by ten consecutive calibration and pH measurements. *P*A and acetone samples were

dissolved at 21 mg/mL and 3% (v/v), respectively. The SIC column and dead column consisted of Teflon FEP Tubing (1/8" outer diameter, 1/16" inner diameter, Upchurch) fitted with a stainless steel frit (2 μm pores, Upchurch). The columns were conditioned after packing for several hours with MES (50 mM, pH 6.00) containing 3% (w/v) NaCl, at 200 μL/min, after which, no further bed settling was observed. Generally, for all experiments where the pH of the mobile phases was constant and cosolvent concentrations incrementally increased, one buffer with no cosolvent and another with the maximum cosolvent concentration were mixed by the HPLC pump to achieve the entire range of desired conditions. Mobile phases for dead column experiments mimicked those of the SIC experiments with the one exception that a concentration of 5% (w/v) NaCl was always used to suppress the potential for electrostatic interactions between mobile phase analytes and the 3HP capped stationary phase.

All chromatographic data were collected on a Hewlett Packard 1050 HPLC and analyzed using Chemstation software. All mobile phases were degassed online. *P*A and acetone samples (2.0 μL) were injected using a Hewlett Packard 1050 autosampler and analyzed at a flow rate of 150 μL/min. The column temperature was regulated with a digital column heater (TC-50, Eppendorf). Eluting samples were detected by UV absorption at 280nm. To ensure reproducibility, *P*A samples were run in quadruplicate, and acetone samples in triplicate. Typical percent coefficient of variations for these replicate injections were <1.0% and <0.5%, respectively.

5.1.7 LC measurements of total soluble *P*A

Our general approach to liquid chromatographic determination of total soluble *P*A is fundamentally similar to previous reports that utilized more traditional forms of chromatography, including analytical size exclusion, hydrophobic interaction, and reversed phase.[1-3] *P*A was adjusted to pH 4.50 with 10% (v/v) acetic acid (as described previously). Samples for LC measurements of total soluble amylase were then prepared by adding appropriate amounts of buffer, salt, and cosolvent to the *P*A slurry. The pH was again adjusted with either 10% (v/v) acetic acid or 10% (w/v) NaOH. All samples were stored at 4°C. Several hours prior to analysis, samples were warmed to room temperature (21 ± 2°C). All samples contained soluble *P*A in equilibrium with precipitated *P*A. Supernatant (2 μL) from each sample was injected onto a SIC dead column (enzyme free column) at a flow rate of 300 μL/min, and column temperature of 23°C. A mobile phase consisting of MES (50 mM, pH 6.00) containing 1% (w/v) NaCl was used for all samples. Peak areas were determined using the Chemstation software auto-integration function. All other instrumental parameters are identical to those used for the SIC experiments. These experiments were run after all SIC experiments had been completed.

5.1.8 BCA assay

The bicinchoninic acid (BCA) protein assay was run according to the manufacturer's (Pierce) recommendations for the standardized test tube procedure. The bovine serum albumin (BSA) standards were measured once

each. The resulting calibration curve was fitted to a fourth order polynomial (R^2= 0.999). Unknowns were typically run in duplicate or triplicate. Theses experiments were used to determine the concentrations of stock and purified *P*A samples as well as *P*A-Amino CDs. CDs were measured by direct assaying of the *P*A-amino particles.

5.1.9 Activity Measurements

Enzyme activity was measured by an endpoint assay. The substrate used was Ceralpha, from Megazyme International Ireland Ltd. (Wicklow, Ireland), which consists of non-reducing-end blocked *p*-nitrophenyl maltoheptaoside (also called BPNPG7), and excess alpha-glucosidase and glucoamylase. Upon hydrolysis of the oligosaccharide by *P*A, the excess quantities of alpha-glucosidase and glucoamylase give instantaneous and quantitative hydrolysis of the *p*-nitrophenyl maltosaccharide fragment to glucose and free *p*-nitrophenol. The substrate was prepared at 1.88 mg/ml BPNPG7 in 50 mM malate, 1% BSA, pH 5.6, and pre equilibrated to 30°C. The reaction was started by the addition of 7 μl of suitably diluted sample into 84 μl of substrate. The reaction was allowed to proceed for 5 minutes at 30°C, until terminated by addition of 105 μl of 200 mM borate, pH 10. Stopped samples were held for 2 minutes, and finally, the intensity of yellow color was quantified, by measuring absorbance at 405 nm. A standard curve was made by the same method, using amylase enzyme of known activity. A regression equation determined from the standard curve, was used to calculate the activity of the unknown sample. The assay was run in an automated format

on a Konelab Aqua 20 auto analyzer (Thermo Electron Corporation, Waltham, MA). All assayed samples were shipped overnight from Colorado State University (Fort Collins, CO) to Genencor (Palo Alto, CA). Beth Fryksdale at Genencor performed all assay measurements.

5.2 Results and Discussion

5.2.1 Purity of *P*A as determine by SEC

Chromatograms in Figure 5.1 show the stepwise purification of *P*A as discussed in section 5.1.1. The *P*A ultra filtrate (Figure 5.1A) contains numerous low MW impurities. Upon lowering the pH to 4.50, *P*A is selectively precipitated (Figure 5.1B). Washing the precipitate with deionized water continues to remove impurities without significantly redisolving the *P*A (Figure 5.1C). Redisolving the *P*A in K_2HPO_4 (100mM, pH 7.5) indicates the overall success of the purification process (Figure 5.1D).

5.2.2 DLS analysis of *P*A

MW and R_H distributions obtained from DLS experiments are presented in Figure 5.2. Notably, these data represent only one of several acquisition trials. Significant cosolvent compatibility limitations as well as lengthy sample preparation and instrument adjustment times prohibited further DLS or SLS experiments. Despite these issues, the data in Figure 5.2 provided important results. The experimentally determined average MW and R_H are 50.44 ± 3.78

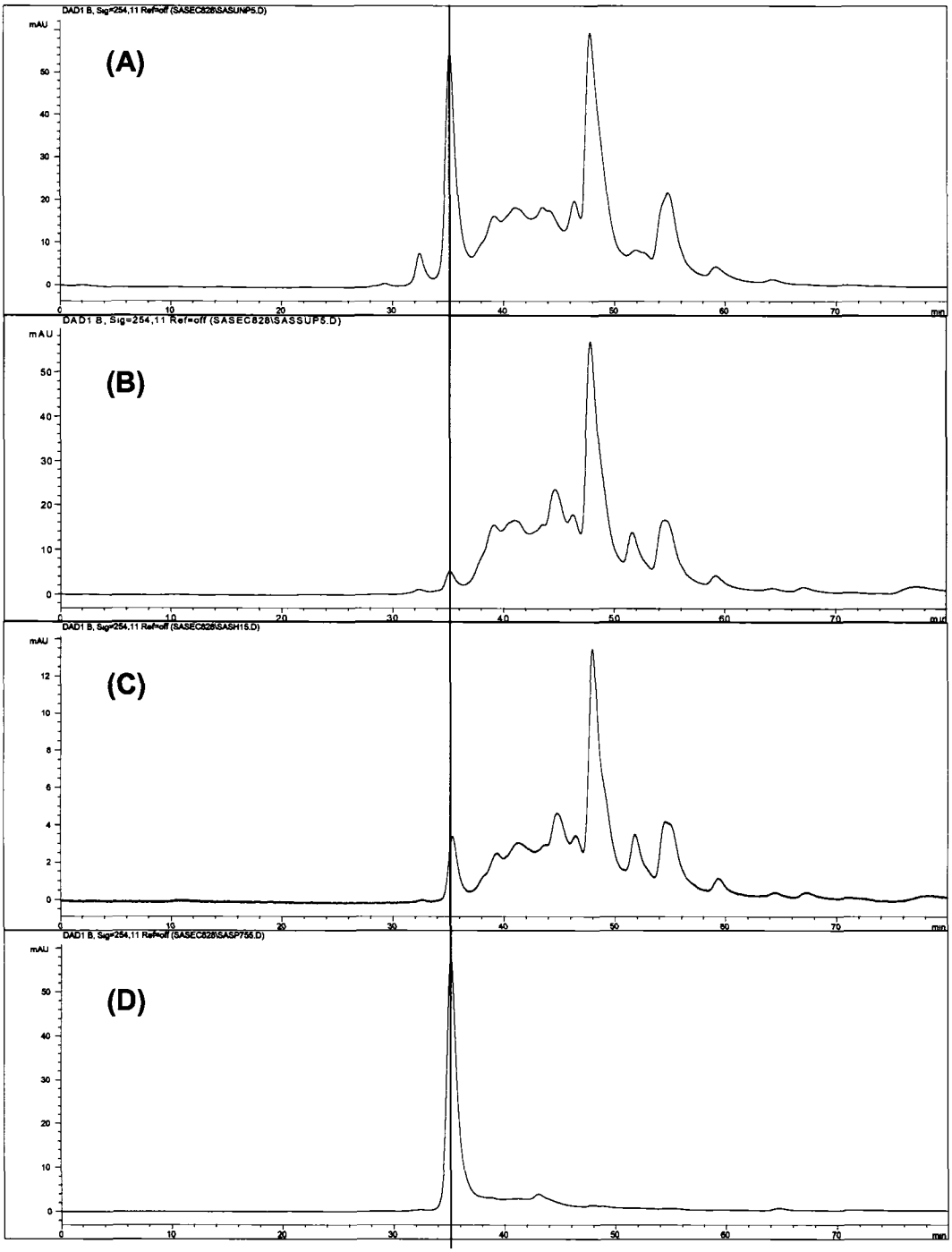

Figure 5.1. (A) Size exclusion chromatography (SEC) of *P*A ultra filtrate at pH 5.60, (B) supernatant from precipitated ultra filtrate at pH 4.50, (C) supernatant from the first wash cycle of the precipitated *P*A at pH 4.50, and (D) purified *PA* dissolved in K_2HPO_4 (100 mM, pH 7.5). The red line was added to help guide the reader's eye for identification of the *P*A peak.

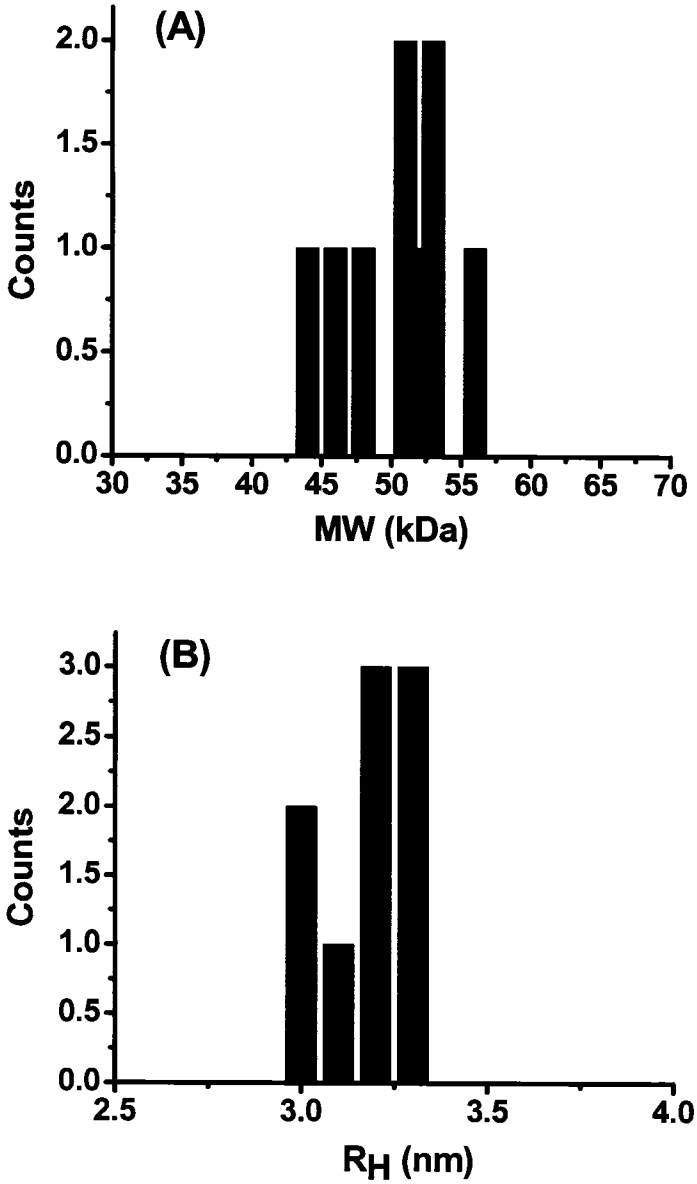

Figure 5.2. The MW (A) and R_H (B) distribution of *P*A as determined by dynamic light scattering (DLS). Solvent conditions were deionized water at 21°C. The averaged MW and R_H are 50.44 ± 3.78 kDa and 3.18 ± 0.12 nm, respectively.

kDa and 3.18 ± 0.12 nm, respectively. The calculated MW of *P*A based on its amino acid composition is 47.6 kDa, consistent with the experimental DLS results. The agreement between these MW values confirms the relative purity of our PA samples used during the SIC studies.

5.2.3 pH dependent elution profile and precipitation behavior of *PA*

The sample SIC chromatograms in Figure 5.3 demonstrate the sensitivity of the *P*A elution profile to changes in pH. Here, the observed peak broadening and shift in maximum absorbance towards longer retention times at lower pH indicates enhanced attraction between mobile and stationary phase *P*A. By contrast, the ACE peak (data not shown) was unaffected by changes in pH or cosolvent concentration, indicating its suitability as a neutral marker, as demonstrated in Chapter 2. The photograph in Figure 5.3 demonstrates pH dependent precipitation of *P*A from the ultra filtrate, consistent with the elution profiles observed by SIC. These elution profiles were representative of the *P*A peak response to changes in solution conditions throughout the *P*A-SIC studies. As a result, we progress our discussion *of PA* physical stability studies to terms of SIC measured trends in B, rather than elution profiles. In all cases, B was calculated from *P*A retention times recorded at maximum peak height.

5.2.4 Preliminary *PA* formulation screening: NaCl and pH

Initial SIC investigations focused on screening the effects of pH and NaCl on B of *P*A. Sixteen combinations of pH and NaCl were chosen as a base set of

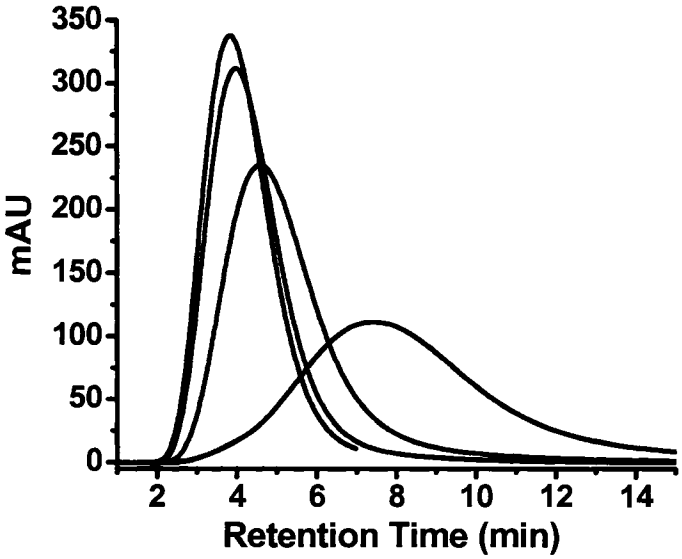

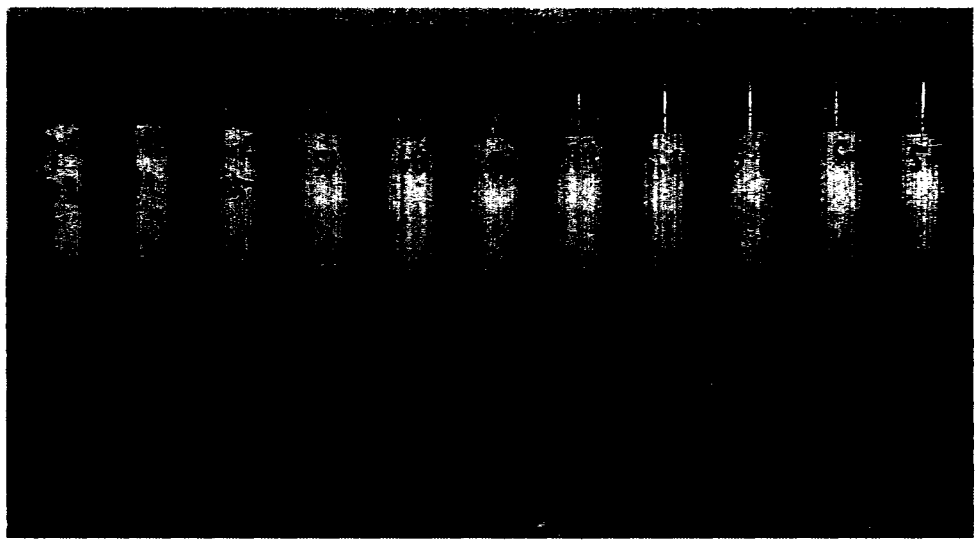

Figure 5.3. Representative elution profiles for *P*A as a function of pH in 50 mM MES (50 mM) containing 3% (w/v) NaCl at pH 6.00 (black line), pH 5.50 (red line), pH 5.00 (green line), and pH 4.50 (blue line). The photograph demonstrates pH dependent precipitation of *P*A from the ultra filtrate.

formulation conditions based on commercial scale manufacturing considerations. The results are presented as a contour plot in Figure 5.4. We first note the extreme sensitivity of B as the pH approaches 4.50. As discussed in more detail in the following sections of this report, changes of only a few hundredths of a pH unit in the range of 4.45-4.55 significantly impact B. At pH 4.55 and 1% (w/v) NaCl, *P*A self-interaction is considerably attractive, as indicated by a B of - 35.05 ± 0.58 × 10^{-4} mol mL/g^2. Increasing the pH to 6.00 while holding the NaCl concentration constant at 1% (w/v) raises B to -5.86 ± 0.23 × 10^{-4} mol mL/g^2 (a net increase of 29.19 ± 0.62 × 10^{-4} mol mL/g^2). On the other hand, increasing the concentration of NaCl to 4% (w/v) at a constant pH of 4.55 brings B up to -23.29 ± 0.24 × 10^{-4} mol mL/g^2 (a net increase of only 11.76 ± 0.63 × 10^{-4} mol mL/g^2). B is largest (-0.44 ± 0.08 × 10^{-4} mol mL/g) at conditions of 4% (w/v) NaCl, pH 6.00. Overall, Figure 5.4 indicates that *P*A B values are most improved when the NaCl concentration is between 2% and 4% (w/v) and the pH is between 5.50 and 6.00. Using SIC, these types of contour plots can be rapidly generated, offering a high-throughput screening approach for evaluation of significant formulation parameter space.

The pH dependent trend shown in Figure 5.4, at all NaCl concentrations, can be explained by considering the relationship between B, protein solubility, net charge, and pH. First, we recall that positive shifts in B indicate favorable shifts toward protein-solvent interactions, which in turn correlate with enhanced

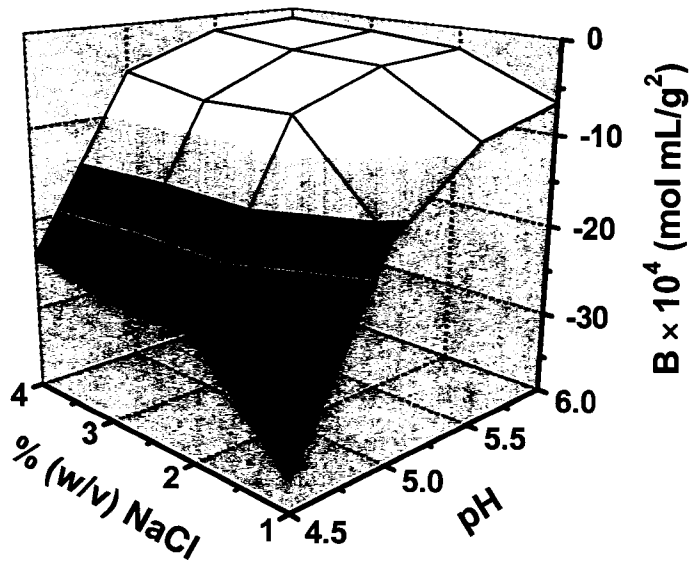

Figure 5.4. Contour plot of *P*A B values as a function of % (w/v) NaCl and pH in MES (50 mM) buffer.

solubility. Proteins are expected to be least soluble at their isoelectric point (pI).[4] The pI is the pH where a protein is electrically neutral, suggesting that the netintermolecular electrostatic repulsion will be at a minimum. The experimental pI of *P*A is 4.2, as determined by the IEF gel shown in Figure 5.5. Notably, two other *Pseudomonas* amylases have reported pIs of 4.7 and 5.0.[5] At pH 4.2, *P*A self-interaction is therefore highly attractive because the net charge of the enzyme is zero. As the pH is raised, excess negative charges accumulate on the surface of *P*A. As a result, Intermolecular electrostatic repulsion intensifies and *P*A self-interaction becomes less favored. This manifests as an increasing trend in measured B values, as shown in Figure 5.4.

The observed trend for NaCl in Figure 5.4 is less expected. NaCl is a weak kosmotropic salt; it should be an effective structure stabilizer and display a general salting-out effect.[6] Salting-out correlates with enhanced self-interaction and a shift towards more negative B values. Instead, we see that the addition of NaCl has a salting-in effect on *P*A, as indicated by positive shifts in B. The same NaCl dependent behavior was observed for NC in Chapter 4. Although not as common, similar NaCl-induced trends in B[7, 8] and solubility[9, 10] have been previously reported.

5.2.5 Stabilization of *P*A by Cosolvents: Sucrose and Sorbitol

Saccharides and polyols are among the most common classes of protein stabilizers found both in nature (where they are referred to as osmolytes) and in

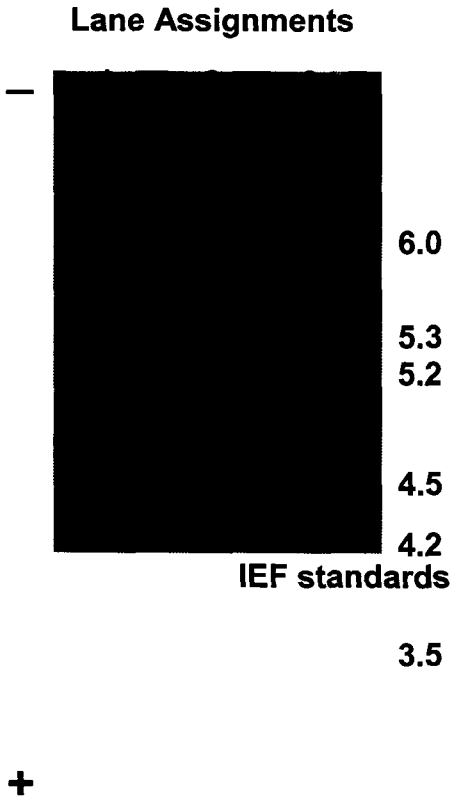

Figure 5.5. Novex IEF Pre-cast Vertical Gel, pH3-7. Lane Assignments: 1- purified *P*A concentrate (dilution, 1:200), 2- purified *P*A concentrate (dilution, 1:100), 3- IEF markers (Amyloglucosidase, 3.5); (Glucose oxidase, 4.2); (Trypsin inhibitor, 4.2); (b-lactoglobulin, 5.2 anodic isoform, 5.3 cathodic isoform); (Carbonic anhydrase, 6.0).

commercial protein formulations (where they are more commonly called cosolvents). Figures 5.6 and 5.7 show SIC measurements of B as a function of sucrose and sorbitol, respectively. The initial solution conditions for these studies were chosen to expand upon the base set of formulations investigated in Figure 5.4.

In Figure 5.6, sucrose was added to three initial solution conditions that differed in NaCl concentration and pH. These differences primarily affected B in the absence of sucrose as well as the overall sucrose induced trend in B. For example, B at conditions of pH 4.53 and either 1% or 5% (w/v) NaCl is -47.93 ± 1.01 and -27.74 ± 0.06 × 10^{-4} mol mL/g^2, respectively. This positive shift in B with increased NaCl concentration is consistent with the data in Figure 5.4. Subsequent addition of 10% (w/v) sucrose to these solutions leads to B values of -8.36 ± 0.07 and -6.47 ± 0.25 × 10^{-4} mol mL/g^2. The respective sucrose induced changes in B are large (39.57 ± 1.00 vs. 21.27 ± 0.26 × 10^{-4} mol mL/g^2) and differ significantly. The final B values though, differ by only 1.89 ± 0.26 × 10^{-4} mol mL/g^2 in the presence of sucrose, as opposed to a difference of 20.19 ± 0.67 × 10^{-4} mol mL/g^2 in the absence of sucrose. A similar, yet slighter sucrose induced trend in B is observed at 1% (w/v) NaCl, pH 6.00, Here, addition of 10% (w/v) sucrose raises B from -8.81 ± 0.93 to -1.78 ± 0.01 × 10^{-4} mol mL/g^2 (a net increase of only 7.03 ± 0.93 × 10^{-4} mol mL/g^2). Beyond a concentration of 10 % (w/v) sucrose, measured B values were largely unaffected by differences in NaCl concentration

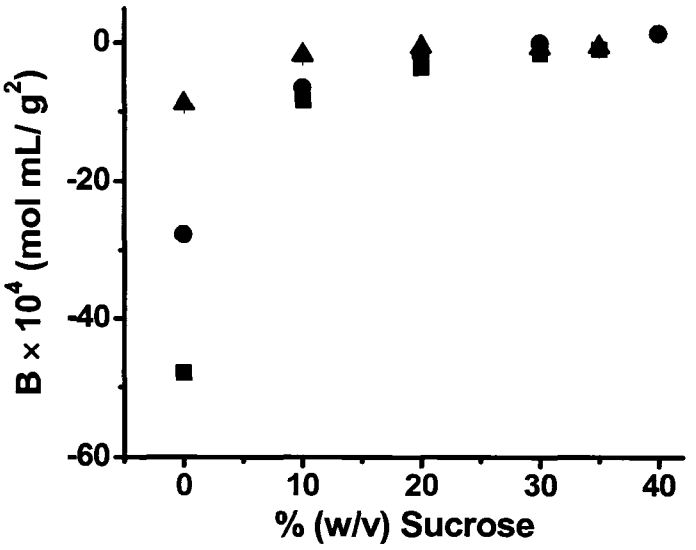

Figure 5.6. Effect of sucrose on *P*A B values. Solution conditions were MES (50 mM) (all symbols) containing 1% (w/v) NaCl at pH 6.00 (black triangles), 5% (w/v) NaCl at pH 4.53 (red circles) or 1% (w/v) NaCl at pH 4.53 (green squares).

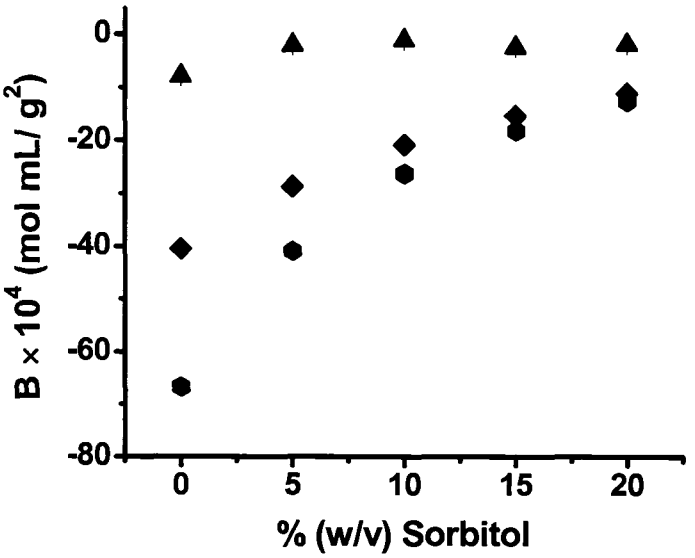

Figure 5.7. Effect of sorbitol on *P*A B values. Solution conditions were MES (50 mM) (all symbols) containing1% (w/v) NaCl at pH 6.00 (black triangles), 5% (w/v) NaCl at pH 4.45 (red diamonds), or 1% (w/v) NaCl at pH 4.45 (green hexagons).

or pH, and only slightly raised by further addition of sucrose. Between sucrose concentrations of 20% to 40% (w/v), the data sets in Figure 5.6 merge and B trends level off to an average value of $-0.95 \pm 1.35 \times 10^{-4}$ mol mL/g^2.

Sorbitol-induced trends in B are shown in Figure 5.7. As with sucrose, sorbitol was added to three initial solutions of different pH and NaCl concentration. Several interesting comparisons can be made between the data in Figures 5.6 and 5.7. First, we note a slight difference in pH that had a large impact on B. In Figure 5.7, B is $-66.79 \pm 0.28 \times 10^{-4}$ mol mL/g^2 at 1% (w/v) NaCl, pH 4.45. In Figure 5, at pH 4.53 and the same NaCl concentration, B is $-47.93 \pm 1.01 \times 10^{-4}$ mol mL/g^2. This large shift in B is due to a change of only 0.08 pH units. These results are not surprising considering the proximity to the pI of *P*A (shown in Figure 5.5). As shown in both Figure 5.6 and 5.7, initial differences in pH and NaCl concentration become less apparent with increasing cosolvent concentration. In Figure 5.7, the merging of data sets as a function of sorbitol was similar, although less abrupt than what was observed for sucrose in Figure 5.6. As already discussed, B values were largely unaffected by sucrose concentrations above 10% (w/v), regardless of NaCl concentration or pH. Conversely, B values in Figure 6 still show significant dependence on both NaCl concentration and pH in the presence of 10 % (w/v) sorbitol. Even at 20% (w/v) sorbitol, B values are somewhat sensitive to pH. For example, in the presence of 20 % (w/v) sorbitol, B is $-12.67 \pm 0.19 \times 10^{-4}$ mol mL/g^2 at 1% (w/v) NaCl, pH

4.45. Increasing the NaCl concentration to 5% (w/v) raises B to -11.19 ± 0.08 × 10^{-4} mol mL/g^2 while increasing the pH to 6.00 raises B to -1.92 ± 0.09 × 10^{-4} mol mL/g^2.

The observed cosolvent-induced trends in B are clarified by considering the nature of protein-cosolvent-water interactions.[11, 12] At pH values near the pI of a protein, intermolecular electrostatic repulsion is minimized and protein self-interaction is dominated by short range, attractive hydrophobic interactions.[13] Both sucrose and sorbitol stabilize proteins through excluded volume[14] and surface tension effects.[15] Their preferential exclusion from the protein surface results in a thermodynamic condition that influences protein conformational dynamics towards the most compact, native-like state.[16,17] The surface hydrophobicity and associated intermolecular hydrophobic attraction are therefore reduced. The magnitude of these effects depends on both the molecular weight and concentration of the individual cosolvent. These dependencies are more easily observed by converting % (w/v) to molarity. When this is done, we see that 20 % (w/v) cosolvent converts to 0.58M sucrose and 1.10 M sorbitol, thus explaining the relative strengths of the sucrose (342.30 g/mol) and sorbitol (182.17 g/mol) induced trends in B. At pH 6.00, far from the pI, long-range electrostatic repulsion between negatively charged *P*A surfaces extends beyond the range of hydrophobic effects. Sucrose and sorbitol induced trends in B are therefore expected to be diminished at these conditions. Additionally, the rate of change in B is another indication of the relative strength

of each cosolvent. The leveling off trend in B, on the other hand, is an indication of the finite degree to which physical protein stability can be enhanced by optimization of individual solution parameters (here, the use of stabilizing cosolvents).

5.2.6 Correlating Trends in B with trends in enzymatic activity and LC measurements of total soluble *P*A

While calculation of absolute protein solubility from B is theoretically possible, it remains experimentally difficult due to the need for a pure monocrystalline form of the starting protein.[18] As an alternative, quantitative experimental measures of total soluble protein are commonly obtained through colorimetric assays[19] and liquid chromatography.[1-3] In the case of enzymes, equally valuable information is often acquired from standardized activity assays. To confirm the ability of SIC to predict the physical stability of *P*A, a comparison study of *P*A solubility and enzymatic activity was performed within the same experimental space described in Figures 5.6 and 5.7. All solubility and activity data were obtained from one set of samples to ensure consistency. As in the previous section, we focus here on the effects of adding sucrose and sorbitol to *P*A solutions around pH 4.50, where previously observed trends in B were strongest. The primary objective is to show that the trends we observe with SIC correspond on a larger scale with trends in the net properties of *P*A, such as solubility and enzymatic activity.

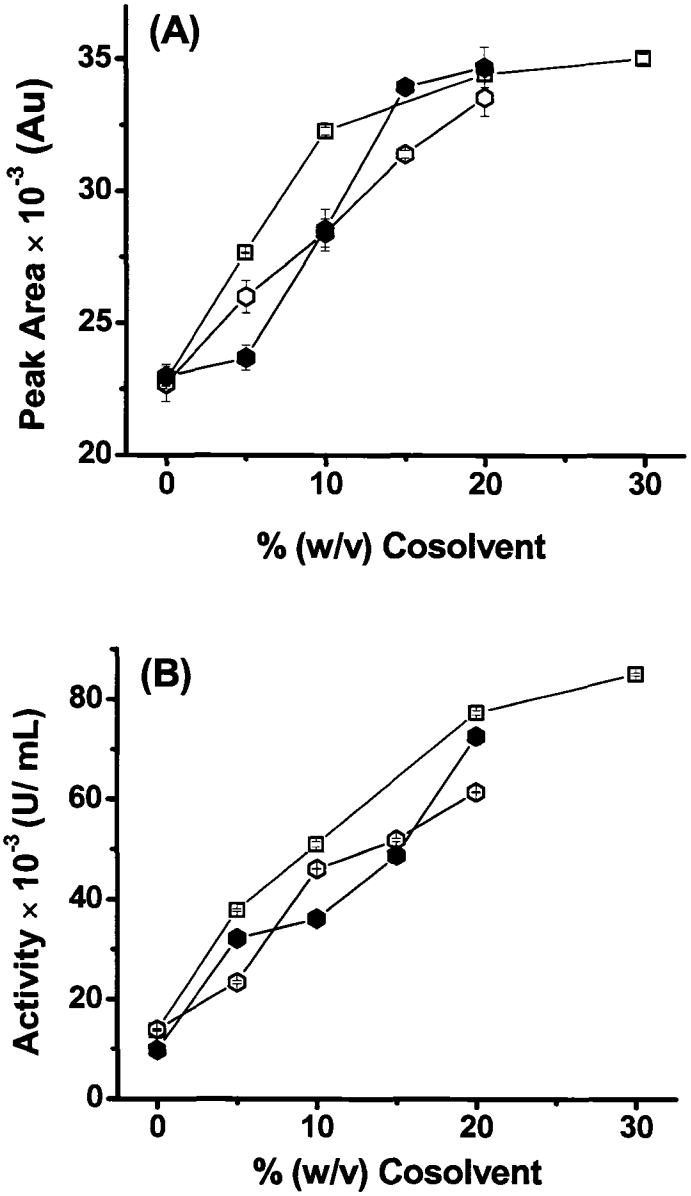

Figure 5.8. Chromatographic peak area (A) and activity (B) of *P*A as a function of sucrose (red squares) and sorbitol (black hexagons). Solution conditions were MES (50 mM) containing 1% (w/v) NaCl at pH 4.53 (open symbols) or pH 4.45 (solid symbols). Lines connecting data trends were added to help guide the eye.

Solubility trends for *P*A as a function of sucrose and sorbitol are presented in Figure 5.8A. For these experiments, NaCl was held constant at a concentration of 1% (w/v) and pH was either 4.45 or 4.53. Results for both cosolvents (sucrose and sorbitol) are presented on the same graph to facilitate comparison. As shown in Figure 5.8A, the overall cosolvent-induced trends in solubility are very similar to previously observed trends in B. At pH 4.53, the amount of total soluble *PA* (measured in terms of integrated peak area) is effectively increased by the addition of up to 20% (w/v) sucrose or sorbitol. The respective integrated peak areas are 34.44 ± 0.22 and 33.54 ± 0.68 × 10^3 Au. Increasing the sucrose concentration to 30% (w/v) did not significantly raise the amount of total soluble *P*A. In terms of molar concentration, sucrose again appears to be the more effective cosolvent, this time from a solubility perspective.

A very interesting aspect of the solubility trends in Figure 5.8A is the overlapping of data sets collected at pH 4.53 and 4.45. These data are in stark contrast with the observed sensitivity of B in this pH range. Recalling that the pI of amylase is 4.2 (as shown in Figure 5.5), we expect to see nominal physical stability at nearby pH. Notably, the theoretical framework for obtaining B from SIC is not optimal at these conditions. Other researchers have proposed that multibody interactions between mobile phase proteins or between one mobile phase protein and multiple stationary phase proteins may lead to skewed B values at physical stability extremes.[20-22] Additional attempts to derive correlations between B and solubility at extreme conditions have encountered similar problems.[23]

Unfortunately, empirical data sets remain limited due to the inherent difficulties of obtaining absolute solubility measurements and B values from proteins in complex solutions.

Unlike B and solubility, there is no established relationship between B and activity, though a qualitative correlation is easily realized. Intuitively, increasing the amount of soluble enzyme should lead to higher enzymatic activity. Indeed, we see that amylase solubility trends in Figure 5.8A are highly correlated with enzymatic activity trends in Figure 5.8B. It then follows that general trends in B and activity should be in agreement. We therefore suggest that measured trends in B are useful predictors of enzymatic activity. One exception would be at conditions of very low physical stability, as previously discussed. Ultimately, small regions of minimum physical stability are unimportant from an industrial formulation development standpoint. The main goal is to identify the overall trends that lead to conditions of maximum physical stability. In these cases we observe strong qualitative agreement between trends in B, solubility, and activity.

5.3 Conclusions

This work demonstrates the use of SIC for rational formulation screening of an industrially relevant enzyme. The identification of formulation conditions that optimize physical stability is still a key hurdle to overcome in developing commercial protein-based products. Using SIC, the individual and combined effects of pH, NaCl, sucrose, and sorbitol on B of a commercial amylase were

rapidly and rationally screened. From these experiments it was determined that increasing pH (from ~4.5 to 6.0), and the addition of NaCl, and sucrose or sorbitol could significantly improve the physical stability of *P*A (as determined by positive shifts in B). To verify the utility of our experimental approach, additional measurements of total soluble *P*A and enzymatic activity were obtained and compared with B. Strong qualitative agreement between trends in B, solubility, and activity were observed, except at conditions near the pI of *P*A, where physical stability was lowest. The outcome of this study suggests that SIC is a useful method to augment current approaches to characterizing the physical stability of protein-based formulations.

5.4 Acknowledgments

The author would like to extend gratitude to Beth Fryksdale, Michael Bodo, Douglas Dale, and Dr. Alfred Gaertner for their contributions to the above studies of *P*A.

5.5 References

1) *An adaptation of hydrophobic interaction chromatography for estimation of protein solubility optima,* Gagnon, P.; Mayes, T.; Danielsson, A., *Journal of Pharmaceutical and Biomedical Analysis* **1997,** 16, (4), 587-592.
2) *Estimating the potential refolding yield of recombinant proteins expressed as inclusion bodies,* Ho, J. G. S.; Middelberg, A. P. J., *Biotechnology and Bioengineering* **2004,** 87, (5), 584-592.
3) *Liquid chromatographic determination of total homocysteine in blood plasma with photometric detection,* Zhloba, A. A.; Blashko, E. L., *Journal of Chromatography B-Analytical Technologies in the Biomedical and Life Sciences* **2004,** 800, (1-2), 275-280.
4) Tanford, C., *Physical Chemistry of Macromolecules*. ed.; John Wiley & Sons Inc: New York, 1961; 'Vol.' p.

5) *Characterization of alpha-maltotetraohydrolase produced by Pseudomonas sp. MS300 isolated from the deepest site of the Mariana Trench,* Kobayashi, H.; Takaki, Y.; Kobata, K.; Takami, H.; Inoue, A., *Extremophiles* **1998,** 2, (4), 401-407.
6) *Salt Effects on Hydrophobic Interactions in Precipitation and Chromatography of Proteins - Interpretation of Lyotropic Series,* Melander, W.; Horvath, C., *Archives of Biochemistry and Biophysics* **1977,** 183, (1), 200-215.
7) *Interactions and aggregation of apoferritin molecules in solution: Effects of added electrolytes,* Petsev, D. N.; Thomas, B. R.; Yau, S. T.; Vekilov, P. G., *Biophysical Journal* **2000,** 78, (4), 2060-2069.
8) *Protein interactions in solution characterized by light and neutron scattering: Comparison of lysozyme and chymotrypsinogen,* Velev, O. D.; Kaler, E. W.; Lenhoff, A. M., *Biophysical Journal* **1998,** 75, (6), 2682-2697.
9) *Abnormal Solubility Behavior of Beta-Lactoglobulin - Salting-in by Glycine and Nacl,* Arakawa, T.; Timasheff, S. N., *Biochemistry* **1987,** 26, (16), 5147-5153.
10) *Effect of salts on the solubility of thermolysin: A remarkable increase in the solubility as well as the activity by the addition of salts without aggregation or dispersion of thermolysin,* Inouye, K.; Kuzuya, K.; Tonomura, B., *Journal of Biochemistry* **1998,** 123, (5), 847-852.
11) *The Control of Protein Stability and Association by Weak-Interactions with Water - How Do Solvents Affect These Processes,* Timasheff, S. N., *Annual Review of Biophysics and Biomolecular Structure* **1993,** 22, 67-97.
12) Timasheff, S. N., Control of protein stability and reactions by weakly interacting cosolvents: The simplicity of the complicated. In *Advances in Protein Chemistry,* **1998**, 51, 355-432.
13) *Hydrophobic Effect and Organization of Living Matter,* Tanford, C., *Science* **1978,** 200, (4345), 1012-1018.
14) *The Stabilization of Proteins by Sucrose,* Lee, J. C.; Timasheff, S. N., *Journal of Biological Chemistry* **1981,** 256, (14), 7193-7201.
15) *Thermal stability of proteins in aqueous polyol solutions: Role of the surface tension of water in the stabilizing effect of polyols,* Kaushik, J. K.; Bhat, R., *Journal of Physical Chemistry B* **1998,** 102, (36), 7058-7066.
16) *Preferential exclusion of sucrose from recombinant interleukin-1 receptor antagonist: Role in restricted conformational mobility and compaction of native state,* Kendrick, B. S.; Chang, B. S.; Arakawa, T.; Peterson, B.; Randolph, T. W.; Manning, M. C.; Carpenter, J. F., *Proceedings of the National Academy of Sciences of the United States of America* **1997,** 94, (22), 11917-11922.
17) *Effects of sucrose on conformational equilibria and fluctuations within the native-state ensemble of proteins,* Kim, Y. S.; Jones, L. S.; Dong, A. C.; Kendrick, B. S.; Chang, B. S.; Manning, M. C.; Randolph, T. W.; Carpenter, J. F., *Protein Science* **2003,** 12, (6), 1252-1261.
18) *Relation between the solubility of proteins in aqueous solutions and the second virial coefficient of the solution,* Haas, C.; Drenth, J.; Wilson, W. W., *Journal of Physical Chemistry B* **1999,** 103, (14), 2808-2811.
19) *Measurement of Protein Using Bicinchoninic Acid,* Smith, P. K.; Krohn, R. I.; Hermanson, G. T.; Mallia, A. K.; Gartner, F. H.; Provenzano, M. D.; Fujimoto, E.

K.; Goeke, N. M.; Olson, B. J.; Klenk, D. C., *Analytical Biochemistry* **1985,** 150, (1), 76-85.
20) *Measurement of lysozyme-lysozyme interactions with quantitative affinity chromatography,* Teske, C. A.; Blanch, H. W.; Prausnitz, J. N., *Journal of Physical Chemistry B* **2004,** 108, (22), 7437-7444.
21) *Rapid measurement of protein osmotic second virial coefficients by self-interaction chromatography,* Tessier, P. M.; Lenhoff, A. M.; Sandler, S. I., *Biophysical Journal* **2002,** 82, (3), 1620-1631.
22) *Self-interaction chromatography: a novel screening method for rational protein crystallization,* Tessier, P. M.; Vandrey, S. D.; Berger, B. W.; Pazhianur, R.; Sandler, S. I.; Lenhoff, A. M., *Acta Crystallographica Section D-Biological Crystallography* **2002,** 58, 1531-1535.
23) *Correlation between the osmotic second virial coefficient and the solubility of proteins,* Ruppert, S.; Sandler, S. I.; Lenhoff, A. M., *Biotechnology Progress* **2001,** 17, (1), 182-187.

CHAPTER 6

SCREENING FOR PHYSICAL STABILITY OF A *BACILLUS* AMYLASE USING SELF-INTERACTION CHROMATOGRAPHY

*B*A was the final protein that I would attempt to study with SIC. Initial *B*A-SIC experiments were designed to investigate solution conditions for which Genencor had previously observed trends in the precipitation behavior of *B*A. The following conditions were known to prevent precipitation of *B*A from the concentrated ultra filtrate: warming to 55°C, dilution by >200%, addition of up to 7% sorbitol, and addition of up to 18% NaCl. We also sought to briefly investigate the reported insensitivity of *B*A precipitation behavior to changes in solution pH. During these studies, we refocused on a previous challenge encountered with NC (Chapter 4). We intended to use the current SIC methodology to evaluate *B*A self-interaction in the presence of the background materials that make up the ultra filtrate solution. This is an extremely relevant issue in the biotechnology industry and was thus selected as a key point of investigation in my internship and collaboration work plan with Genencor. These experiments would represent the most complex protein-cosolvent systems that we had ever attempted to study with SIC or any other B measurements techniques. In Chapter 4 these studies were unsuccessful do to the prohibitively high absorbance of species in the

background at the same wavelengths where NC could be detected. As described in the current chapter, we were able to successfully extract valuable information from SIC experiments of *B*A using the background materials as a mobile phase component. This was an important step in determining the potential for widespread application of SIC as a tool for assessing the physical stability of commercially produced protein based formulations.

6.1 Experimental

6.1.1 Purification of *B*A

Three different purification techniques were employed. The first consisted of Nanosep 3 kDa molecular weight cutoff (MWCO) centrifuge tubes (Pall life sciences). Four 0.70 mL aliquots of the *B*A ultra filtrate were added to individual nanosep tubes. Each sample was centrifuged at 8k rpm for 5 minutes. The <3k MWCO fraction was removed from the bottom of tubes and an equal volume of K_2HPO_4 (100 mM, pH 6.80) was added to the remaining >3K MWCO *B*A solution. This process was repeated four times until ~200μL of <3kDa MWCO filtrate was collected from each sample. The second technique consisted of a buffer exchange process using 10 kDa MWCO dialysis tubing (Pierce). *B*A ultra filtrate (10. 0mL) was added to the dialysis tubing, which was then submerged in 1.0 L of acetic acid (ACTE) (100mM, pH 5.40) containing 3% NaCl for 24 hours at 4°C. The resulting dialyzed *B*A sample was ~15 mL. The third purification process utilized an Amicon 8400 filter cell fitted with a 10kDa MWCO regenerated cellulose ultra filtration membrane (Millipore). The first filtration stage yielded 75

mL of <10kDa filtrate after 10 hours under a nitrogen backpressure of 60 psi. Filtration was continued at a reduced backpressure of 30 psi for 14 hours to obtain an additional 75 mL of filtrate. The filtrate (<10kDa MWCO) and fractionated *B*A ultra filtrate (>10kDa) were sterile filtered with Nalgene filter units fitted with 0.20 μm polyethersulfone (PES) membranes. Samples from all purification procedures were stored at 4°C.

6.1.2 SEC

All SEC data were collected on a Hewlett Packard 1050 HPLC and analyzed using Chemstation software. Concentrated *B*A (fractionated and original ultra filtrate), MWCO fractions, and dialyzed *B*A were analyzed on a Biosep-SEC-3000-S, 600 x 7.8 mm column. The mobile phase for the MWCO fractions and fractionated *B*A concentrate consisted of K_2HPO_4 (100mM, pH 6.80). The mobile phase for the dialyzed *B*A consisted of ACTE (100mM, pH 5.40). The original *B*A ultra filtrate was run in both mobile phases. For all SEC experiments, 5-10μL of sample was injected onto the column at a flow rate of 1.0mL/min. Ambient temperature was 22 ± 2 °C. The eluting samples were detected at 254nm and 280nm.

6.1.3 SDS-PAGE

Sodium dodecyl sulphate-polyacrylamide gel electrophoresis (SDS-PAGE) of *B*A was performed using a Novex Pre-Cast 4-12% Bis-Tris gel with 4-Morpholineethanesulfonic acid (MES) SDS running buffer and an Xcell II mini cell

unit obtained from Invitrogen (Carlsbad, CA). The LDS sample buffer, reducing agent, antioxidant, and SeeBlue Plus2 molecular weight (MW) standards were also obtained from Invitrogen. Each lane was loaded with a 10 µL mixture of sample buffer (2.5 µL), reducing agent (1.0 µL), deionized water (4.5 -5.5 µL), and either dialyzed *B*A (1 µL diluted with 10 parts water) or MW standards (2 µL). The gel was run under variable current conditions (120-80 mA) at 200 V for 35 minutes. Afterwards, the gel was fixed in a solution of 12% (w/v) trichloroacetic acid for 30 minutes. Staining was performed with Coomassie Brilliant Blue R-250 obtained from Bio-Rad (Hercules, CA). Destaining was performed in a solution of 10% ethanol and 7.5% acetic acid until the desired level of background was obtained.

6.1.4 IEF

Isoelectric Focusing (IEF) of *B*A was performed using a Novex Pre-Cast gel (pH 3-10) and an Xcell II mini cell unit obtained from Invitrogen (Carlsbad, CA). Novex running buffers, sample buffer, and Serva IEF 3-10 markers were also obtained from Invitrogen. Each lane was loaded with a 10 µL mixture of sample buffer (5 µL), deionized water (3 µL), and either dialyzed *B*A (2 µL diluted with 50 parts deionized water) or IEF markers (2 µL). The gel was run under constant current conditions (5 mA) at 100 V for 1 h, 200 V for 2 h, and 300 V for 45 min. After focusing, the gel was fixed in a solution of 12% (w/v) trichloroacetic acid for 30 minutes. Staining was performed with Coomassie Brilliant Blue R-250

obtained from Bio-Rad (Hercules, CA). Destaining was performed in a solution of 10% ethanol and 7.5% acetic acid until the desired level of background was obtained.

6.1.5 Immobilization of BA to stationary phases

Attempts were made to covalently bond (immobilize) *B*A on to AF-Amino-650M and AF-Formyl-650M particles. For the AF-Amino-650M coupling trials, 800 μL of particles were washed five times with 1.0mL aliquots of ACTE (100mM, pH 5.40) containing 3% (w/v) NaCl. Dialyzed *B*A (1.3 mL), 3.0 mg EDC, and 0.5 mg NHS were added to the particles. The reaction mixture was put in a room temperature rotary mixer overnight. The *B*A-modified particles were removed from the mixer, washed with the original ACTE buffer, and then placed back in the rotary mixer, overnight, with 3HP (1.3 mL, 0.2 M), EDC (3.0 mg) and NHS (0.5 mg) for the purpose of capping any unreacted amine groups. These particles were again washed with the original ACTE buffer and stored at 4°C until use. A second *B*A-Amino particle coupling experiment was performed as described above, with the exception that the rotary mixer was kept at 4°C.

For the first AF-Formyl-650M coupling trial, 50 mg K_2HPO_4 was added to 3.0 mL of dialyzed *B*A. The pH of this solution was 7.30. AF-Formyl-650M particles (800 μL) were washed five times with 1.0 mL aliquots of K_2HPO_4 (100 mM, pH 7.30). Dialyzed *B*A (1.3 mL) was added to the particles. After brief mixing and subsequent settling of the particles, the supernatant (1.3 mL) was removed and

replaced with another 1.3 mL of dialyzed *B*A and 12 mg of $NaCNBH_3$. The reaction mixture was put in a rotary mixer at 4°C overnight. The *B*A-modified particles were washed with the original ACTE buffer and then placed back in the rotary mixer, overnight, with 1.3 mL of ethanolamine (1.0 M, pH 8.0) and 12 mg of $NaCNBH_3$ for the purpose of capping any unreacted Formyl groups. The particles were again washed five times with 1.0 mL aliquots of K_2HPO_4 (100 mM, pH 7.30) and stored at 4°C. The second *B*A-Formyl coupling trial consisted of two iterations of the above procedure and utilized K_2HPO_4 (400 mM, pH 7.90) as a coupling and wash buffer. Ethanolamine-Formyl particles (used for the protein-free "dead" column) were prepared according to the final "capping" step of the coupling chemistry. Particles from all immobilization trials were stored at 4°C.

6.1.6 BCA assay

The BCA protein assay was run according to the manufacturer's (Pierce) recommendations for the standardized test tube procedure. The BSA standards were measured once each. The resulting calibration curve was fitted to a fourth order polynomial (R^2=0.999). Unknowns were typically run in duplicate or triplicate. The concentration of *B*A immobilized to the stationary phase was determined by direct assaying of the particles.

6.1.7 SIC procedures

All mobile phase solutions were prepared with 18 MΩ water (Nanopure, Barnstead) and buffered with ACTE. Buffer pH was adjusted with either NaOH or

HCl and measured using a digital pH meter (UB-5, Denver Instruments). The pH meter was calibrated before each measurement. BA and acetone samples were dissolved at 29 mg/mL and 3% (v/v), respectively. The SIC column and dead column consisted of Teflon FEP Tubing (1/8" outer diameter, 1/16" inner diameter, Upchurch) fitted with a stainless steel frit (2 μm pores, Upchurch). The column length for *B*A-SIC experiments was 33 cm. Each column was conditioned after packing for several hours with ACTE (50 mM, pH 4.00) (SIC column) or ACTE (50 mM, pH 4.00) containing 5% NaCl (dead column), at 200 μL/min, after which, no further bed settling was observed. Generally, for all experiments where the pH of the mobile phases remained constant and cosolvent concentrations incrementally increased, two buffers were used. One buffer with no cosolvent and another with the maximum cosolvent concentration were mixed by the HPLC pump to achieve the entire range of desired conditions. Mobile phases for dead column experiments mimicked those of the SIC experiments with the one exception that a concentration of 5% (w/v) NaCl was always used to suppress the potential for electrostatic interactions between mobile phase analytes and the ethanolamine capped stationary phase.

All chromatographic data were collected on a Hewlett Packard 1050 HPLC and analyzed using Chemstation software. All mobile phases were degassed online. Sample volumes of 1.0-2.0 μL were injected using a Hewlett Packard 1050 autosampler and analyzed at a flow rate of 150 μL/min. The column temperature

was regulated with a digital column heater (TC-50, Eppendorf). Eluting samples were detected by UV absorption at 280 nm with a bandwidth of 10-25 nm. To ensure reproducibility, BA samples were typically run in triplicate or quadruplicate. Acetone samples were run in triplicate. Typical percent coefficient of variations for replicate injections were <1.5% (based on n=4). In all cases, retention times were recorded at maximum peak height.

6.1.8 Bench scale stability studies

Bench scale simply refers to stability studies performed in 15 mL centrifuge tubes as opposed to HPLC scale where we are dealing with μL size injections of *B*A. Stock *B*A concentrate, fractionated *B*A concentrate, and background (<10 kDa MWCO) samples were added to 15 mL centrifuge tubes and photographed before and after such processes as dilution or addition of NaCl. In the case of bench scale studies using NaCl as a solution additive, supernatant from samples were assayed with BCA. Dilution factors were included in concentration calculations where applicable.

6.2 Results and Discussion

6.2.1. Purity of BA as determined by SEC, SDS-PAGE, and IEF

Chromatograms from SEC experiments of fractionated and dialyzed *B*A, as well as stock *B*A ultra filtrate, are shown in Figure 6.1. Note that the *B*A peak absorbs more strongly at 280 nm (Figure 6.1B and 6.1D) than at 254 nm (Figure 6.1A and 6.1C), while the opposite is true for the background impurities. This was an initial

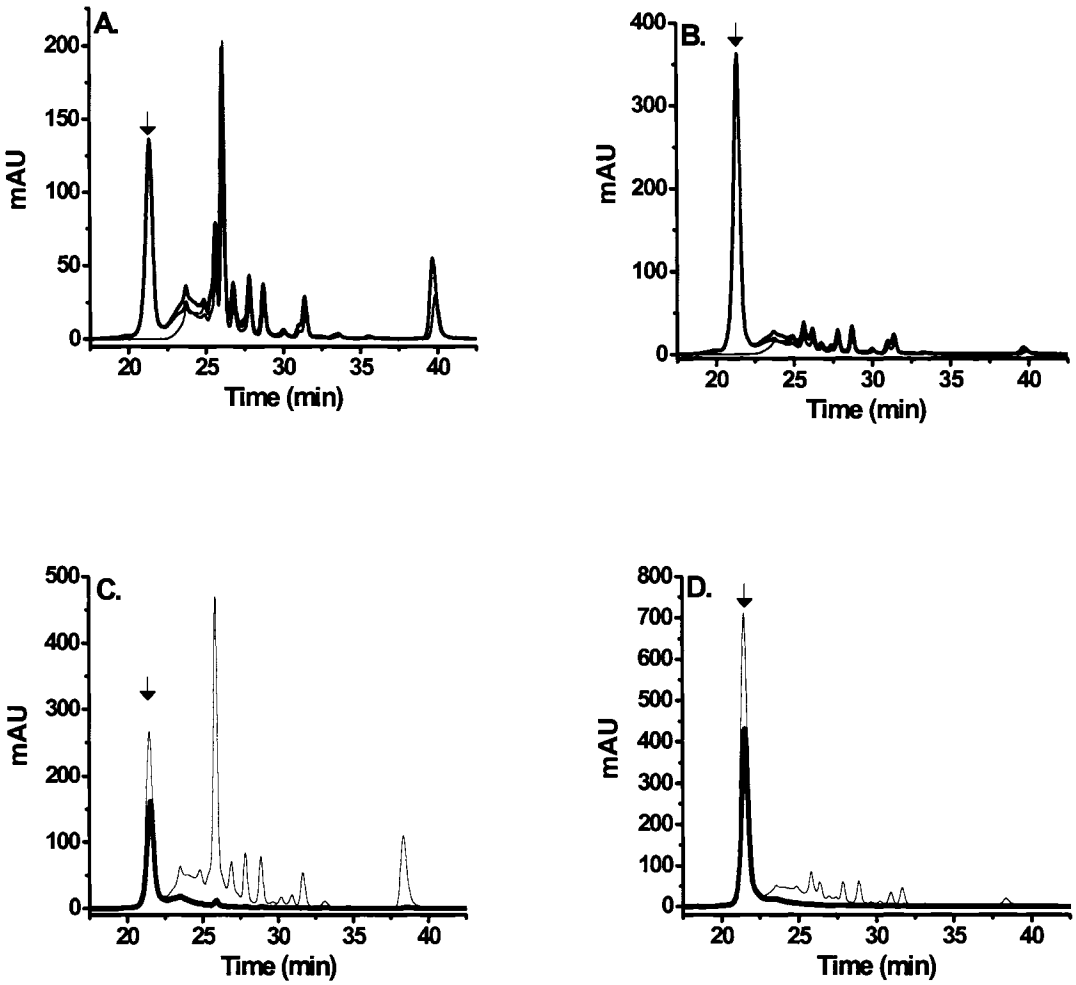

Figure 6.1. SEC elution profile of fractionated, dialyzed, and stock *B*A ultra filtrate recorded at 254nm (A and C) and 280nm (B and D). In all graphs, the *B*A peak is labeled with a black arrow. A and B) Stock BA ultra filtrate (red line), >3kDa MWCO fraction (red line), and <3kDa MWCO fraction (green line). C and D) Stock BA ultra filtrate (red line) and dialyzed *B*A (black line).

indication that *B*A-SIC studies using background materials from the ultra filtrate as mobile phase components may be more feasible than in the past (Chapter 4). In Figure 6.1A and 6.1B, fractionation of *B*A ultra filtrate with a 3kDa MWCO membrane indicated that all the impurities (non *B*A peaks) represented chemical species smaller than 3kDa. No amount of *B*A was detected in the <3kDa fraction. Still, minor amounts of impurities remained in the >3kDa fraction. It is likely that these impurities could have been removed with increased repetitions of the fractionation process described in section 6.1.1, however this option was not pursued due to the poor ratio of labor to purified product. The dialysis approach to purifying *B*A (Figure 6.1C and 6.1D) was much more successful in terms of product yield and removal of impurities. The relatively minor absorption at 280 nm of the remaining impurities indicated that the dialyzed BA sample was sufficiently pure to be used in the *B*A-stationary phase immobilization procedures and as the injection sample for *B*A-SIC experiments. Figure 6.2 shows chromatograms from the Amicon filter cell purification method. As expected, no *B*A was observed in the <10kDa MWCO fraction. The effect of MWCO fractionation and concentration on the physical stability of *B*A will be discussed in the results and discussion section of this chapter.

Gels from SDS-PAGE and IEF of *B*A are shown in Figure 6.3. The SDS gels in Figure 6.3A indicate a molecular weight of ~55 kDa, consistent with the theoretical MW as calculated from the amino acid sequence. Notably, lane 2a of the first SDS gel in Figure 6.3A demonstrates two faint bands between 14 and 6

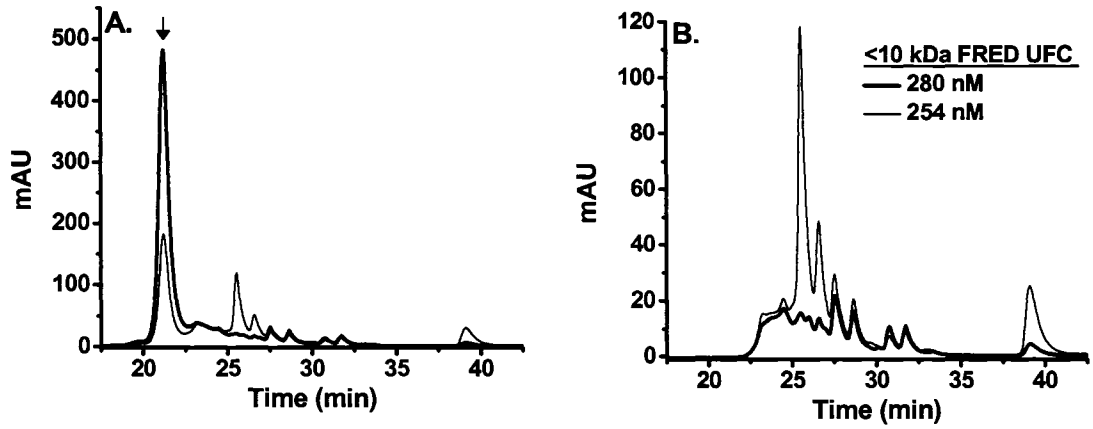

Figure 6.2. SEC elution profile of *B*A ultra filtrate fractions from the Amicon filter cell purification process. A) the >10kDA MWCO fraction. B) the <10kDA MWCO fraction Elution profiles were measured at 254 nm (black line) and 280 nm (red line). The BA peak is labeled with a black arrow in graph A.

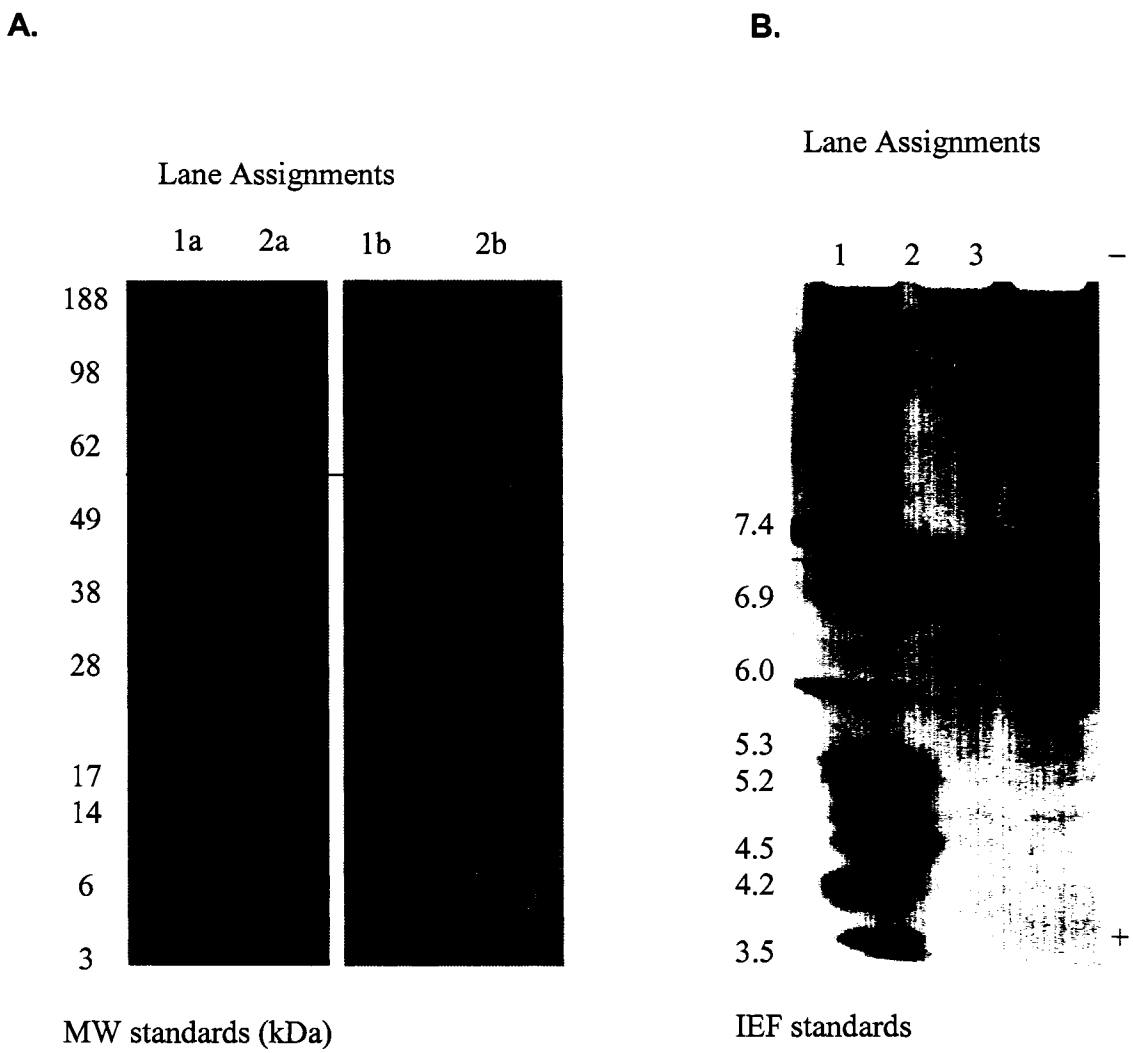

Figure 6.3. Gels from SDS-PAGE (A) and IEF (B) of dialyzed *B*A. The black lines are meant to guide the reader's eye as a marker for *B*A. A) Lanes 1a and 1b contained MW standards. Lane 2a contained 1 μL of dialyzed *B*A. Lane 2b contained 1 μL of dialyzed *B*A diluted with ten parts deionized water. B) Lane 1 contained 2.5 μL of IEF standards. Lanes 2 and 3 contained 2 μL and 3 μL of dialyzed *B*A diluted with fifty parts deionized water, respectively.

kDa. These likely represent background components (impurities) remaining in the dialyzed *B*A. Again, we point to the relative abundances of *B*A verses these impurities as indication that such impurities will not interfere with *B*A-SIC studies. The BA band in the first gel (A) is badly smeared as a result of overloading. In the second gel (B), the *B*A band is again smeared even though the amount of protein loaded into the lane had been significantly reduced. This pattern of smearing during SDS-PAGE is commonly observed with highly glycated proteins such as *B*A.[1-3]

The IEF gel in Figure 6.3B indicates that the experimental pI of *B*A is 7.4. By comparison, the theoretical pI was calculated to be 6.5. We observed a similar discrepancy between the experimental and theoretical pI when working with *P*A in Chapter 5. Moreover, it is generally accepted that the current methods for calculating theoretical pI values[4, 5] are accurate to within ± one pH unit of the experimental pI.[6]

An interesting feature of *B*A is the fact that it remains quite soluble at its pI. Proteins are generally expected to be least soluble at their pI.[7] During the preparation the second batch of *B*A-Formyl particles, K_2HPO_4 (400 mM) was added to the dialyzed *B*A solution (29 mg/mL) to bring the pH from 5.40 to 7.90. No precipitation of *B*A was observed during this process. One explanation for this somewhat counterintuitive behavior can be realized by considering the number of ionizable residues belonging to *B*A. Even though the net charge of *B*A is zero at

pH 7.4, there are well over one hundred ionizable residues belonging to each *B*A molecule. The abundance of these individual charges would potentially explain the largely pH independent precipitation behavior observed both in our laboratory and in previous studies at Genencor. Another very likely explanation comes from the fact that *BA* highly glycated. The literature contains numerous reports of glycation conferring enhanced solubility to proteins across large pH ranges, including the range of their isoelectric point.[8-10]

6.2.2. Impact of AB-Formyl CD on measured B value

*B*A-Formyl particles were used for all SIC studies. *B*A-Amino coupling trials yielded unacceptably low coupling densities (CDs) (< 1 mg of *B*A/ mL of particles). The two batches of *B*A-Formyl particles produced initial CDs of 8.5 ± 0.3 and 14.1 ± 1.6 mg of *B*A/ mL of particles. All B values were obtained from a single column packed with the former set of *B*A-Formyl particles. *B*A-SIC experiments were conducted for five weeks. Afterwards, the CD of the *B*A-Formyl particles was again determined. To our surprise, this final CD was measured as 3.7 ± 0.4 mg of *B*A/mL Formyl particles. This is 44% of the initial CD measured before the start of the SIC studies. The most plausible explanation for these results was that the initial CD of the *B*A Formyl particles was actually a measure of mg of total protein/ mL Formyl particles. More specifically, cysteine, cystine, tryptophan, and tyrosine as free amino acids or as parts of protein fragments or peptides would have contributed to the overall BCA assay signal. There is a very high possibility that any number of these chemical species are background

components of the *B*A concentrate. SEC (Figure 6.1) indicated relatively low amounts of <10 kDa MWCO background components remaining in the dialyzed *B*A. However, exact concentrations or identification of chemical species were not determined.

We proposed that some of the background species were non-covalently bound to the immobilized *B*A and thus contributed to the initial CD of the *B*A-Formyl particles. It was then important that we determined when and/or at what rate the background components were washed off the column. Taking the second set of *B*A-Formyl particles that had been stored in the refrigerator and exposing them to solution conditions representative of those used in the *B*A-SIC studies answered these questions. The CD of these particles was measured as 12.3 ± 0.7 mg of *B*A/mL of Formyl particles; consistent with the CD of 14.1 ± 1.6 mg of *B*A/mL Formyl of particles measured immediately after the coupling process was completed nearly six weeks earlier. This indicated that the CD had not degraded simply as a function of time. Aliquots of the particles were exposed to the solution conditions listed in Table 6.1. At room temperature (21 ± 2°C) only the solution of background diluted with 1 part deionized water contributed to a reduction of CD. Particles exposed to this particular solution condition yielded 81.7 ± 4.3% of their initial CD. Additionally, overnight incubation of the particles at 55°C significantly reduced the CD.

Table 6.1 Solution conditions that we tested for their effect on the CD of *BA*-Formyl particles. Particles were stirred in the solutions listed below for ~18 hours.

Solution Conditions	**Temperature**	**% of initial CD**
ACTE (50mM, pH 4.00) containing 1% NaCl	21 ± 2°C	104.4 ± 6.9
ACTE (50mM, pH 4.00) containing 2% NaCl and 5% background	21 ± 2°C	94.0 ± 6.4
ACTE (50mM, pH 4.00) containing 15% background	21 ± 2°C	101.9 ± 3.4
Background diluted with one part deionized water	21 ± 2°C	81.7 ± 4.3
Background diluted with one part ACTE (50 mM, pH 4.00) containing 1% NaCl	55°C	82.6 ± 5.4
ACTE (50mM, pH 4.00)	55°C	55.7 ± 4.8

Particles suspended in background diluted with one part ACTE (50 mM, pH 4.00) at 55°C retained 82.6 ± 5.4% of their original CD, while particles suspended in ACTE (50 mM, pH 4.00) at 55°C retained only 55.7 ± 4.8% of their original CD. The supernatant from both of these samples were also assayed. A measurable BCA signal from the supernatant of the latter particle sample supports the idea that protein/peptide species are being releases into solution from the particles. Since the background already contains considerable amounts of species that produce a BCA signal it was not possible to determine the portion of signal that was due to the release of such species from the former set of particles.

In light of these recent BCA results we can reasonably assume that the majority of CD reduction occurred within the first twenty four hours that the particles were exposed to solution conditions of ACTE (50 mM, pH 4.00) at 55°C. *B*A-SIC experiments with the particles from April 9th, 2006 (initial CD of 8.5 ± 0.3 mg of *B*A/ mL of particles) began on April 13th, 2006. This particular set of experiments was run at 25°C. On April 14th and 15th, 2006, respective column temperatures of 40°C and 45°C were used. The column temperature was first raised to 55°C on April 16th, 2006, where an ACTE buffer (100 mM, pH 5.40) was used. However, no B values were recorded. The first B values were recorded from a sequence run on April 18th, 2006 in an ACTE buffer (50mM, pH 4.00) at 25°C. The very next sequence run the following day used the same buffer conditions at a column temperature of 55°C. Therefore, all B values were calculated using the final CD

of 3.61 mg of *BA*/ mL of Formyl particles. This converts to 3.74×10^{15} *BA* molecules/ m^2 Formyl particle surface area. This is the average CD based on BCA two independent sets of BCA assay results.

The fact that the particles used in the above studies retained more CD in the presence of background is an important result. It supports our hypothesis that the reduction in CD was due to the release of non-covalently bound background species from the immobilized (covalently bound) *BA*. This makes further sense when considering that the presence of background already in solution would potentially shift the equilibrium in favor of more background remaining bound to the immobilized *BA*, consistent with our observations. As discussed in the following sections, this line of reasoning is further supported by results from BA-SIC experiments in the temperature range of 25-55°C and in the presence of background.

6.2.3 Bench scale precipitation behavior of BA

The following bench scale experiments were performed after an unexpected observation of dilution dependent precipitation behavior of the fractionated BA concentrate. Genencor reported that dilution in excess of 200% prevented precipitation of BA from the stock concentrate. However, it was not specified whether precipitation of any other chemical species was observed. Stock and fractionated BA concentrate and background samples were removed from the refrigerator and centrifuged. Figure 6.4A demonstrates the presence of a white

precipitate in the stock *B*A ultra filtrate (2A) and the background (<10kDa MWCO) filtrate (3A), but not in the fractionated BA ultra filtrate (>10kDa MWCO) (1A). Supernatant from each of these samples was then diluted with four parts deionized water. The stock and fractionated *B*A ultra filtrate samples immediately turned cloudy, the background did not. After centrifugation a grey, oily precipitate was observed in samples 1B (supernatant from >10kDa MWCO fractionated *B*A ultra filtrate) and 2B (supernatant from stock *B*A ultra filtrate). Further dilution of these samples continued to produce precipitate. No precipitate was observed from the dilution of sample 3B (supernatant from <10kDa MWCO background fraction). It is believed that the precipitate is a lipid phase that is preferentially bound to soluble *B*A in a concentration dependent manner. Whether this material is binding to the BA backbone or to the glycosyl substituents remains unclear. As we will see in the next section, this precipitation behavior significantly impacts the elution profile of *B*A.

6.2.4 BA-SIC elution profiles

Initial *B*A-SIC experiments focused on evaluation of the *B*A elution profile prior to calculation of B values. In this section, the elution profile of *B*A as a function of flow rate, temperature, pH, NaCl, and sorbitol is discussed. Many of the chromatograms presented here were used to calculate B in the next section. As we will show, valuable information was obtained from analysis of the raw chromatograms.

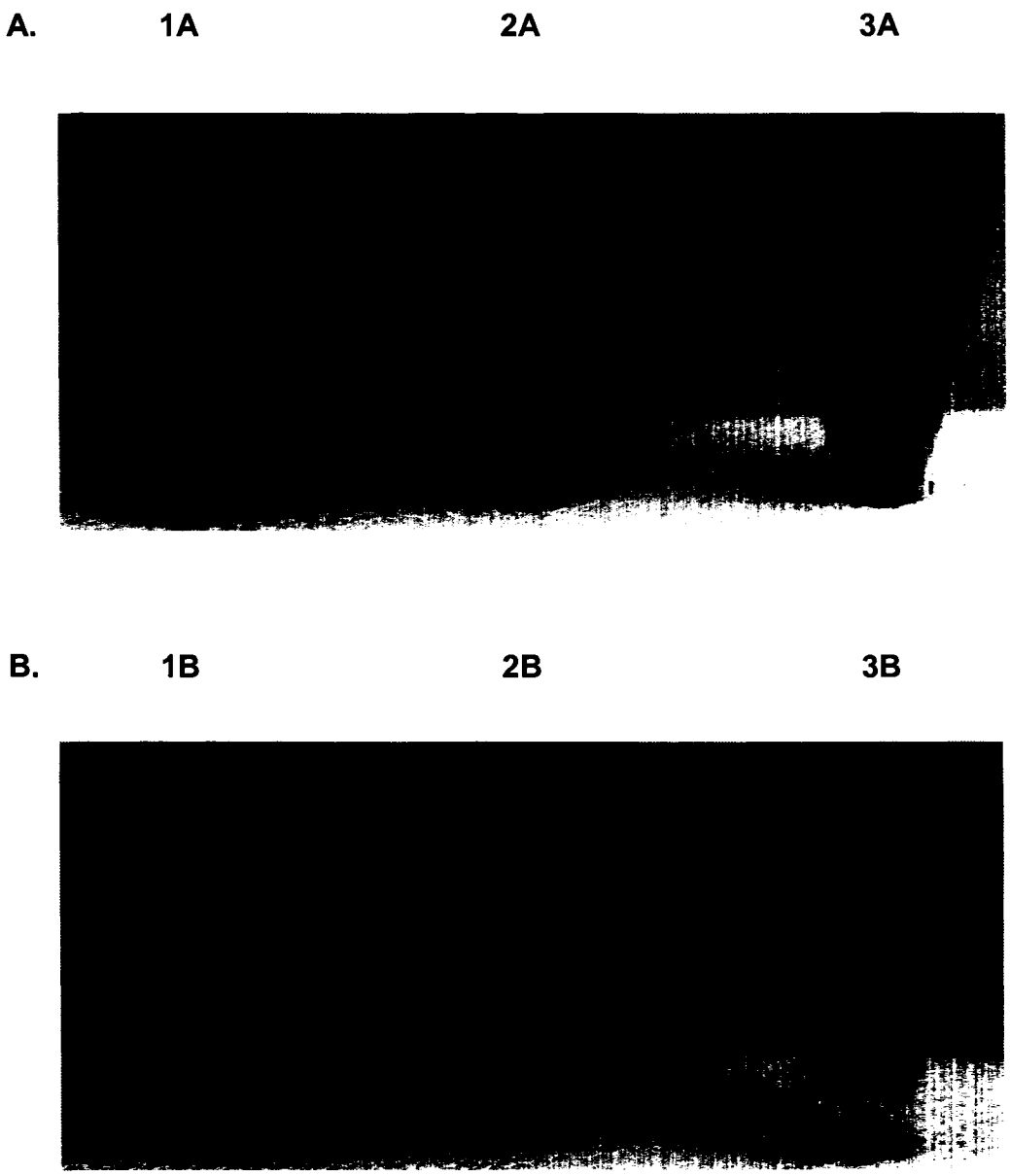

Figure 6.4. Bench scale precipitation behavior of *B*A. A) Precipitate obtained from centrifugation of the >10 kDa MWCO concentrated *B*A ultra filtrate (1A), the stock (unfractionated) *B*A ultra filtrate (2A), and the <10kDa MWCO background fraction of the ultra filtrate (3A). B) Precipitate observed from the dilution of supernatant from samples in (A). Samples were diluted with four parts water.

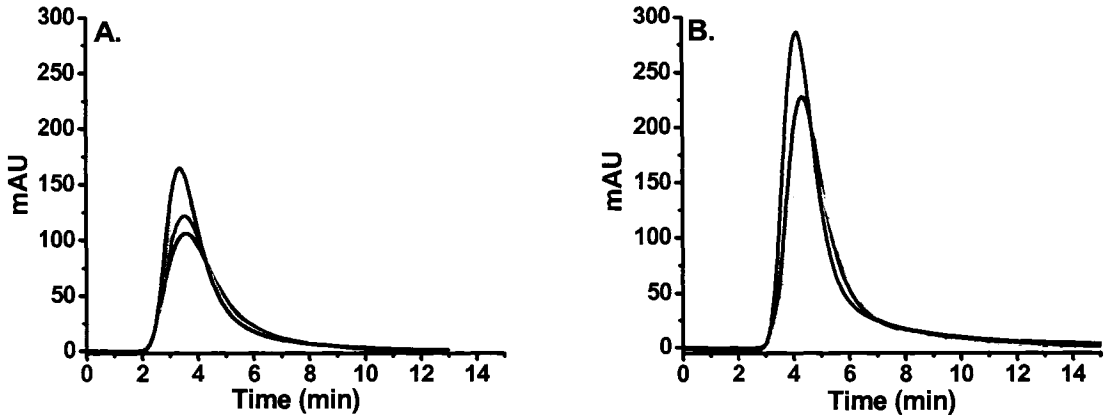

Figure 6.5. Elution profile of *B*A as a function of temperature. Buffer conditions were ACTE (100 mM, pH 5.4) at 25°C (blue line), 30°C (brown line), 35°C (grey line), 40°C (black line), 45°C (green line), or 55°C (red line). The flow rates were 200 μL/min (A) and 150 μL/min (B). The axes for both graphs are equal to facilitate comparison.

Figure 6.5 demonstrates the elution profile of *B*A as a function of temperature and flow rate. Buffer conditions of ACTE (100 mM, pH 5.40) were chosen to match the pH of the stock *B*A ultra filtrate. Temperatures of 25°C, 30°C, 35°C, and 40°C were run on first (Figure 6.5A). Temperatures of 35°C, 45°C, and 55°C were run second (Figure 6.5B). The former data set was obtained at a flow rate of 200 μL/min and the latter at 150 μL/min. Higher flow rates lead to faster elution times and narrower peaks. Lower flow rates, on the other hand, allow for more time on the column, which improves the sensitivity of SIC to minor changes in solution conditions. Generally, a compromise is made to ensure sensitivity while maintaining well-defined peaks. Therefore, all subsequent *B*A-SIC studies were run at a flow rate of 150 μL/ min.

As shown in Figure 6.5 the *B*A peak shifts towards shorter retention times as a function of increased temperature. For example, increasing the temperature from 35-55°C shifted the maximum absorption of the *B*A peak from 4.50 ± 0.03 to 4.12 ± 0.03 min. This indicates that *B*A self-interaction is less favored at elevated temperatures, consistent with the "normal" temperature dependent precipitation behavior of *B*A observed at Genencor. Perhaps the most striking feature of the BA elution profiles in Figure 6.5 is the significant dependence of peak height and area on temperature. If this were due solely to temperature induced changes in *B*A self-interaction we would expect to see the peaks become shorter and broader with conditions that favor *B*A self-interaction. Conversely, peaks should become taller and narrower at conditions that favor *B*A-solvent interactions. In

Figure 6.5 the height of the *B*A peaks are dramatically affected by changes in temperature while the peak width remains relatively constant. During calibration runs where the column temperature was raised and stabilized prior to any injections we observed quite large peaks eluting from the column. This suggested that a portion of the *B*A injected into the mobile phase was remaining on the SIC column in a temperature dependent manner. At this stage of the *B*A-SIC studies it was unclear whether it was the *B*A molecules or the background components that were remaining on the column.

The pH dependent elution profile of BA is presented in Figure 6.6. The buffers for these experiments contained ACTE (25 mM) and K_2HPO_4 (25 mM) to ensure buffering capacity at pH 4.00, pH 6.00 and pH 7.00. Each of these pH conditions was run at 25°C and 45°C. As shown in Figure 6.6, *B*A peaks at pH 7.00 and pH 6.00 are very tall and narrow, differing only by a slightly lower maximum absorption and slightly longer retention time of the pH 6.00 peak. By contrast, the pH 4.00 peak is much shorter, broader, and more strongly retained on the column suggesting that *B*A self-interaction is substantially enhanced as the pH is lowered from 6.00 to 4.00. This is counterintuitive considering that the experimental pI of *B*A is 7.4 (Figure 6.3). Again, we speculate that the pH dependent solubility behavior of *B*A is due to the glycation of this protein.

Another interesting outcome of these experiments was observed when the column temperature was set to 45°C (Figure 6.6B). A very broad tailing peak

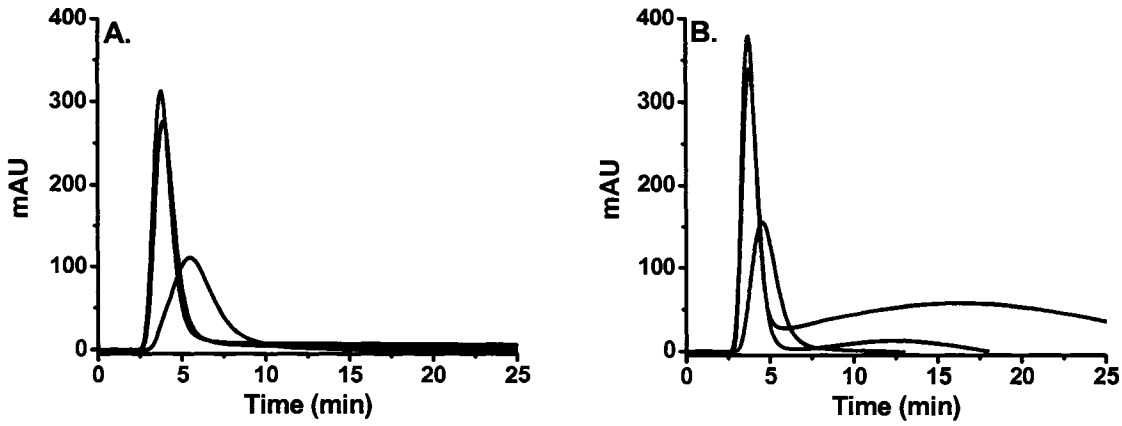

Figure 6.6. Elution profile of *B*A as a function of pH. Buffer conditions were ACTE (25mM), K_2HPO_4 (25mM) containing 2% NaCl at pH 7.00 (green line), pH 6.00 (red line), or pH 4.00 (black line). Column temperatures were 25°C (A) and 45°C (B).

begins to appear at pH 6.00 and becomes more pronounced at pH 7.00. Initially, we speculated that these elution profiles were a result of highly attractive self-interaction between portions of the mobile phase *B*A that saturated the stationary phase. The sharp initial peak would thus represent the unretained portion of the mobile phase *B*A while the broad tailing peak would be due to the proposed highly attractive self-interaction. This hypothesis was ruled out when we observed similar behavior while using an ethanolamine-Formyl column (a dead column). It was discovered that the *B*A injection samples became cloudy after several days at room temperature. We believed that soluble aggregates were forming, and when injected, interacted very strongly with the *B*A-SIC column. The issue was resolved by frequently replacing the *B*A injection sample with fresh portions of the dialyzed *B*A that was being stored in the refrigerator at 4°C. When *B*A was stored at 4°C, the sample remained free of any visible cloudiness. It is important to point out that the *B*A peaks obtained at 45°C demonstrate higher maximum absorbencies than their corresponding peaks obtained at 25°C. This points to the idea of injected material remaining on the column in a temperature dependent manner.

Figure 6.7 demonstrates how the elution profile of BA is affected by the addition of up to 4% NaCl to an ACTE buffer (50mM, pH 4.00) and at a column temperature of either 25°C (left graph) or 55°C (right graph). Here, we chose to work at pH 4.00 based on theoretical estimates of BA's net charge as a function of pH. At pH 4.00 BA is highly positively charged in excess of +50 according to

theoretical estimates). NaCl was used as a general salting out agent; it should shield electrostatic repulsion between like charges, thus favoring protein self-interaction due to short range hydrophobic interactions.[11] Indeed, the chromatograms in Figure 6.7 demonstrate that the addition of up to 4% NaCl to the mobile phase shifts the maximum absorption of the *B*A peaks towards longer retention times, reflecting enhanced *B*A self-interaction. Comparison between the NaCl induced elution profiles at the two different temperatures indicates that *B*A retention times are shorter and less affected by NaCl at 55°C (Figure 6.7B) than at 25°C (Figure 6.7A). For example, increasing the NaCl concentration from 0-3% at 25°C shifts the maximum retention of BA from 3.26 ± 0.09 to 6.74 ± 0.02 min. The same change in NaCl concentration at 55°C shifts the maximum retention of *B*A from 3.10 ± 0.01 to 4.57 ± 0.02 min. These data are again consistent with the reported normal temperature dependent precipitation behavior of *B*A. Figure 6.7 demonstrates substantial shouldering and splitting of the *B*A peaks. At the 3% NaCl, 25°C condition a front shoulder is observed. At 4% NaCl the shoulder begins to split away from a much broader peak. This particular elution profile was not acceptable for use in calculating B due to the extremely broad nature of the primary peak. However, it is still qualitatively valuable for demonstrating the salting out behavior of NaCl on *B*A.

Similar shouldering behavior of the *B*A elution profile is observed at 55°C. Here, the 0% NaCl condition results in a shoulder on the backside of the primary peak. The retention time of this shoulder is 3.98 ± 0.03 min. At 4% NaCl, there is a

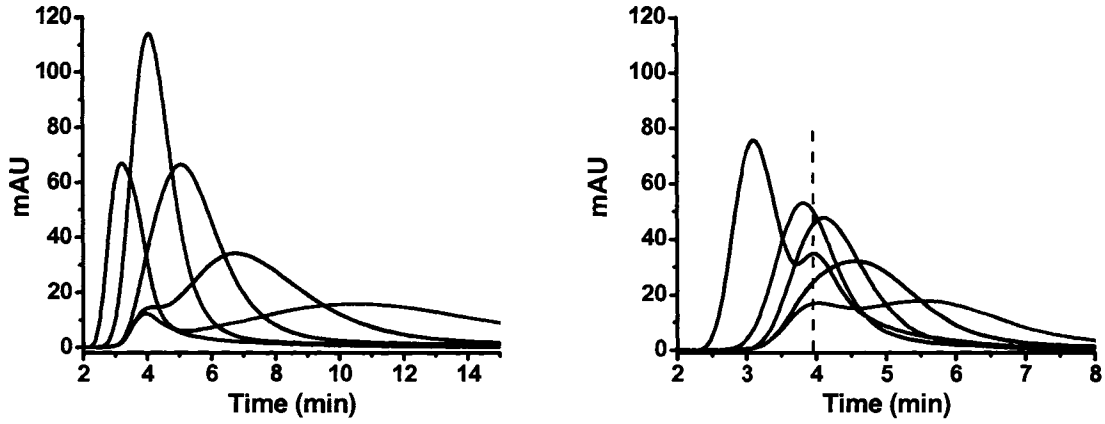

Figure 6.7. Elution profile of BA as a function of NaCl. Buffer conditions were ACTE (50mM, pH 4.00) containing 0% NaCl (black line), 1% NaCl (red line), 2% NaCl (green line), 3% NaCl (dark blue line), or 4% NaCl (light blue line). Column temperatures were 25°C (A) and 55°C (B). Note that the X-axes are scaled differently.

shoulder at 4.02 ± 0.01 min, in front of the primary peak. From 1-3% NaCl, no splitting/shouldering is observed, however, the 3% NaCl peak is distorted in the region where the shoulders for the 1% and 4% NaCl conditions were observed (the dotted line has been added to help guide the eye). Note that the shouldering previously observed in the pH studies (Figure 6.6) is quite different from what we observed here. The *B*A elution profiles in Figure 6.7 demonstrate that the majority of the *B*A peak moves around a shoulder that remains at a constant retention time. This behavior was not observed in dead column experiments and injection samples were periodically checked and replaced with fresh aliquots from the stock dialyzed *B*A sample.

We believe that the shouldering of the *B*A peaks in Figure 6.7 is the result of dilution dependent precipitation that occurs when the injected *B*A sample enters the mobile phase. As shown in Figure 6.4B, dilution of *B*A solutions results in the precipitation of a grey, oily substance. The fact that this precipitate was not observed in the <10kDa filtrate suggests that it is bound to the soluble *B*A. Injection of *B*A into the mobile phase causes sufficient dilution to result in disassociation and phase separation of this oily substance. Visual inspection of the column indicated that this material was not being deposited onto the stationary phase. We should therefore observe this material in our chromatograms. However, it will only be viewable when the soluble portion of the *B*A injection is not covering it up. This will be discussed in more detain in the next section.

The sorbitol induced elution profile of *B*A is presented in Figure 6.8. Up to 12% sorbitol was mixed into a mobile phase of ACTE (50mM, pH 4.00) containing 3% NaCl at 25°C (Figure 6.8A) and 55°C (Figure 6.8B). The constant presence of 3% NaCl in the mobile phases for this set of experiments was based on previous results (Chapters 2 and 5) which demonstrated that the effect of polyol based cosolvents on protein self-interaction was strongest when long range electrostatics were suppressed. This has been accomplished here by the addition of 3% NaCl. Referring back to Figure 6.7, we observed that 3% NaCl induced considerable salting out of *B*A without affecting the peak beyond the point of accurate analysis. In Figure 6.8A, the addition of up to 12 % sorbitol at 25°C induced a significant shift in the maximum absorbance of *B*A towards shorter retention times (from 6.15 ± 0.08 to 4.78 ± 0.01 min). At 55°C, the same amount of sorbitol was less effective at reducing *B*A retention times, inducing a shift from 4.84 ± 0.02 to 4.07 ± 0.01 (Figure 6.8B). Other notable features of the elution profiles in Figure 6.8 include the overall shorter retention times of *B*A at 55°C (Figure 6.8B) than at 25°C (Figure 6.8A) and the shoulder appearing at ~4 min on the *B*A peak at the 0% sorbitol, 25°C condition (Figure 6.8A).

As a final set of SIC experiments we sought to evaluate *B*A self-interaction as a function of the background material that composes the stock *B*A ultra filtrate. The isolation of this background material was described in section 6.1.1. Using this material as a mobile phase component represented unique challenges that

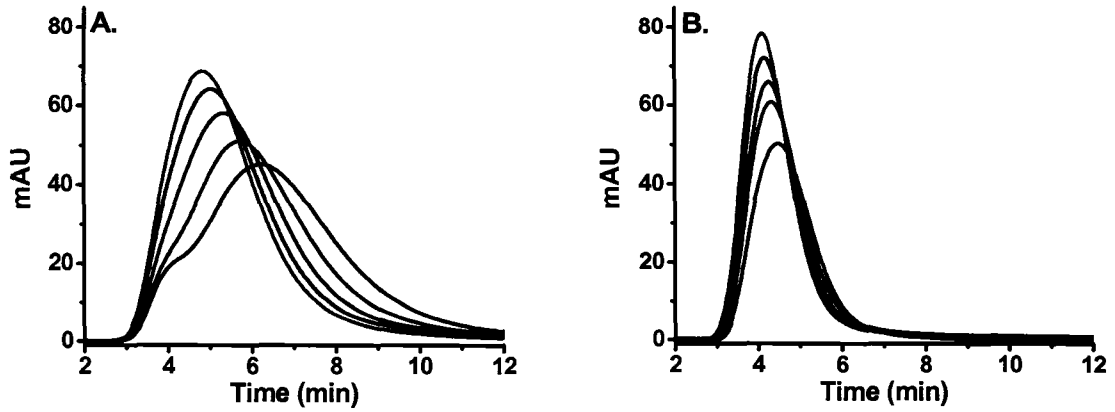

Figure 6.8. Elution profile of *B*A as a function of sorbitol. The buffer conditions were ACTE (50mM, pH 4.00) containing 3% NaCl and 0% sorbitol (black line), 3% sorbitol (red line), 6% sorbitol (green line), 9% sorbitol (dark blue line), or 12% sorbitol (light blue line). Column temperatures were 25°C (A) and 55°C (B).

required extended calibration times and minor modifications to our detection parameters. For these experiments, the background sample obtained from the Amicon filtration process (see section 6.1.1) was diluted with one part deionized water to a final volume of 300 mL. The pH was measured as 5.20. Therefore, the percent background numbers reported in the following discussion refer to the diluted background sample. Corresponding percents for the undiluted background sample would be half of the reported values. For consistency, only diluted percent values are discussed.

The results of the initial attempt at running background as a mobile phase component are shown in Figure 6.9. The buffer condition for this set of experiments was ACTE (10 mM, pH 5.20). These conditions were chosen to mimic the pH of the background while minimizing the introduction of new buffer species. The chromatograms indicate that the presence of up to 5% background shifts the maximum absorption of *B*A towards longer retention times. One of the challenges encountered during this experiment was a large increase in the baseline due to the background. Mixing 5% background into the mobile phase raised the baseline by ~1 AU and required >70 minutes to stabilize. In the absence of any background, column stabilization times average ~30 minutes and typically generate minimal baseline shifts (<50 mAU). The baseline noise introduced by the background required minor adjustments to our detection parameters and injection volumes. For example, the Chemstation integration parameters had to be adjusted to a peak width threshold of 0.2 for the data in

Figure 6.9. The setting for all previous experiments was 0.05. Another modification was to double our injection volumes of *B*A and acetone from 1 μL to 2 μL. This effectively increased the signal to noise ratio. To maintain consistency with previous stages of the *B*A experiments, larger injection volumes or masses were avoided.

Severe baseline noise was encountered in the presence of 10% background. Figure 6.10 demonstrates the effect of increased bandwidth on this noise and on the elution profile of *B*A. The mobile phase used to obtain these chromatograms was ACTE (50 mM, pH 4.00) containing 10% background at 25°C. These conditions were chosen to build upon solution parameter space investigated in previous *B*A-SIC experiments (Figure 6.7). To date, all *B*A-SIC data had been obtained using a detection wavelength of 280 nm with a bandwidth of 10 nm. The data in Figure 6.10 show that these detection parameters yielded an extremely noisy signal in the presence of 10% background. Increasing the bandwidth reduced this noise but also significantly affected the *B*A elution profile. In consideration of these results, a bandwidth of up to 25 nm was deemed an acceptable setting for reducing baseline noise while maintaining an elution profile representative of what would be observed at a bandwidth of 10 nm. Using these detection parameters, we see that the elution profile of *B*A in the presence 10% background demonstrates a front shoulder at ~4 minutes and a maximum absorption of the primary *B*A peak near six min. In the absence of background

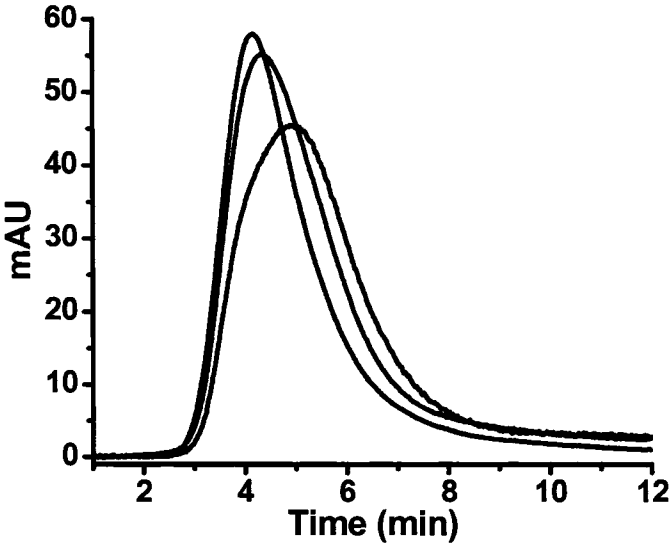

Figure 6.9. Elution profile of *B*A as a function of % background (<10kDa MWCO) in the mobile phase. Buffer conditions were ACTE (10mM, pH 5.20) containing 0.0% background (black line), 2.5% background (red line), or 5.0% background (green line) at 25°C.

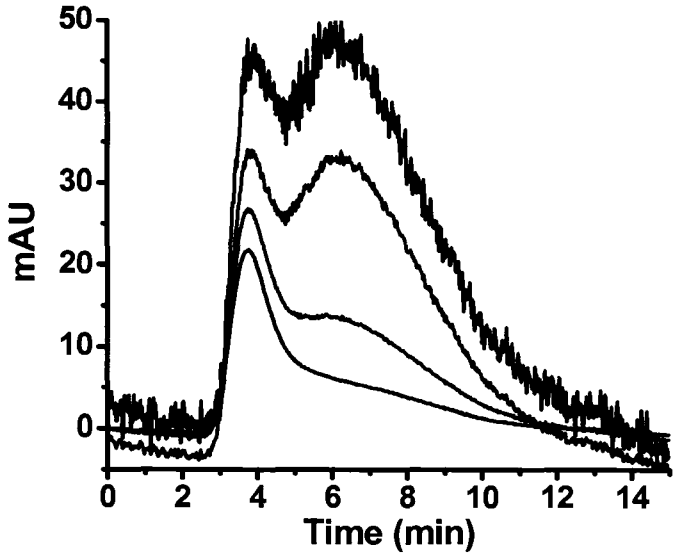

Figure 6.10. Elution profile of *B*A as a function of bandwidth. Buffer conditions were ACTE (50 mM, pH 4.00). Detection wavelength was 280nm with a bandwidth of 10 nm (black line), 25 nm (red line), 50 nm (green line), or 100 nm (blue line). Column temperature was 25°C.

(with all other buffer conditions equal) the average retention time for the maximum absorption of *B*A was 3.26 ± 0.10 min. These data clearly indicate that the presence of background as a mobile phase component leads to increased retention times of maximum *B*A absorption.

For the next experiment, up to 4% NaCl was added to constant buffer conditions of ACTE (50 mM, pH 4.00) containing 5% background at 25°C (Figure 6.11). Figure 6.7 shows the elution profile of *B*A as a function of the same solution conditions, minus the background. By comparing the results of the two experiments we are able to better understand how the presence of background in the mobile phase affects the elution profile of *B*A. In Figure 6.11 we again observed splitting of the BA peak as the NaCl concentration was increased. *B*A peaks at the 3% and 4% NaCl conditions have a shoulder at ~4 minutes. An interesting feature in the chromatograms from both Figures 6.7 and 6.11 is the significantly reduced peak area of BA at the 0% NaCl condition. As the NaCl concentration is raised from 1%-4% the shift towards longer retention times of the *B*A peak is accompanied by reductions in peak height and increases in peak width. This behavior is expected based on the salting out effect of NaCl on *B*A. The *B*A peak at the 0% NaCl condition does not fit the trend. In Figure 6.11, significant tailing that continued for nearly twenty minutes was observed in the *B*A peak at 0% NaCl. The tail was far to broad to be treated as a separate peak or accurately measure its maximum retention. It was concluded that the

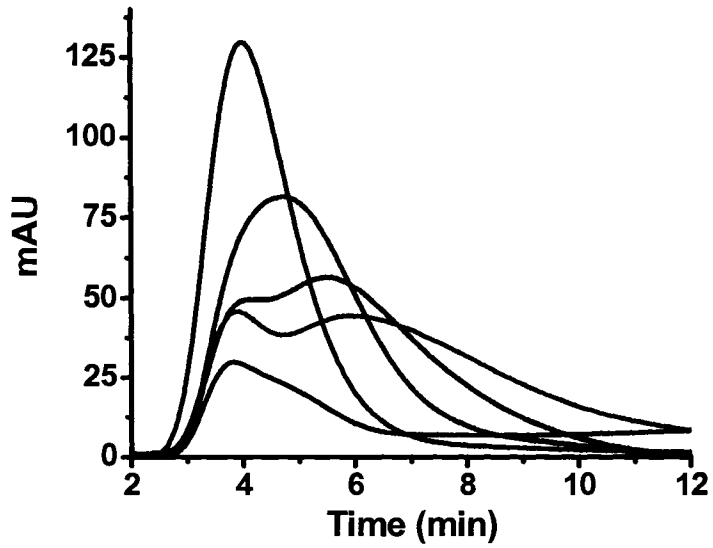

Figure 6.11. Elution profile of *B*A as a function of NaCl. Buffer conditions were ACTE (50 mM, pH 4.00) containing 5% background and 0% NaCl (black line), 1% NaCl (red line), 2% NaCl (green line), 3% NaCl (dark blue line), or 4% NaCl (light blue line). The detection wavelength was 280nm with a 25 nm bandwidth. The column temperature was 25°C.

tailing was the result of highly attractive interactions between a portion of the mobile phase *B*A and the stationary phase. This conclusion was supported by the observation of a very large peak (maximum absorbance of ~300 mAU) eluting from the column during the calibration run from 0% to 1% NaCl. It was impossible to determine the compositional nature of this peak. Since this behavior was not observed during any other conditioning runs it was determined that the overall NaCl induced trend in the elution profile of *B*A accurately reflected changes in the self-interaction between stationary and mobile phase *B*A.

6.2.5 B of BA

In this section we present B of *B*A as measured by SIC. The previous analysis of *B*A elution profiles was instrumental in ensuring the accurate determination of trends in B as a function of solution conditions. It is important to note that our discussion focuses on trends in B rather than absolute B values. As with previous studies on multiple other proteins, we assert here that the following trends in B are representative of changes in the physical stability of *B*A.

NaCl was the most widely studied solution additive for *B*A. Figure 6.12 shows measured trends in B as a function of NaCl at 25°C and 55°C and in the presence of 5% background. The data show that the addition of up to 4% NaCl enhances *B*A self-interaction, as indicated by the falling trend in B. The strength of the NaCl induced trend in B is sensitive to both temperate and the presence of

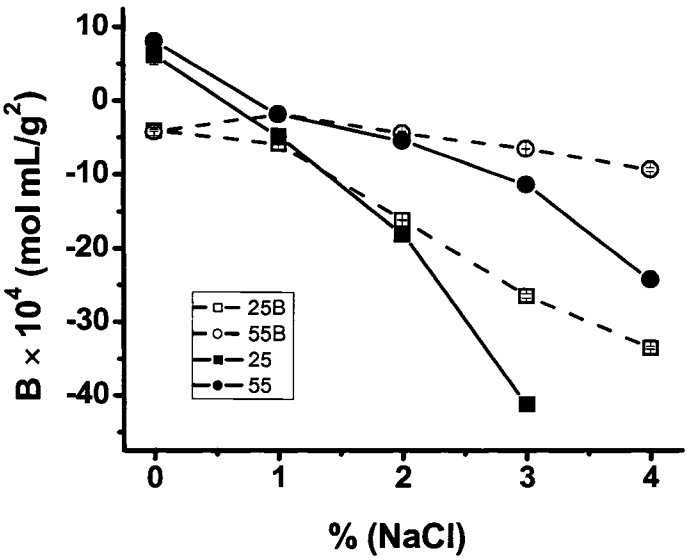

Figure 6.12. B trends of *B*A as a function of NaCl. Buffer conditions were ACTE (50 mM, pH 4.00) (solid symbols, solid lines) or ACTE (50mM, pH 4.00) containing 5% background (open symbols, dashed lined). Column Temperatures were 55°C (red symbols and lines) or 25°C (black symbols and lines). Solid and dashed lines were added to help guide the reader's eyes.

background. In the absence of NaCl, B is relatively unaffected by changes in temperature from 25-55°C. As the concentration of NaCl is increased, B falls faster at 25°C than at 55°C. The presence of 5% background, on the other hand, lowers B in the absence of NaCl and reduces the overall strength of the NaCl induced trend in B. The sensitivity of B to temperature again depends on the concentration of NaCl, just as it did in the absence of background. Together, these data support several of our conclusions from the *B*A elution profile analyses in the previous section. NaCl has a general salting out effect on BA, as indicated by the trend towards lower B values. The physical stability of *B*A is improved by raising the temperature from 25-55°C, as indicated by the trend towards increased B values. Moreover, the temperature dependence of B is more pronounce as the concentration of NaCl is increased.

Figure 6.13 compares trends in B and solubility as a function of NaCl. The solubility data was obtained from BCA assay measurements of the supernatants from the photographed samples. The amount of precipitate in these samples clearly increases as a function of NaCl concentration. The solubility and B trends demonstrate excellent qualitative agreement. These data support the validity of SIC measured trends in B as accurate indicators of solubility trends, and thus the physical stability of *B*A. Previous studies performed at Genencor revealed that the addition of up to 18% NaCl effectively prevented precipitation of *B*A from the ultra filtrate. This is contrary to our observations. The apparent discrepancy is

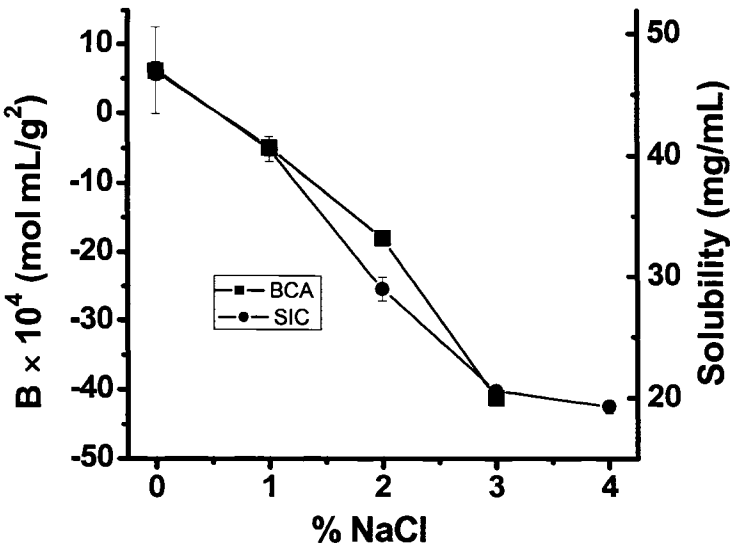

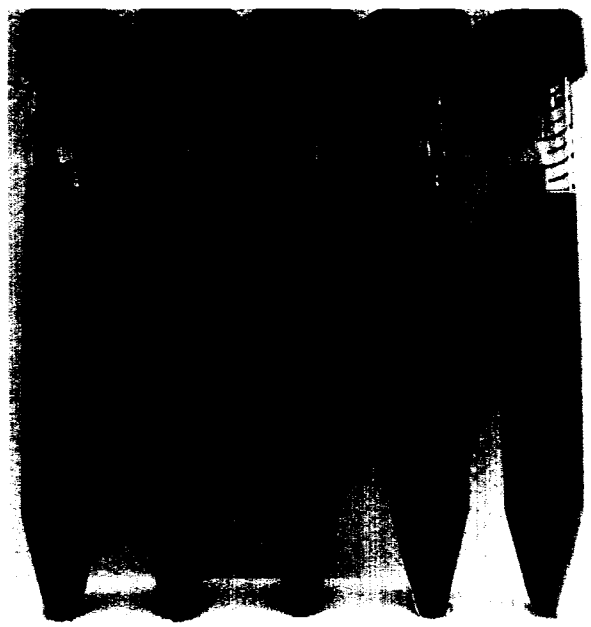

Figure 6.13. B (black squares) and solubility (red) trends of *B*A as a function of NaCl. Buffer conditions for B data were ACTE (50 mM, pH 4.00) at 25°C. Buffer conditions for solubility data were fractionated *B*A ultra filtrate (sample 1A in Figure 6.4) adjusted to pH 4.00 with 5% ACTE at ambient temperature (22 ± 2 °C). Solubility of *B*A was measured by BCA assay using supernatant from the samples in the photograph.

easily resolved when considering the vastly different solution environments in which the opposite behaviors were observed. The improved physical stability of *B*A afforded by NaCl was observed in the presence of the ultra filtrate. *B*A-SIC experiments were performed after purification processes that removed much of ultra filtrate (<10kDa MWCO background). When we reintroduced as little as 5% of the background material we saw a reduction in the over NaCl induced trend in B (Figure6.12). It is therefore plausible that additional reintroduction of the background material to its original concentration could result in a complete reversal of NaCl's effect on the physical stability of B.

Figure 6.14 shows the results of a *B*A-SIC screening study for the effects of NaCl and pH on B. Each contour plot contains eighteen B values (six NaCl concentrations (0%-5%) at each of three pH values (4.50, 5.00, and 5.40)). B for each condition was measured at 25 and 55°C to yield a total of 36 data points between the two plots. Both plots utilize a common shading scale to facilitate comparison. The B trends in both plots can be visualized as a saddle, curving downward at the top left and bottom right corners (indicating reduced physical stability), and upward at the top right and bottom left corners (indicating enhanced physical stability. At both temperatures, the addition of up to 5% NaCl demonstrates a general salting out effect (lowering of B) at pH 4.50 and a general salting in effect (raising of B) at pH 5.40. Higher temperatures promote higher B values and reduce the strength of the NaCl and pH induced trends in B,

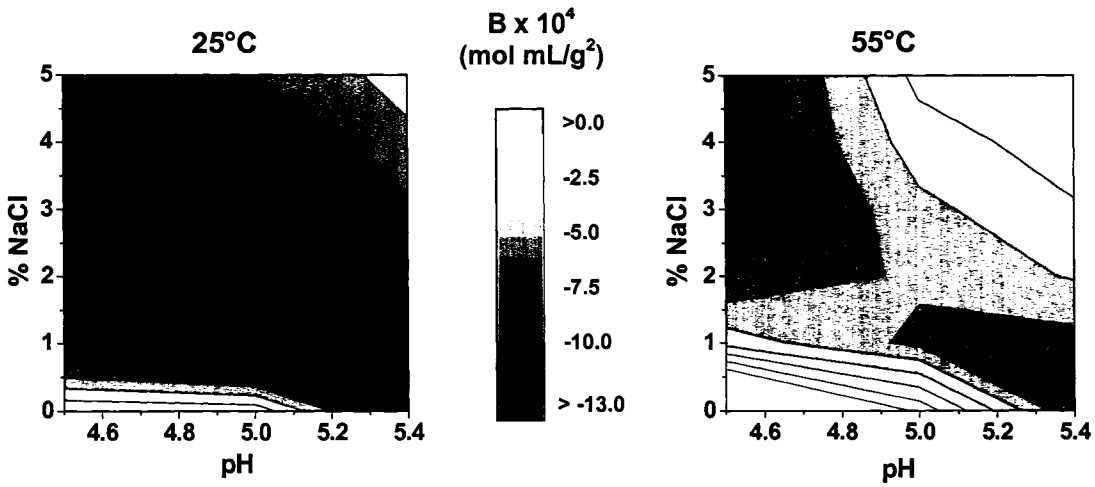

Figure 6.14. Contour plots of *B*A B values as a function of NaCl and pH at 25°C (left plot) and 55°C (right plot). All solutions were buffered with ACTE (50 mM).

as previously observed. The lowest B value (-19.11 ± 0.50 × 10^{-4} mol mL/ g^2) was obtained at 3% NaCl, pH 4.50, 25°C, and the highest (4.76 ± 0.43 × 10^{-4} mol mL/ g^2) was obtained at 0% NaCl, pH 4.50, 55°C.

Increasing the pH from 4.50 to 5.40 at 0% NaCl shifted B towards more negative values while the same increase in pH in the presence of 5% NaCl had the opposite effect. Compared to NaCl induces trends in B, pH induced trends were relatively weak. The strongest pH dependent trend in B was measured at conditions of 5% NaCl, 25°C, where raising the pH from 4.50 to 5.40 increased B by 11.64 ± 0.77 × 10^{-4} mol mL/ g^2. The difference between the highest and lowest B values for this set of experiments (given in the previous paragraph) was 23.87 ± 0.66 ± 0.77 × 10^{-4} mol mL/ g^2. Therefore, it is reasonable to say that we observed a pH dependent trend in the physical stability of *B*A in the pH range of 4.50 to 5.40. These data seemingly conflict with the reported pH independent precipitation behavior of *B*A observed at Genencor. Again we point to the different solution environments in which the two sets of studies were conducted. Even though our measured trends in B indicate shifts in the physical stability of *B*A, it was not determined whether those trends were sufficient to actually induce precipitation.

Figure 6.15 demonstrates the effect of sorbitol on B of *B*A. The addition of up to 12% sorbitol effectively shifts B towards higher values, indicating enhanced physical stability of *B*A. These data are consistent with results from Genencor

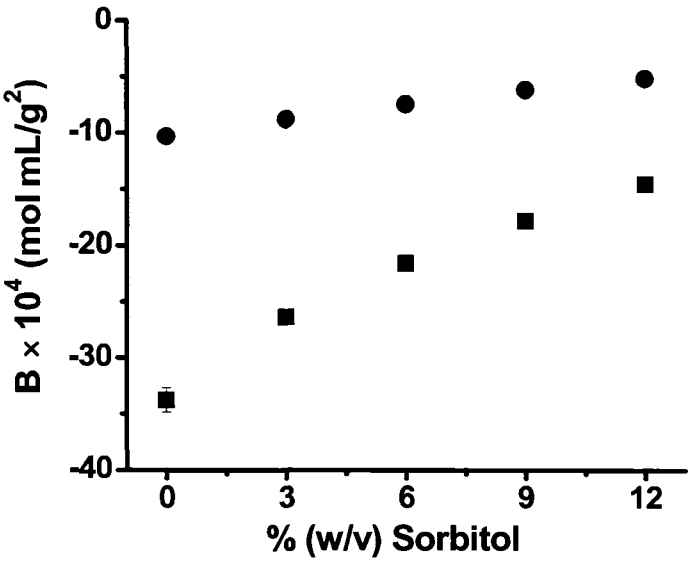

Figure 6.15. Sorbitol induced trends in B of *B*A. Solution conditions were ACTE (50 mM, pH 4.00) containing 3% NaCl at 55°C (red circles) or 25°C (black squares).

that up to 7% sorbitol inhibited precipitation of *B*A. In this case, the difference in solution environments between the stock ultra filtrate and the purified *B*A did not seem to significantly alter the overall effect of sorbitol induced stabilization of *BA*. In Figure 6.15 we also observe higher B values and a reduction in the strength of the sorbitol induced trend in B. These data support previous reports of the normal temperature dependent physical stability of *B*A (observed in our SIC studies and in independent studies at Genencor). Additionally, a reduced NaCl induced trend in B was observed at 55°C, consistent with the sorbitol results in Figure 6.15.

6.3 Conclusions

The physical stability of *B*A was evaluated as a function of solution parameter dependent trends in B. The effects of temperature, pH, NaCl, sorbitol, and the addition <10kDa MWCO background from the ultra filtrate on B were measured by SIC. Careful analysis of the *B*A elution profile during these studies alluded to a concentration dependent phase separation of non-specifically bound material from the soluble *B*A. This proved useful for understanding the observed trends in B, and thus the physical stability of *B*A.

As a function of temperature, B of *B*A at 55°C was always greater than or equal to B of *B*A at 25°C. The separation between trends in B at each temperature scaled with concentrations of NaCl and sorbitol. At pH 4.00, the addition of up to sorbitol 12% induced shifts towards more positive B values. At the same pH, the

addition of up to 4% NaCl demonstrated a strong salting out effect (lowering of B) on *B*A. As the pH was raised to 5.40 the NaCl induced trend in B reversed.

B of *B*A was shifted towards lower values as the pH was raised from 4.50 to 5.40. These results conflicted with the reported pH independent precipitation of BA observed in independent studies at Genencor, and are seemingly counter intuitive considering the experimental pI of *B*A was determined to be 7.4. Differences between the solution environment of the stock *B*A ultra filtrate used during studies at Genencor and the purified *B*A concentrate used for SIC studies were identified as the most likely source of discrepancy between results obtained from each laboratory. Additionally, it is likely that pH dependent trend in B could indicate a reduction in the physical stability of *B*A without necessarily inducing precipitation. The pH dependent physical stability of *B*A, and the fact that *B*A remained soluble even at its pI, was clarified by considering the abundance of ionizable residues belonging to each *B*A molecule and the highly glycated nature of *B*A.

A particularly interesting result of this work came from the <10kDa MWCO background studies. We observed that the addition of up to 5% of this background material to the mobile phase enhanced *B*A self-interaction (lowered B) and reduced the overall strength of the NaCl induced trend in B. We also determined that reductions in the CD of the *B*A-Formyl particles were caused by exposure to solution conditions at 55°C. The CD reduction was explained by the

temperature and concentration dependent release of non-specifically bound background components from the *B*A immobilized to the Formyl particles. Therefore, the increased physical stability of *B*A at elevated temperature may be explained by the temperature dependent release of such materials from the soluble *B*A. This suggests that *B*A would be physically more stable in a reduced background solution environment. In support, fractionated *B*A concentrate (filtered by a 10kDa MWCO membrane) stored at 4°C remained free of precipitate. BCA assay of this sample indicated a total protein concentration of 83.33 ± 0.14 mg/mL. Both the background sample (<10kDA MWCO fractionate) (9.73 ± 0.51 mg/mL) and the stock BA ultra filtrate (48.11 ± 2.65 mg/mL) contain visible amounts of precipitate.

6.4 Acknowledgments

The author would like to extend gratitude to Beth Fryksdale, Douglas Dale, and Dr. Alfred Gaertner for their contributions to the above studies of BA.

6.5 References

1) *Heterogeneity in utilization of N-glycosylation sites Asn(624) and Asn(138) in human lactoferrin: A study with glycosylation-site mutants,* vanBerkel, P. H. C.; vanVeen, H. A.; Geerts, M. E. J.; deBoer, H. A.; Nuijens, J. H., *Biochemical Journal* **1996,** 319, 117-122.
2) *Glycosylation provides both stimulatory and inhibitory effects on cell surface and soluble CD44 binding to hyaluronan,* Skelton, T. P.; Zeng, C. X.; Nocks, A.; Stamenkovic, I., *Journal of Cell Biology* **1998,** 140, (2), 431-446.
3) *Glycosylation Analysis of a Polyreactive Human Monoclonal Igg Antibody Derived from a Human-Mouse Heterohybridoma,* Leibiger, H.; Hansen, A.; Schoenherr, G.; Seifert, M.; Wustner, D.; Stigler, R.; Marx, U., *Molecular Immunology* **1995,** 32, (8), 595-602.

4) *Isoelectric Points of Proteins - Theoretical Determination,* Sillero, A.; Ribeiro, J. M., *Analytical Biochemistry* **1989,** 179, (2), 319-325.
5) *Polypeptide Amino-Acid-Composition and Isoelectric Point .2. Comparison between Experiment and Theory,* Patrickios, C. S.; Yamasaki, E. N., *Analytical Biochemistry* **1995,** 231, (1), 82-91.
6) *The effect of net charge on the solubility, activity, and stability of ribonuclease Sa,* Shaw, K. L.; Grimsley, G. R.; Yakovlev, G. I.; Makarov, A. A.; Pace, C. N., *Protein Science* **2001,** 10, (6), 1206-1215.
7) Tanford, C., *Physical Chemistry of Macromolecules*. ed.; John Wiley & Sons Inc: New York, **1961**.
8) *Covalent Binding of Glycosyl Residues to Bovine Casein - Effects on Solubility and Viscosity,* Courthaudon, J. L.; Colas, B.; Lorient, D., *Journal of Agricultural and Food Chemistry* **1989,** 37, (1), 32-36.
9) *Covalent Binding of Glycosyl Residues to Beta-Lactoglobulin - Effects on Solubility and Heat-Stability,* Kitabatake, N.; Cuq, J. L.; Cheftel, J. C., *Journal of Agricultural and Food Chemistry* **1985,** 33, (1), 125-130.
10) *Induction of new physicochemical and functional properties by the glycosylation of whey proteins,* Nacka, F.; Chobert, J. M.; Burova, T.; Leonil, J.; Haertle, T., *Journal of Protein Chemistry* **1998,** 17, (5), 495-503.
11) *Hydrophobic forces between protein molecules in aqueous solutions of concentrated electrolyte,* Curtis, R. A.; Steinbrecher, C.; Heinemann, A.; Blanch, H. W.; Prausnitz, J. M., *Biophysical Chemistry* **2002,** 98, (3), 249-265.

APPENDIX 1: RESEARCH PROPOSAL

PRENYLATED FLAVONOIDS AS POTENTIAL INHIBITORS OF BETA AMYLOID PEPTIDE AGGREGATION: IMPLICATIONS FOR PREVENTATIVE TREATMENT OF ALZHEIMER'S DISEASE

A. Specific Aims. Alzheimer's disease (AD) is a progressive neurodegenerative brain disorder with no known cure. Recent surveys estimate that over 18 million people world wide, including more that 4.5 million Americans, have AD.[1] The annual cost of AD treatment in the United States alone is estimated to be between $80 and $100 billion[1]. A hallmark of AD pathology is the extracellular deposition of amyloid plaques composed of fibrillar beta amyloid (Aβ) peptides $A\beta_{1-40}$ and $A\beta_{1-42}$. A key preventative approach to AD therapy involves the use of small molecules that effectively inhibit this process.[2] The flavonoids represent one such class of naturally occurring small molecules that have demonstrated numerous beneficial health effects,[3] including recent reports of neuroprotective[4] and anti-amyloidogenic activities.[5] *Here, we propose to study the effects of a unique and exciting sub-class of flavonoids for their potential to stabilize the soluble, monomeric forms of the Aβ peptides.* The unique feature of our chosen set of flavonoids is the presence of one or more prenyl groups. These substituents, composed of five carbon isoprene units, confer increased hydrophobicity, and thus lipophilicity to the parent flavonoid. In theory, the prenyl substituents would preferably interact with the hydrophobic regions of the Aβ peptides, thus deterring Aβ aggregation, and subsequent formation of amyloid plaques. *Our primary hypothesis, then, is that rational screening of prenylated-flavonoids may lead to novel therapeutic targets for the treatment or prevention of AD.* To test this hypothesis, we will achieve the following specific aims.

A.1 Screen the potential of prenylated flavonoids to inhibit fibril formation of $A\beta_{1-40}$ and $A\beta_{1-42}$ using a standardized Thioflavine T (Th T) assay.

A.2 Quantify the ability of prenylated flavonoids to influence the conformational dynamics of $A\beta_{1-40}$ and $A\beta_{1-42}$ secondary structure using Circular Dichroism (CD) Spectroscopy.

The direct outcome of this project will be an in depth understanding of how prenylated flavonoids affect the propensity for Aβ peptide aggregation. The broader impacts of this project may ultimately prove useful for identification of therapeutic targets for the preventative treatment of AD, as well as other amyloidoses and protein misfolding diseases.

B. Background. Amyloidoses collectively refer to human disease states that result from the abnormal folding and extracellular deposition of insoluble aggregates of otherwise normal proteins.[6, 7] Currently, over 20 naturally occurring proteins are known to be involved in amyloidoses.[8] Many of these proteins perform necessary functions throughout the human body. For others, no specific activity has yet been identified. What is common to all of these proteins is that for largely inexplicable reasons, their conformational dynamics shift in favor of predominantly β-sheet content.[9] These alterations to the proteins secondary structures promote aggregation in the form of β-sheet rich, toxic amyloidogenic species known as fibrils and plaques. Atop the list of amyloidoses, in terms of both recognition and prevalence, is AD. The amyloidogenic $A\beta_{1-40}$ and $A\beta_{1-42}$ peptides of AD are produced from the proteolysis of the transmembrane amyloid precursor protein (APP).[10] These peptides are soluble monomers at subnanomolar concentrations in the cerebrospinal fluid of healthy persons.[11] In persons afflicted with AD, the Aβ peptides aggregate to form intracellular neurofibrillary tangles and extracellular amyloid plaques. The exact mechanisms responsible for these deleterious events, and thus, a clear preventative strategy, remain elusive.

Therapeutic intervention strategies for AD are generally classified as either preventative or symptomatical. Both approaches are encountered with unique challenges and potentials for success, and are discussed in several recent reviews.[12-14] For example, a widely applied symptomatical strategy targets the Cholinergic system[15] with drugs that either boost levels of acetylcholine (an essential neurotransmitter) or inhibit the action of acetylcholinesterase.[16] One current preventative approach, on the other hand, targets potential inhibitors, activators, and modulators of the various secretases that process the APP, and thus produce the Aβ peptides.[17, 18] Another attractive preventative approach is the use of small molecules that promote stabilization of the soluble, monomeric states of Aβ peptides.[2, 19] To date, the list of compounds that have effectively prevented Aβ fibrillation and/or disrupted preformed fibrils and amyloid plaques includes: neurotransmitters,[20] saccharides,[21] surfactants,[22] synthetic peptides,[23] apomorphine derivatives,[24] dyes,[25] melatonin,[26] nicotine,[27] and recently, several flavonoids,[5, 28, 29]

B.1 Flavonoids. Flavonoids are a diverse set of naturally occurring polyphenolic compounds found throughout the plant kingdom[30]. They commonly find their way into the human diet through consumption of fruits, vegetables, herbs, spices, and

beverages. The flavonoid structure is based on a diphenylpropane (C_6-C_3-C_6) skeleton. The oxidation state and heterocyclization of the propane group is used to characterize flavonoids into six major classes (Figure 1): chalcones **(1)**, flavones **(2)**, flavonones **(3)**, flavonols **(4)**, anthocyanins **(5)**, and isoflavonoids **(6)**. Together, these compounds are responsible for a remarkable number of reported biological and pharmacological effects including: antioxidant[31, 32], anti-inflammatory,[33, 34] antiallergic,[35] antihepatotoxic,[35] antimicrobial,[36] antiviral,[37] and anticarcinigenic[38, 39] activities.

Traditionally, the antioxidant activity of certain flavonoids has received a great deal of attention. This is in light of the now widely accepted and scientifically supported notion that many human diseases (including AD) are promoted by damage caused by reactive oxygen and nitrogen species (ROS/RNS).[40-42] Therefore, the free radical scavenging activity of certain flavonoids offers an attractive therapeutic approach to reducing oxidative stress associated with disease states.[43, 44]

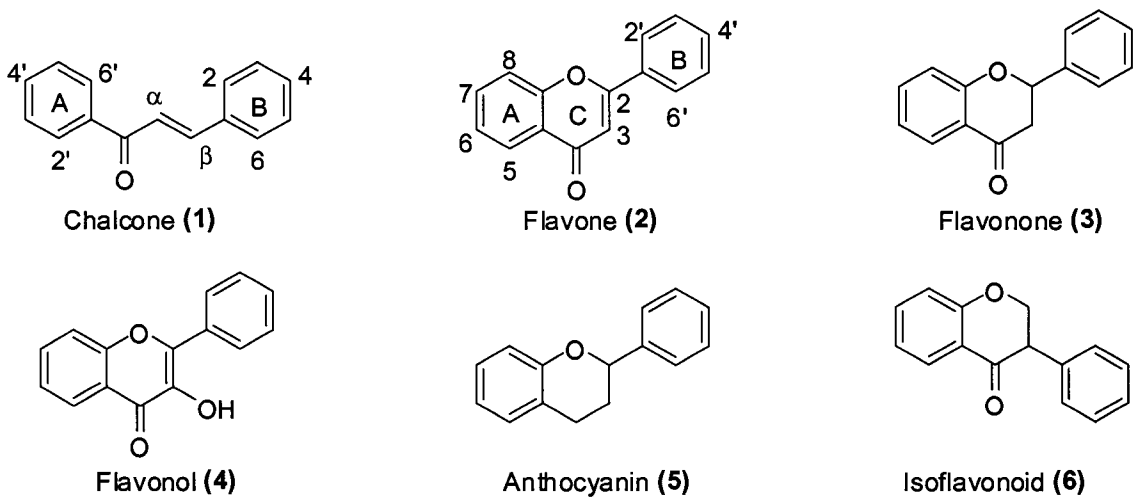

Figure 1: The skeleton structures of the six major classes of naturally occurring flavonoids

B.2 Flavonoids and AD. As recently as 2000, flavonoids were not mentioned in a review of Aβ peptide polymerization inhibitors.[45] More recent reports have demonstrated the neuroprotective and anti-amyloidogenic activities of flavonoids and pointed out that antioxidant activity does not necessarily scale with therapeutic treatment or prevention of AD.[5, 46, 47] Instead it has been suggested that structure specificity and interaction with Aβ peptides, rather than general antioxidant properties, should be more carefully considered as a crucial aspect of the flavonoids for AD treatment and prevention. Needless to say, extensive research efforts are, and will continue to focus on the isolation, identification, and

characterization of naturally occurring and synthetic flavonoids for their potentially beneficial impacts on human health.

B.3 Prenylated Flavonoids. Prenylated flavonoids, while scarcely distributed in the plant kingdom, have recently generated considerable interest in the scientific community. Studies have shown that prenyl groups can alter the intermolecular interactions of proteins as well as the activities of flavonoids. Prenylated proteins demonstrate increased protein-protein interactions as well as protein-membrane interactions.[48] It is believed that the enhanced hydrophobicity and thus, lipophilicity, conferred by prenyl groups is responsible for these observed effects. In the case of flavonoids, the presence of prenyl groups have been shown to greatly enhanced antioxidant activity.[49, 50]

Some of the biological and pharmacological activities of the more than 700 known prenylated flavonoids are discussed in reviews by Barron and Ibrahim,[51] and more recently, Botta, et al.[52] To the best of our knowledge, there are no reports on the effects of prenylated flavonoids on Aβ peptide conformational dynamics. However, one very recent report identified four prenylated isoflavonoids from the extract of *Flemingia macrophylla* that reduced $A\beta_{25-35}$ induced apoptosis of neonatal cortical neurons.[53] Interestingly, all four prenylated flavonoids demonstrated antioxidant activity as well. As previously noted, the link between antioxidant, neuroprotective, and anti-amyloidogenic activity is murky at best. Clearly then, we believe that these issues, along with the recently reported connection between prenylated flavonoids and AD,[53] merit further investigation. *Specifically, our proposed project would rationally screen a diverse set of prenylated flavonoids for their potential to affect the fibrillation and associated conformational dynamics of Aβ peptides.*

B.4 Thioflavine T (Th T) assay. The Th T assay is a standardized method for determining the presence and rate of fibril formation. Th T is a fluorescent dye that has a characteristic excitation at 385 nm and emission at 445 nm when free in solution. In the presence of non-fibrillar peptides and proteins, the dye remains free in solution, and its fluorescence is unaffected. Th T binds only to fibrillar species, giving rise to enhanced absorption and emission at 450 nm and 482 nm, respectively.[54] This fibril dependent fluorescence shift is demonstrated in Figure 2. Here, the fluorescence emission intensity reflects the degree of fibril formation while it's time dependence indicates the rate of fibril formation.[55]

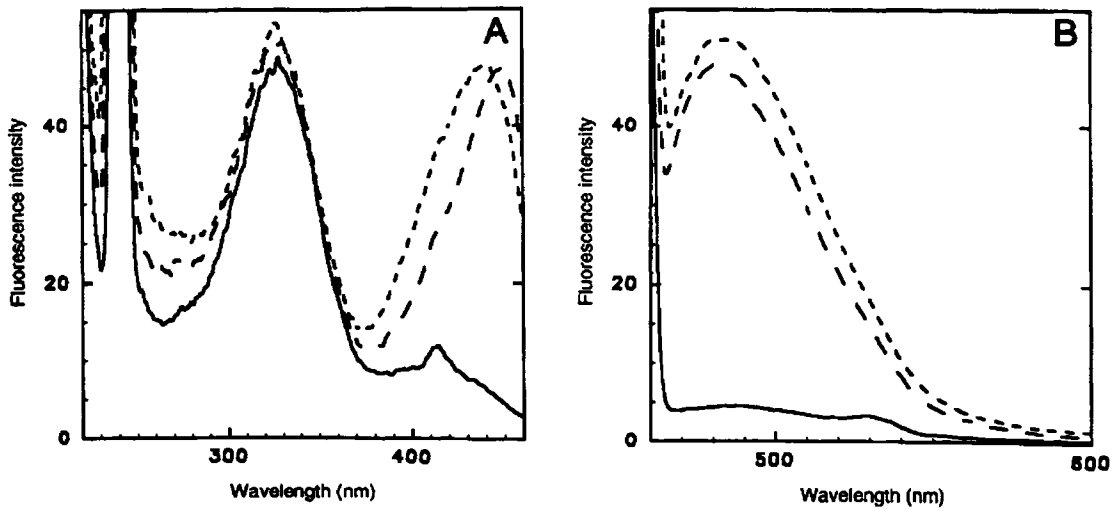

Figure 2. Excitation (A) and emission (B) spectra of Th T free in solution (solid line) and bound to $A\beta_{1-28}$ fibrils (short dashed line) and $A\beta_{1-40}$ fibrils (long dashed line).[54]

B.5 Circular Dichroism (CD). The conformational dynamics of proteins and peptides have been studied in great detail with far UV (190-250 nm) CD spectroscopy.[56] CD studies on synthetic Aβ peptides have shown that transitions towards increasing β-sheet content are consistent with fibril formation and ultimately, amyloid plaques.[57] These conformational dynamics are most easily observed as a decrease in spectral intensity at 194 nm (a characteristic maximum of β-sheets) and the appearance of random coil spectral features. The approximate percent of these secondary structure types is determined from analysis of reference spectra.[58] Figure 3 demonstrates the inhibitory effect of melatonin on $A\beta_{1-42}$ fibril formation.[26] Here, we see that melatonin induces a shift in Aβ secondary structure from β-sheet towards random coil. We would similarly analyze the conformational dynamics of $A\beta_{1-42}$ and $A\beta_{1-40}$ with special attention paid to the dose dependent effects of prenylated flavonoids.

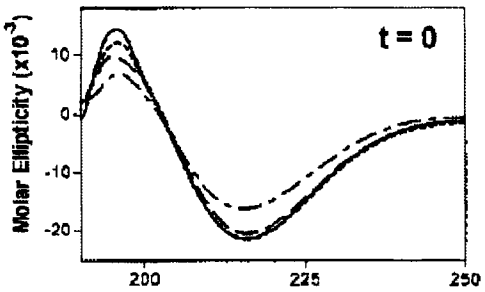

	Aβ	+NAT	+PBN	+Mel
α-helix	2	3	2	4
β-sheet	89	85	80	65
β-turn	1	1	3	10
random	8	11	15	21

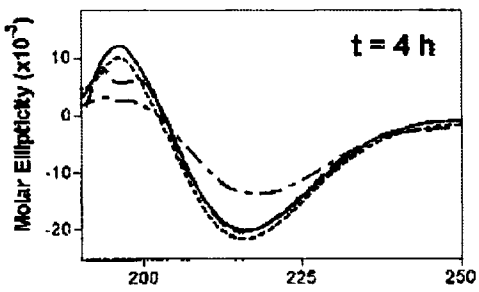

	Aβ	+NAT	+PBN	+Mel
α-helix	2	3	3	3
β-sheet	95	90	77	59
β-turn	2	3	4	10
random	1	4	16	28

Figure 3. CD spectra and corresponding percentages of secondary structure types of $A\beta_{1-42}$ alone in solution (solid line), and the presence of either 5-hydroxy-*N*-acetyl-tryptamine (NAT) (short dashes), *N*-t-butyl-a-phenylnitrone (PBN) (long dashes), or melatonin (short and long dashes).[26]

C. Research Methods/ Experimental Design. In the proposed project we will conduct Th T assay and CD spectroscopic studies on the dose dependent effects of prenylated flavonoids and some non-prenylated analogs on $A\beta_{1-40}$ and $A\beta_{1-42}$ fibril formation and corresponding conformational dynamics. We hypothesize that prenylated flavonoids will more effectively inhibit fibrillation and reduce β-sheet content relative to their non-prenylated counterparts. Additionally, we expect that the degree of prenylation will scale with their inhibitory effects. The results of this project will provide a basis data set for evaluating the potential of prenylated flavonoids as therapeutic agents for the treatment and prevention of AD.

Our chosen set of prenylated and non-prenylated flavonoids covers four **(1-4)** of the six major classes, as well as one subclass known as dihydroflavonols. Dihydroflavonols are characterized by the reduction of the 2,3 double bond in **(4)**. The non-prenylated flavonoids in Figure 4 will serve as internal standards. Several of these compounds have been investigated as potential therapeutic agents for the treatment and prevention of AD. For example, **(9-11)** have been screened by Th T assay for their effects on $A\beta_{1-42}$ fibril formation; **(10)** strongly inhibited fibril formation while **(9)** and **(11)** had no measurable effects[5]. Furthermore, **(8-10)** and **(12)** were screened by 3-[4,5-dimethylthiazol-2-yl]-2,5-diphenyl-tetrazolium bromide (MTT) assay for potential neuroprotective effects against $A\beta_{25-35}$ induced apoptosis; only **(12)** provided measurable neuroprotection.[59] To the best of our knowledge, there are no reports of the effects of these compounds on Aβ conformational dynamics as measured by CD.

Thus, our first task will be to confirm the previously observed Th T assay results for **(9-11)** and perform CD studies of the dose dependent effect of **(9-11)**, with the expectation that we will observe for **(10)** a shift in the conformational dynamics of the Aβ peptides that correspond with its ability to inhibit fibril formation. We will perform similar experiments for **(7)**, **(8)**, and **(12)** to create a basis set for understanding the role of prenylation. This methodology will be extended to the rational screening of the prenylated flavonoids discussed in the following sections.

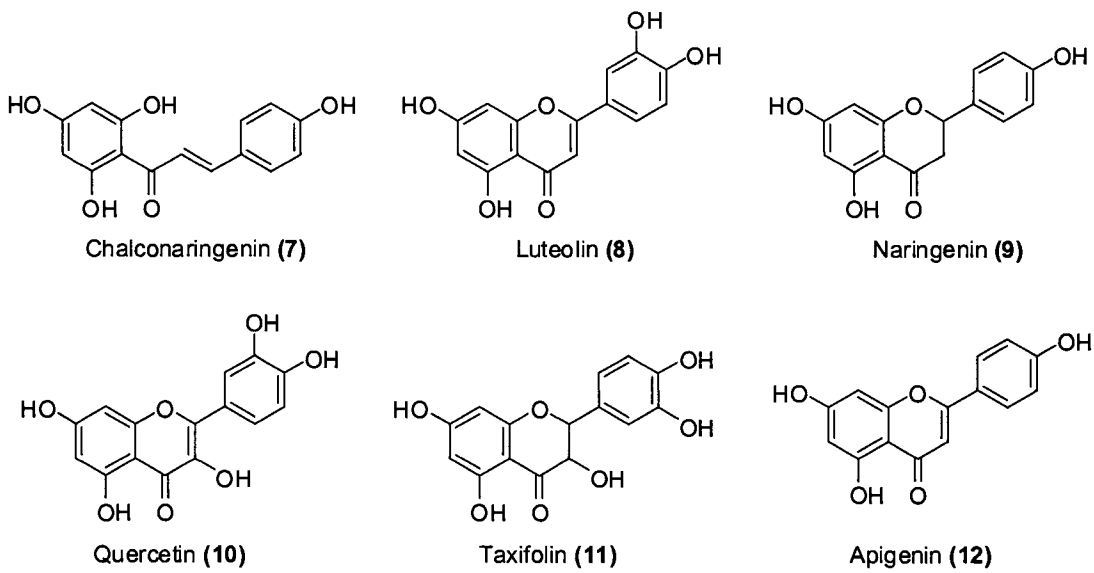

Figure 4: Non-prenylated flavonoids.

For clarity and brevity, the prenylated flavonoids that we are proposing to study are organized in the text according to their natural plant source and referred to by number, which correspond to a structure presented in Figure 5. In Figure 5, the compounds are organized according to their parent flavonoid structure. Finally, in Table 1, structure numbers are associated with compound names, their natural plant source, and literature references for isolation procedures.

C.1 Prenylated Flavonoids obtained from *Humulus lupulus (H. lupulus).* A particularly relevant source of prenylated flavonoids is the female hops plant (*H. lupulus*)[60]. This plant has been identified as the primary contributor to the dietary intake of prenylated flavonoids, when consumed in the form of beer. Recent studies attesting to the health benefits of the prenylated flavonoids of *H. lupulus* have identified **(13)** and **(22)** as useful chemopreventative agents for several cancers[61, 62] and HIV-1,[63] and **(21)** as the most potent phytoestrogen known to date.[64] The various biological and pharmacological activities as well as biotechnological aspects of the *H. lupulus* flavonoids are summarized in several reports by Stevens and coworkers.[49, 50, 61, 65, 66] For the purpose of this project, we have selected ten naturally occurring **(13-22)** and three semi-synthetic **(23-25)**

flavonoids originating from *H. lupulus* that demonstrate various patterns and degrees of prenylation. For example, **(13-16)** are 3' monoprenylated chalcones differing in their content of hydroxy and methoxy substituents. While these variations in non-prenyl substituents are not the focus of this project, we still consider it a necessary aspect of our rational screening approach. **(16)** and **(17)** are the respective 3' prenylated and 3' geranylated analogs of **(7)**. **(18)** displays a unique rearrangement of the 3' prenyl group to form a chromene group with the A ring of the parent chalcone. **(19)** is a 3', 5'-diprenyl chalcone. **(20-22)** are prenylated flavonones. **(21)** is the flavone isomer of **(16)**, which is the prenylated analog of **(9)**. Relationships such as these will enable us to make comparison between prenylated verses non-prenylated analogs, as well as prenylated isomers of different parent flavonoid structure.

C.2 Prenylated Flavonoids obtained from *Macaranga pleiostemona (M. pleiostemona)*. *M. Pleiostemona* is a common shrub of New Guinea. It's leaves are used by the natives as a topical antibiotic for the treatment of minor cuts and bruises, to reduce swelling, and relieve headaches.[67] Extracts from the leaves of *M. Pleiostemona* have led to the isolation of four flavonones **(26-29)** that have demonstrated varying degrees of antibacterial activity.[67] **(26-29)** were chosen for this project because they represent unique prenylated and geranylated analogs of **(9)**. Both **(26)** and **(28)** are geranylated, the former at the 5' position of the B ring and the latter at the 6 position of the A ring. By contrast, **(27)** and **(29)** are diprenylated. Both of these compounds contain a prenyl group at the 5' position of the B ring, with their second prenyl group at the 6 or 8 position of the A ring for **(27)** and **(28)**, respectively. As previously mentioned, it was recently reported that **(9)** had no measurable effect on the fibrillation of $A\beta_{1-42}$.[5] We believe that the prenyl and geranyl substituents of **(26-29)** will confer some degree of antifibrillation properties to these flavonoids.

C.3 Prenylated Flavonoids obtained from *Morus Cathayana (M. Cathayana)*. *M. Cathayana* is a Chinese Mulberry tree. It's leaves provide a vital food source for silk worms, while it's root bark is valued in traditional Chinese medicine an anti-inflammatory, diuretic, and expectorant[68]. Fukai and coworkers have isolated a wide variety of prenylated and geranylated flavonoids form this plant[68, 69]. We have chosen to focus on Sanggenols A-E **(30-34)**. There are two unique aspects about these compounds that we believe will significantly contribute to our proposed studies. First, **(31-34)** are the only flavonoids in our list of flavonoids that contain both geranyl and prenyl substituents. Second, **(34)** is the first tri-substituted flavonoid (containing two prenyl groups and one geranyl group) that we have proposed to study.

C.4 Prenylated Flavonoids obtained from *Dorstenia Psilurus (D. Psilurus)*. The genus *Dorstenia* is an exceptionally rich source of naturally occurring prenylated and geranylated flavonoids. *D. manni,*[70, 71] *D. zenkeri,*[72] *D. prorepens,*[72] *D. poinsettifolia,*[73, 74] and *D. psilurus*[75, 76] are among the members of

this genus that are valued medicinal plants to many native cultures of Africa and Central and South America.[52] For the purpose of this project, we have chosen to focus on *D. psilurus*, an indigenous herb of the African tropical rain forests. In tribal medicine, leaves of this plant are used for the treatment of headaches, stomach pains, and rheumatism.[75] We have chosen to focus on three prenylated flavones **(35-37)** and one prenylated flavonol **(38)** obtained from the roots of *D. psilurus*. These compounds are unique from the other flavonoids chosen for this study by virtue of the fact that they are all triprenylated. Additionally, **(36-38)** contain various rearrangements of one of their prenyl groups. In **(36)**, a chromane group is formed between a prenyl group and the A ring of the parent flavone. In **(37)**, the C8 prenyl group has rearranged into a 3-methylbut-3-en-2-ol substituent. Finally, a chromene group is formed between a prenyl group and the B ring in **(38)**.

Summary. AD is the most common form of age-related neurological degeneration and clinical dementia. The clinical and therapeutic aspects of AD (as well as other amyloidoses) still represent major challenges. Potential treatments and preventative agents of AD are continually being explored. One of the most promising preventative approaches is the use of small molecules that alter the conformational dynamics of the Aβ peptides to inhibit fibrillation, and subsequent deposition of amyloid plaques. The results of this project will add valuable new information to this key area of AD research. The unique feature of our proposed studies is the focus on the prenyl substituents of several naturally occurring and semi-synthetic flavonoids. The rational screening of prenylated flavonoids and their unprenylated analogs will directly result in data sets that rank the efficiency of prenyl group substitutions to alter the Aβ fibrillation process, as determined by the standardized Thioflavine T (Th T) assay. Additionally, CD spectroscopic studies will augment Th T assay data by providing information about the direct effect of prenylated and nonprenylated flavonoids on the conformational dynamics of Aβ peptides. *Ultimately, these studies will determine the utility of prenylated flavonoids as possible targets for the development of novel therapeutics for the treatment and prevention of AD, as well as other amyloidoses.*

Figure 5. Structures of prenylated and non-prenylated flavonoids proposed for use in this study. Numbers correspond to use in text.

Chalcones

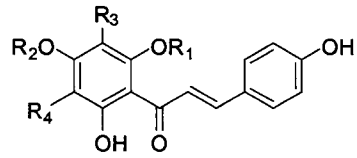

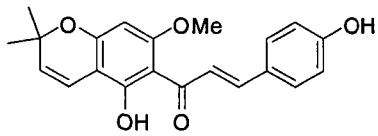

R1,R2,R3,R4=H	(7)
R1=Me, R2,R3=H, R4=Prenyl	(13)
R1,R3=H, R2=Me, R4=Prenyl	(14)
R1,R2=Me, R3=H, R4=Prenyl	(15)
R1,R2,R3=H, R4=Prenyl	(16)
R1,R2,R3=H, R4=Geranyl	(17)
R1=Me, R2=H, R3,R4=Prenyl	(19)
R1,=Me, R2,R3,R4=Prenyl	(23)

(18)

Prenyl

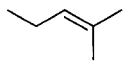

Geranyl

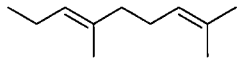

Flavonones

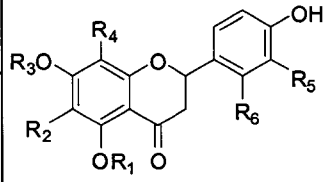

R1,R2,R3,R4,R5,R6=H	(9)
R1,R3,R4,R5,R6=H, R2=Prenyl	(20)
R1,R2,R3,R5,R6=H, R4=Prenyl	(21)
R1=Me, R2,R3,R5,R6=H, R4=Prenyl	(22)
R1,R3,R5,R6=H, R2,R4,=Prenyl	(24)
R1,R2,R3,R5,R6=H, R4=Geranyl	(25)
R1,R2,R3,R4,R6=H, R5=Geranyl	(26)
R1,R3,R4,R6=H, R2,R5=Prenyl	(27)
R1,R3,R4,R5,R6=H, R2=Geranyl	(28)
R1,R2,R3,R6=H, R4,R5=Prenyl	(29)
R1, R2,R3,R4,R6=H, R6=OH, R5=Geranyl	(30)

Dihydroflavonols

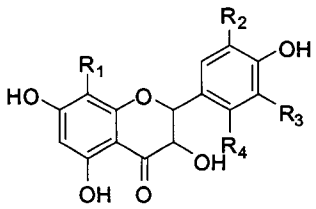

R1,R2,R4=H, R3=OH	(11)
R1=Prenyl, R2,R4=H, R3=Geranyl	(32)
R1=H, R2=Prenyl, R3=Geranyl, R4=OH	(33)
R1, R2=Prenyl, R3=Geranyl, R4=OH	(34)

Flavonols

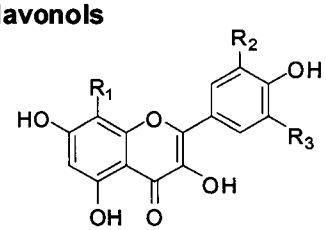

R1,R3=H, R2=OH	(10)
R1=Prenyl, R2=H, R3=Geranyl	(31)

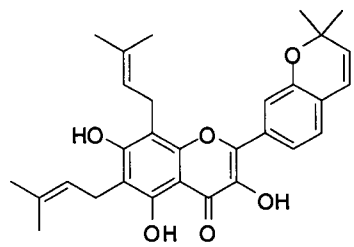

(38)

Flavones

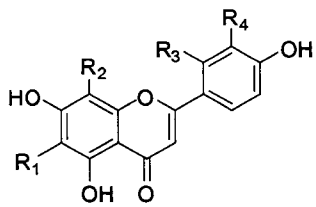

R1,R2,R3=H, R4=OH	(8)
R1,R2,R3,R4=H	(12)
R1,R2,R4=Prenyl, R3=OH	(35)

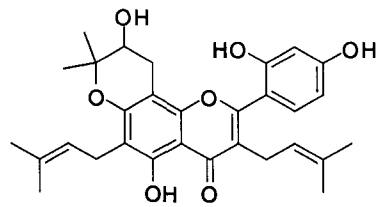

(36)

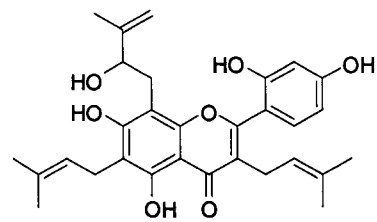

(37)

Table 1. The names of all compounds proposed for use in this project are linked to structure numbers used in Figures 4 and 5, along with literature reference for isolation procedures, where appropriate.

Name	Structure (#)	Source	Parent Flavoniod	Ref.
Chalconaringenin	**(7)**	Synthesized from **(9)**	Chalcone	[49]
Xanthohumol	**(13)**	Humulus lupulus	Chalcone	[60]
Xanthogalenol	**(14)**	Humulus lupulus	Chalcone	[60]
4'-O-Methylxanthohumol	**(15)**	Humulus lupulus	Chalcone	[60]
Desmethylxanthohumol	**(16)**	Humulus lupulus	Chalcone	[60]
2',4',6',4-tetrahydroxy-3'-C-geranylchalcone	**(17)**	Humulus lupulus	Chalcone	[60]
Dehydrocyclo-xanthohumol	**(18)**	Humulus lupulus	Chalcone	[60]
5'-Prenylxanthohumol	**(19)**	Humulus lupulus	Chalcone	[60]
4'-O-5'-C-diprenylxanthohumol	**(23)**	Synthesized from **(13)**	Chalcone	[49]
Naringenin	**(9)**	commercial (Sigma)	Flavonone	
6-Prenylnaringenin	**(20)**	Humulus lupulus	Flavonone	[60]
8-Prenylnaringenin	**(21)**	Humulus lupulus	Flavonone	[60]
Isoxanthohumol	**(22)**	Humulus lupulus	Flavonone	[60]
6,8-Diprenylnaringenin	**(24)**	Synthesized from **(9)**	Flavonone	[77, 78]
8-Geranylnaringenin	**(25)**	Synthesized from **(9)**	Flavonone	[77, 78]
Macarangaflavanone A	**(26)**	Macaranga Pleiostemona	Flavonone	[67]
Macarangaflavanone B	**(27)**	Macaranga Pleiostemona	Flavonone	[67]
Bonannione A	**(28)**	Macaranga Pleiostemona	Flavonone	[67]
Euchrestaflavanone A	**(29)**	Macaranga Pleiostemona	Flavonone	[67]
Sanggenols A	**(30)**	Morus cathayana	Flavonone	[69]
Luteolin	**(8)**	commercial (Sigma)	Flavone	
Apigenin	**(12)**	commercial (Sigma)	Flavone	
Dorsilurin A	**(35)**	Dorstenia Psilurus	Flavone	[75]
Dorsilurin B	**(36)**	Dorstenia Psilurus	Flavone	[75]
Dorsilurin C	**(37)**	Dorstenia Psilurus	Flavone	[76]
Taxifolin	**(11)**	commercial (Sigma)	Dihydroflavonol	
Sanggenols C	**(32)**	Morus cathayana	Dihydroflavonol	[69]
Sanggenols D	**(33)**	Morus cathayana	Dihydroflavonol	[69]
Sanggenols E	**(34)**	Morus cathayana	Dihydroflavonol	[69]
Quercetin	**(10)**	commercial (Sigma)	Flavonol	
Sangennols B	**(31)**	Morus cathayana	Flavonol	[69]
Dorsilurin D	**(38)**	Dorstenia Psilurus	Flavonol	[76]

References

1. *The Facts on Alzheimer's Disease*; American Health Assistance Foundation 2005; p www.ahaf.org.
2. Cohen, F. E.; Kelly, J. W., Therapeutic approaches to protein-misfolding diseases. *Nature* **2003,** 426, (6968), 905-909.
3. Bravo, L., Polyphenols: Chemistry, dietary sources, metabolism, and nutritional significance. *Nutrition Reviews* **1998,** 56, (11), 317-333.
4. Youdim, K. A.; Spencer, J. P. E.; Schroeter, H.; Rice-Evans, C., Dietary flavonoids as potential neuroprotectants. *Biological Chemistry* **2002,** 383, (3-4), 503-519.
5. Kim, H.; Park, B. S.; Lee, K. G.; Choi, C. Y.; Jang, S. S.; Kim, Y. H.; Lee, S. E., Effects of naturally occurring compounds on fibril formation and oxidative stress of beta-amyloid. *Journal of Agricultural and Food Chemistry* **2005,** 53, (22), 8537-8541.
6. Stefani, M.; Dobson, C. M., Protein aggregation and aggregate toxicity: new insights into protein folding, misfolding diseases and biological evolution. *Journal of Molecular Medicine-Jmm* **2003,** 81, (11), 678-699.
7. Sipe, J. D., Amyloidosis. *Critical Reviews in Clinical Laboratory Sciences* **1994,** 31, (4), 325-354.
8. Obici, L.; Perfetti, V.; Palladini, G.; Moratti, R.; Merlini, G., Clinical aspects of systemic amyloid diseases. *Biochimica Et Biophysica Acta-Proteins and Proteomics* **2005,** 1753, (1), 11-22.
9. Selkoe, D. J., Folding proteins in fatal ways. *Nature* **2003,** 426, (6968), 900-904.
10. Mattson, M. P., Cellular actions of beta-amyloid precursor protein and its soluble and fibrillogenic derivatives. *Physiological Reviews* **1997,** 77, (4), 1081-1132.
11. Shoji, M.; Golde, T. E.; Ghiso, J.; Cheung, T. T.; Estus, S.; Shaffer, L. M.; Cai, X. D.; McKay, D. M.; Tintner, R.; Frangione, B.; Younkin, S. G., Production of the Alzheimer Amyloid-Beta Protein by Normal Proteolytic Processing. *Science* **1992,** 258, (5079), 126-129.
12. Lleo, A.; Greenberg, S. M.; Growdon, J. H., Current pharmacotherapy for Alzheimer's disease. *Annual Review of Medicine* **2006,** 57, 513-533.
13. Sramek, J. J.; Cutler, N. R., Recent developments in the drug treatment of Alzheimer's disease. *Drugs & Aging* **1999,** 14, (5), 359-373.
14. Selkoe, D. J., Alzheimer's disease: Genes, proteins, and therapy. *Physiological Reviews* **2001,** 81, (2), 741-766.
15. Kasa, P.; Rakonczay, Z.; Gulya, K., The cholinergic system in Alzheimer's disease. *Progress in Neurobiology* **1997,** 52, (6), 511-535.
16. Grutzendler, J.; Morris, J. C., Cholinesterase inhibitors for Alzheimer's disease. *Drugs* **2001,** 61, (1), 41-52.
17. Wolfe, M. S., Secretase targets for Alzheimer's disease: Identification and therapeutic potential. *Journal of Medicinal Chemistry* **2001,** 44, (13), 2039-2060.
18. Citron, M., Secretases as targets for the treatment of Alzheimer's disease. *Molecular Medicine Today* **2000,** 6, (10), 392-397.
19. Lansbury, P. T., Inhibition of amyloid formation: a strategy to delay the onset of Alzheimer's disease. *Current Opinion in Chemical Biology* **1997,** 1, (2), 260-267.
20. Li, J.; Zhu, M.; Manning-Bog, A. B.; Di Monte, D. A.; Fink, A. L., Dopamine and L-dopa disaggregate amyloid fibrils: implications for Parkinson's and Alzheimer's disease. *Faseb Journal* **2004,** 18, (6).
21. Fung, J.; Darabie, A. A.; McLaurin, J., Contribution of simple saccharides to the stabilization of amyloid structure. *Biochemical and Biophysical Research Communications* **2005,** 328, (4), 1067-1072.
22. Sabate, R.; Estelrich, J., Stimulatory and inhibitory effects of alkyl bromide surfactants on beta-amyloid fibrillogenesis. *Langmuir* **2005,** 21, (15), 6944-6949.
23. Soto, C.; Kindy, M. S.; Baumann, M.; Frangione, B., Inhibition of Alzheimer's amyloidosis by peptides that prevent beta-sheet conformation. *Biochemical and Biophysical Research Communications* **1996,** 226, (3), 672-680.

24. Lashuel, H. A.; Hartley, D. M.; Balakhaneh, D.; Aggarwal, A.; Teichberg, S.; Callaway, D. J. E., New class of inhibitors of amyloid-beta fibril formation - Implications for the mechanism of pathogenesis in Alzheimer's disease. *Journal of Biological Chemistry* **2002,** 277, (45), 42881-42890.
25. Bandiera, T.; Lansen, J.; Post, C.; Varasi, M., Inhibitors of A beta peptide aggregation as potential anti-Alzheimer agents. *Current Medicinal Chemistry* **1997,** 4, (3), 159-170.
26. Pappolla, M.; Bozner, P.; Soto, C.; Shao, H. Y.; Robakis, N. K.; Zagorski, M.; Frangione, B.; Ghiso, J., Inhibition of Alzheimer beta-fibrillogenesis by melatonin. *Journal of Biological Chemistry* **1998,** 273, (13), 7185-7188.
27. Ono, K.; Hasegawa, K.; Yamada, M.; Naiki, H., Nicotine breaks down preformed Alzheimer's beta-amyloid fibrils in vitro. *Biological Psychiatry* **2002,** 52, (9), 880-886.
28. Ono, K.; Hasegawa, K. U.; Yoshiike, Y.; Takashima, A.; Yamada, M.; Naiki, H., Nordihydroguaiaretic acid potently breaks down pre-formed Alzheimer's beta-amyloid fibrils in vitro. *Journal of Neurochemistry* **2002,** 81, (3), 434-440.
29. Ono, K.; Hasegawa, K.; Naiki, H.; Yamada, M., Anti-amyloidogenic activity of tannic acid and its activity to destabilize Alzheimer's beta-amyloid fibrils in vitro. *Biochimica Et Biophysica Acta-Molecular Basis of Disease* **2004,** 1690, (3), 193-202.
30. Manach, C.; Scalbert, A.; Morand, C.; Remesy, C.; Jimenez, L., Polyphenols: food sources and bioavailability. *American Journal of Clinical Nutrition* **2004,** 79, (5), 727-747.
31. Montoro, P.; Braca, A.; Pizza, C.; De Tommasi, N., Structure-antioxant activity relationships of flavonoids isolated from different plant species. *Food Chemistry* **2005,** 92, (2), 349-355.
32. Mandel, S.; Amit, T.; Reznichenko, L.; Weinreb, O.; Youdim, M. B. H., Green tea catechins as brain-permeable, natural iron chelators-antioxidants for the treatment of neurodegenerative disorders. *Molecular Nutrition & Food Research* **2006,** 50, (2), 229-234.
33. Wei, B. L.; Weng, J. R.; Chiu, P. H.; Hung, C. F.; Wang, J. P.; Lin, C. N., Antiinflammatory flavonoids from Artocarpus heterophyllus and Artocarpus communis. *Journal of Agricultural and Food Chemistry* **2005,** 53, (10), 3867-3871.
34. Middleton, E., Effect of plant flavonoids on immune and inflammatory cell function. In *Flavonoids in the Living System*, 1998; Vol. 439, pp 175-182.
35. Di Carlo, G.; Mascolo, N.; Izzo, A. A.; Capasso, F., Flavonoids: Old and new aspects of a class of natural therapeutic drugs. *Life Sciences* **1999,** 65, (4), 337-353.
36. Cowan, M. M., Plant products as antimicrobial agents. *Clinical Microbiology Reviews* **1999,** 12, (4), 564-+.
37. Buckwold, V. E.; Wilson, R. J. H.; Nalca, A.; Beer, B. B.; Voss, T. G.; Turpin, J. A.; Buckheit, R. W.; Wei, J. Y.; Wenzel-Mathers, M.; Walton, E. M.; Smith, R. J.; Pallansch, M.; Ward, P.; Wells, J.; Chuvala, L.; Sloane, S.; Paulman, R.; Russell, J.; Hartman, T.; Ptak, R., Antiviral activity of hop constituents against a series of DNA and RNA viruses. *Antiviral Research* **2004,** 61, (1), 57-62.
38. Okuyama, T.; Takata, M.; Takayasu, J.; Hasegawa, T.; Tokuda, H.; Nishino, A.; Nishino, H.; Iwashima, A., Studies on the Anti-Tumor-Promoting Activity of Naturally-Occurring Substances .5. Anti-Tumor-Promotion by Principles Obtained from Angelica-Keiskei. *Planta Medica* **1991,** 57, (3), 242-246.
39. Kimura, Y.; Baba, K., Antitumor and antimetastatic activities of Angelica keiskei roots, part 1: Isolation of an active substance, xanthoangelol. *International Journal of Cancer* **2003,** 106, (3), 429-437.
40. Markesbery, W. R., Oxidative stress hypothesis in Alzheimer's disease. *Free Radical Biology and Medicine* **1997,** 23, (1), 134-147.
41. Berlett, B. S.; Stadtman, E. R., Protein oxidation in aging, disease, and oxidative stress. *Journal of Biological Chemistry* **1997,** 272, (33), 20313-20316.
42. Devi, G. S.; Prasad, M. H.; Saraswathi, I.; Raghu, D.; Rao, D. N.; Reddy, P. P., Free radicals antioxidant enzymes and lipid peroxidation in different types of leukemias. *Clinica Chimica Acta* **2000,** 293, (1-2), 53-62.

43. Luximon-Ramma, A.; Bahorun, T.; Crozier, A.; Zbarsky, V.; Datla, K. P.; Dexter, D. T.; Aruoma, O. I., Characterization of the antioxidant functions of flavonoids and proanthocyanidins in Mauritian black teas. *Food Research International* **2005,** 38, (4), 357-367.
44. Lopes, G. K. B.; Schulman, H. M.; Hermes-Lima, M., Polyphenol tannic acid inhibits hydroxyl radical formation from Fenton reaction by complexing ferrous ions. *Biochimica Et Biophysica Acta-General Subjects* **1999,** 1472, (1-2), 142-152.
45. Findeis, M. A., Approaches to discovery and characterization of inhibitors of amyloid beta-peptide polymerization. *Biochimica Et Biophysica Acta-Molecular Basis of Disease* **2000,** 1502, (1), 76-84.
46. Weinreb, O.; Mandel, S.; Amit, T.; Youdim, M. B. H., Neurological mechanisms of green tea polyphenols in Alzheimer's and Parkinson's diseases. *Journal of Nutritional Biochemistry* **2004,** 15, (9), 506-516.
47. Bastianetto, S.; Yao, Z. X.; Papadopoulos, V.; Quirion, R., Neuroprotective effects of green and black teas and their catechin gallate esters against beta-amyloid-induced toxicity. *European Journal of Neuroscience* **2006,** 23, (1), 55-64.
48. Zhang, F. L.; Casey, P. J., Protein prenylation: Molecular mechanisms and functional consequences. *Annual Review of Biochemistry* **1996,** 65, 241-269.
49. Miranda, C. L.; Stevens, J. F.; Ivanov, V.; McCall, M.; Frei, B.; Deinzer, M. L.; Buhler, D. R., Antioxidant and prooxidant actions of prenylated and nonprenylated chalcones and flavanones in vitro. *Journal of Agricultural and Food Chemistry* **2000,** 48, (9), 3876-3884.
50. Stevens, J. F.; Miranda, C. L.; Frei, B.; Buhler, D. R., Inhibition of peroxynitrite-mediated LDL oxidation by prenylated flavonoids: The alpha,beta-unsaturated keto functionality of 2 '-hydroxychalcones as a novel antioxidant pharmacophore. *Chemical Research in Toxicology* **2003,** 16, (10), 1277-1286.
51. Barron, D.; Ibrahim, R. K., Isoprenylated flavonoids - A survey. *Phytochemistry* **1996,** 43, (5), 921-982.
52. Botta, B.; Vitali, A.; Menendez, P.; Misiti, D.; Delle Monache, G., Prenylated flavonoids: Pharmacology and biotechnology. *Current Medicinal Chemistry* **2005,** 12, (6), 713-739.
53. Shiao, Y. J.; Wang, C. N.; Wang, W. Y.; Lin, Y. L., Neuroprotective flavonoids from Flemingia macrophylla. *Planta Medica* **2005,** 71, (9), 835-840.
54. Levine, H., Thioflavine-T Interaction with Synthetic Alzheimers-Disease Beta-Amyloid Peptides - Detection of Amyloid Aggregation in Solution. *Protein Science* **1993,** 2, (3), 404-410.
55. LeVine, H., Quantification of beta-sheet amyloid fibril structures with thioflavin T. In *Amyloid, Prions, and Other Protein Aggregates*, 1999; Vol. 309, pp 274-284.
56. Woody, R. W., Circular-Dichroism. In *Biochemical Spectroscopy*, 1995; Vol. 246, pp 34-71.
57. Barrow, C. J.; Yasuda, A.; Kenny, P. T. M.; Zagorski, M. G., Solution Conformations and Aggregational Properties of Synthetic Amyloid Beta-Peptides of Alzheimers-Disease - Analysis of Circular-Dichroism Spectra. *Journal of Molecular Biology* **1992,** 225, (4), 1075-1093.
58. Pelton, J. T.; McLean, L. R., Spectroscopic methods for analysis of protein secondary structure. *Analytical Biochemistry* **2000,** 277, (2), 167-176.
59. Wang, C. N.; Chi, C. W.; Lin, Y. L.; Chen, C. F.; Shiao, Y. J., The neuroprotective effects of phytoestrogens on amyloid beta protein-induced toxicity are mediated by abrogating the activation of caspase cascade in rat cortical neurons. *Journal of Biological Chemistry* **2001,** 276, (7), 5287-5295.
60. Stevens, J. F.; Ivancic, M.; Hsu, V. L.; Deinzer, M. L., Prenylflavonoids from Humulus lupulus. *Phytochemistry* **1997,** 44, (8), 1575-1585.
61. Miranda, C. L.; Stevens, J. F.; Helmrich, A.; Henderson, M. C.; Rodriguez, R. J.; Yang, Y. H.; Deinzer, M. L.; Barnes, D. W.; Buhler, D. R., Antiproliferative and cytotoxic effects of prenylated flavonoids from hops (Humulus lupulus) in human cancer cell lines. *Food and Chemical Toxicology* **1999,** 37, (4), 271-285.
62. Gerhauser, C.; Alt, A.; Heiss, E.; Gamal-Eldeen, A.; Klimo, K.; Knauft, J.; Neumann, I.; Scherf, H. R.; Frank, N.; Bartsch, H.; Becker, H., Cancer chemopreventive activity of Xanthohumol, a natural product derived from hop. *Molecular Cancer Therapeutics* **2002,** 1, (11), 959-969.

63. Wang, Q.; Ding, Z. H.; Liu, J. K.; Zheng, Y. T., Xanthohumol, a novel anti-HIV-1 agent purified from Hops Humulus lupulus. *Antiviral Research* **2004,** 64, (3), 189-194.
64. Milligan, S. R.; Kalita, J. C.; Heyerick, A.; Rong, H.; De Cooman, L.; De Keukeleire, D., Identification of a potent phytoestrogen in hops (Humulus lupulus L.) and beer. *Journal of Clinical Endocrinology and Metabolism* **1999,** 84, (6), 2249-2252.
65. Stevens, J. F.; Miranda, C. L.; Buhler, D. R.; Deinzer, M. L., Chemistry and biology of hop flavonoids. *Journal of the American Society of Brewing Chemists* **1998,** 56, (4), 136-145.
66. Stevens, J. F.; Page, J. E., Xanthohumol and related prenylflavonoids from hops and beer: to your good health! *Phytochemistry* **2004,** 65, (10), 1317-1330.
67. Schutz, B. A.; Wright, A. D.; Rali, T.; Sticher, O., Prenylated Flavanones from Leaves of Macaranga-Pleiostemona. *Phytochemistry* **1995,** 40, (4), 1273-1277.
68. Fukai, T.; Pei, Y. H.; Nomura, T.; Xu, C. Q.; Wu, L. J.; Chen, Y. J., Isoprenylated flavanones from Morus cathayana. *Phytochemistry* **1998,** 47, (2), 273-280.
69. Fukai, T.; Pei, Y. H.; Nomura, T.; Xu, C. Q.; Wu, L. J.; Chen, Y. J., Components of the root bark of Morus cathayana .1. Structures of five new isoprenylated flavonoids, sanggenols A-E and a diprenyl-2-arylbenzofuran, mulberrofuran V. *Heterocycles* **1996,** 43, (2), 425-436.
70. Dufall, K. G.; Ngadjui, B. T.; Simeon, K. F.; Abegaz, B. M.; Croft, K. D., Antioxidant activity of prenylated flavonoids from the West African medicinal plant Dorstenia mannii. *Journal of Ethnopharmacology* **2003,** 87, (1), 67-72.
71. Ngadjui, B. T.; Abegaz, B. M.; Dongo, E.; Tamboue, H.; Fogue, K., Geranylated and prenylated flavonoids from the twigs of Dorstenia mannii. *Phytochemistry* **1998,** 48, (2), 349-354.
72. Abegaz, B. M.; Ngadjui, B. T.; Dongo, E.; Ngameni, B.; Nindi, M. N.; Bezabih, M., Chalcones and other constituents of Dorstenia prorepens and Dorstenia zenkeri. *Phytochemistry* **2002,** 59, (8), 877-883.
73. Tsopmo, A.; Tene, M.; Kamnaing, P.; Ngnokam, D.; Ayafor, J. F.; Sterner, O., Geranylated flavonoids from Dorstenia poinsettifolia. *Phytochemistry* **1998,** 48, (2), 345-348.
74. Ngadjui, B. T.; Kapche, G. W. F.; Tamboue, H.; Abegaz, B. M.; Connolly, J. D., Prenylated flavonoids and a dihydro-4-phenylcoumarin from Dorstenia poinsettifolia. *Phytochemistry* **1999,** 51, (1), 119-123.
75. Ngadjui, B. T.; Dongo, E.; Happi, E. N.; Bezabih, M. T.; Abegaz, B. M., Prenylated flavones and phenylpropanoid derivatives from roots of Dorstenia psilurus. *Phytochemistry* **1998,** 48, (4), 733-737.
76. Ngadjui, B. T.; Tabopda, T. K.; Dongo, E.; Kapche, G. W. F.; Sandor, P.; Abegaz, B. M., Dorsilurins C, D and E, three prenylated flavonoids from the roots of Dorstenia psilurus. *Phytochemistry* **1999,** 52, (4), 731-735.
77. Stevens, J. F.; Taylor, A. W.; Clawson, J. E.; Deinzer, M. L., Fate of xanthohumol and related prenylflavonoids from hops to beer. *Journal of Agricultural and Food Chemistry* **1999,** 47, (6), 2421-2428.
78. Stevens, J. F.; Taylor, A. W.; Deinzer, M. L., Quantitative analysis of xanthohumol and related prenylflavonoids in hops and beer by liquid chromatography tandem mass spectrometry. *Journal of Chromatography A* **1999,** 832, (1-2), 97-107.